

**A NOVEL PEG-ELASTIN COPOLYMER FOR  
TISSUE ENGINEERED VASCULAR GRAFTS**

A Thesis  
Presented to  
The Academic Faculty

by

Dhaval Pradipkumar Patel

In Partial Fulfillment  
of the Requirements for the Degree  
Doctor of Philosophy in the  
School of Chemical & Biomolecular Engineering

Georgia Institute of Technology  
December 2012

**A NOVEL PEG-ELASTIN COPOLYMER FOR TISSUE  
ENGINEERED VASCULAR GRAFTS**

Approved by:

Dr. Lakeshia J. Taite, Advisor  
School of Chemical & Biomolecular  
Engineering  
*Georgia Institute of Technology*

Dr. Elliot Chaikof  
Department of Surgery  
*Beth Israel Deaconess Medical Center*  
School of Chemical & Biomolecular  
Engineering  
*Georgia Institute of Technology*

Dr. Andrés García  
School of Mechanical Engineering  
*Georgia Institute of Technology*

Dr. Larry McIntire  
School of Chemical & Biomolecular  
Engineering  
*Georgia Institute of Technology*

Dr. Athanassios Sambanis  
School of Chemical & Biomolecular  
Engineering  
*Georgia Institute of Technology*

Date Approved: August 14, 2012

-For my loving parents-  
-Who sacrificed their dreams so that their sons may get the best opportunities in life-

## ACKNOWLEDGEMENTS

First and foremost, I wish to thank my advisor Dr. Lakeshia J. Taite for taking me on as a student. Throughout the past five years, I know that I have not lived up to your expectations as a model graduate student, but your patience with me has driven me to this stage of my career. You always told me to never give up and always keep trying regardless of the result. When I started graduate school, I never imagined being a student of an advisor such as you: dynamic and caring. You allowed me to pursue my hobbies while in graduate school and I could not have asked for a better advisor than you. Thank you very much for the wonderful 5 years and I am going to miss the lab that Shahana and I built with you!

I wish to thank my committee members, Dr. Elliot Chaikof, Dr. Andrés García, Dr. Larry McIntire, and Dr. Athanassios Sambanis, for their support and guidance on my project.

I wish to thank my lab colleagues, Shahana Safdar and Kai Chang. All the ridiculous conversations we have had in the past totally made the lab environment more dynamic and fun. Both of you have helped me tremendously throughout my tenure as a graduate student and I would not be here without your help.

I wish to thank my amazing undergraduate students, Rohan Menon, Susan Vandromme, Michael Reid, and Madiha Zafar for helping me with my project. Rohan, you have helped me bring this project to life ever since you joined the Taite lab. Your ability to quickly learn and adapt new techniques has made my life a lot easier over the

past five years. Your companionship as a friend and mentee has made the experience memorable for a lifetime!

I wish to thank my parents for their support throughout my graduate studies even though I chose a career path they did not intend. I know that both of you wanted me to become a medical doctor, but your support in my life decisions has made this experience ever so sweeter. Ever since we immigrated to the United States, both of you have worked harder than I ever can to ensure that my brother and I get the best education possible. I am here at this stage because of my loving parents who gave me the strength and intelligence to fight through any obstacle life may throw at me.

*JAI SWAMINARAYAN AND JAI SHRI KRISHNA*

## TABLE OF CONTENTS

LIST OF TABLES .....	X
LIST OF FIGURES .....	XI
LIST OF SYMBOLS AND ABBREVIATIONS .....	XIII
SUMMARY .....	XVI
CHAPTER 1 .....	1
1.1 Summary .....	1
1.2 Cardiovascular Diseases .....	1
1.3 Anatomy of a Blood Vessel .....	2
1.4 Tissue Engineering of Vascular Grafts .....	4
1.4.1 Synthetic Materials for Engineering Vascular Grafts .....	6
1.4.2 Natural Material for Engineering Vascular Grafts .....	11
1.5 Synthetic and Natural Polymers for Engineering Vascular Grafts .....	15
CHAPTER 2 .....	19
2.1 Summary .....	19
2.2 Introduction .....	20
2.3 Materials and Methods .....	22
2.3.1 Circular Dichroism Studies .....	22
2.3.2 Peptide Synthesis .....	22
2.3.3 Cell Culture and Maintenance .....	23
2.3.4 Peptide Influence on Elastin and Desmosine Formation .....	24
2.3.5 Peptide Competition with $\alpha$ -Lactose & RGDS .....	25
2.3.6 Fastin Assay for Assessment of Elastin Production .....	26
2.3.7 Desmosine enzyme linked immunosorbent assay (ELISA) .....	26
2.3.8 Immunofluorescence Staining .....	27

2.3.9 Quantification of tropoelastin and LOX mRNA levels .....	28
2.3.10 Blockage of integrins .....	29
2.3.11 Statistical Analysis.....	31
2.4 Results.....	31
2.4.1 Circular Dichroism Studies.....	31
2.4.2 Peptide influence on Elastin and Desmosine Production .....	32
2.4.3 Peptide competition with $\alpha$ -lactose .....	34
2.4.4 Peptide competition with Soluble RGDS .....	37
2.4.5 Visualizing Peptide Activity via Immunofluorescence .....	38
2.4.6 Tropoelastin and LOX mRNA levels .....	39
2.4.7 Role of Integrins in Elastin Fiber Assembly.....	40
2.5 Discussion.....	42
2.6 Conclusion .....	51
CHAPTER 3 .....	52
3.1 Summary.....	52
3.2 Introduction.....	52
3.3 Materials and Methods.....	53
3.3.1 Peptide synthesis.....	53
3.3.2 Cell culture and maintenance.....	54
3.3.3 PEG-DA synthesis .....	55
3.3.4 Conjugation of peptides to monoacrylate PEG derivative.....	55
3.3.5 Determining the Grafting Efficiencies of Peptide onto PEG-DA Surfaces.....	56
3.3.6 Optimizing Cell Adhesion and Proliferation on PEG-peptide Hydrogels.....	57
3.3.7 Cell Spreading on PEG-peptide Hydrogels .....	58
3.3.8 Cell viability on PEG-peptide hydrogels .....	58

3.3.9 Biochemical analysis of PEG-peptide hydrogels.....	59
3.3.10 Hydrogel elastin content .....	60
3.3.11 Statistical Analysis.....	60
3.4 Results.....	60
3.4.1 Grafting efficiencies of Different Peptides over PEG-DA Hydrogel Surfaces	60
3.4.2 Optimizing cell adhesion using varying concentrations of elastin mimetic peptides .....	61
3.4.3 Quantifying SMC Spreading over PEG-peptide Surfaces.....	63
3.4.4 Quantifying and Visualizing Cell Viability over PEG-peptide Surfaces.....	64
3.4.5 Quantifying Elastin Deposition over PEG-peptide Surfaces.....	66
3.5 Discussion.....	66
3.6 Conclusion .....	71
CHAPTER 4 .....	72
4.1 Summary.....	72
4.2 Introduction.....	72
4.3 Materials and Methods.....	73
4.3.1 Peptide synthesis.....	73
4.3.2 Cell culture and maintenance.....	74
4.3.3 PEG-DA synthesis .....	74
4.3.4 Synthesis of PEG-peptide Copolymers.....	75
4.3.5 Hydrogel Degradation Studies.....	76
4.3.6 Cell Encapsulation .....	77
4.3.7 Biochemical Analysis of PEG-peptide-PEG hydrogels.....	78
4.3.8 Hydrogel Compression Testing .....	79
4.3.9 Cell Viability.....	81
4.3.10 Statistical Analysis.....	82

4.4 Results.....	82
4.4.1 Gel Degradation in the Presence of Elastase .....	82
4.4.2 Elastin Content in Peptide Polymerized Hydrogels.....	83
4.4.3 Hydroxyproline Content .....	85
4.4.4 Estimating the Compressive Modulus of Different PEG-peptide-PEG Hydrogels.....	86
4.5 Discussion.....	88
4.6 Conclusion .....	95
CHAPTER 5 .....	96
5.1 Results and Implications.....	96
5.1.1 EM-23 is a Promising Candidate for Vascular Graft Applications .....	96
5.2 Future Work.....	98
5.2.1 Further Characterization of EM-23 as a 3D template.....	98
5.2.2 Dynamic Mechanical Stimulation.....	100
5.2.3 Alternative Materials and Techniques for Engineering Vascular Grafts.....	102
APPENDIX.....	104
REFERENCES .....	108

## LIST OF TABLES

	Page
Table 4.1: Hydrogel Formulations.....	77

## LIST OF FIGURES

Figure 1.1 – Anatomy of a blood vessel .....	3
Figure 1.2 – Structure of Desmosine and Isodesmosine.....	16
Figure 1.3 – Mechanism of Elastin Production .....	17
Figure 2.1 – CD Spectra of the Elastin Mimetic Peptides .....	32
Figure 2.2 – Elastin and Desmosine Production in the Presence of the Elastin Mimetic Peptides.....	33
Figure 2.3 – Desmosine Production in the Presence of EM-19G and EM-23G.....	34
Figure 2.4 – Elastin and Desmosine Production in the Presence of $\alpha$ -lactose and the Elastin Mimetic Peptides .....	35
Figure 2.5 – Elastin and Desmosine Production in the Presence of Soluble RGDS and the Elastin Mimetic Peptides .....	37
Figure 2.6 – Immunofluorescent Images of Peptide Bioactivity <i>In Vitro</i> .....	38
Figure 2.7 – Tropoelastin and LOX mRNA Levels.....	40
Figure 2.8 – Elastin and Desmosine Production in the Presence of $\alpha_v\beta_3$ or $\alpha_5\beta_1$ Antibodies and the Elastin Mimetic Peptides .....	41
Figure 2.9 – Elastin and Desmosine Production in the Presence of an Isotype Control and the Elastin Mimetic Peptides .....	42
Figure 2.10 – Proposed Mechanism of EM-19 Cross-linking with Elastin Matrix .....	44
Figure 2.11 – Proposed Mechanism of EM-23 Cross-linking with Elastin Matrix .....	45
Figure 2.12 – Binding of $\alpha$ -lactose to the EBP.....	47
Figure 3.1 – PEG-DA Hydrogel Formation.....	53
Figure 3.2 – Peptide Grafting Efficiencies onto PEG-DA Surfaces.....	61
Figure 3.3 – SMC Adhesion on PEG-peptide Surfaces after 12 hours.....	62
Figure 3.4 – SMC Adhesion on PEG-peptide Surfaces after 48 hours.....	63
Figure 3.5 – SMC Spreading on PEG-peptide Surfaces after 48 hours.....	64

Figure 3.6 – Quantification and Visualization of SMC Adhesion, Viability, and Spreading on Different PEG-peptide Surfaces .....	65
Figure 3.7 – Elastin Deposition over PEG-peptide Surfaces.....	66
Figure 3.8 – Reaction of PEG-SVA with a Peptide Bearing a Free Amine .....	67
Figure 3.9 – Synergistic activity between $\alpha_v\beta_3$ and the EBP in Promoting SMC Adhesion and Elastin Deposition over PEG-DA Surfaces.....	69
Figure 4.1 – Gel Degradation in the Presence of Elastase .....	83
Figure 4.2 – Elastin Content in Different Gel Formulations .....	84
Figure 4.3 – Hydroxyproline Content in Different Gel Formulations .....	85
Figure 4.4 – Compressive Modulus of Different Gel Formulations.....	87
Figure 4.5 – SMC Viability in Different Gel Formulations.....	88
Figure 5.1 – Proposed Mechanism of Controlling Diacrylation of EM-23 .....	99
Figure 5.2 – Bioreactor Design.....	101
Figure A.1 – Characterizing Peptide Conjugation with PEG-SVA at a 1:1 Mole Ratio	104
Figure A.2 – Molecular Weight Distributions of PEG-peptide.....	104
Figure A.3 – Characterizing EM-23 Conjugation with PEG-NHS at a 1:2 Mole Ratio.	105
Figure A.4 – Characterizing EM-23S Conjugation with PEG-NHS at a 1:2 Mole Ratio .....	105
Figure A.5 – Characterizing DS Conjugation with PEG-NHS at a 1:2 Mole Ratio.....	106
Figure A.6 – Characterizing EM-23SR Conjugation with PEG-NHS at a 1:2 Mole Ratio .....	106
Figure A.7 – Characterizing EM-23X Conjugation with PEG-NHS at a 1:2 Mole Ratio .....	107

## LIST OF SYMBOLS AND ABBREVIATIONS

$K_2CO_3$	Potassium Carbonate
mm	Millimeters
ml	Milliliters
mM	Millimolar
mW	Milliwatt
M	Molar
$\mu\text{mol}$	Micromole
2D	Two-dimensional
3D	Three-dimensional
A	Alanine
AAPPTec	Advanced Automated Peptide Protein Tehnologies
ANOVA	Analysis of Variance
BSA	Bovine Serum Albumin
CD	Circular Dichroism
cDNA	Complementary Deoxyribonucleic Acid
DAPI	4',6-Diamidino-2-Phenylindole
DCM	Dichloromethane
DI	Deionized
DMAP	2, 2 Dimethyl-2-Phenyl-Acetophenone
DS	Degradable Sequence
EBP	Elastin Binding Protein
EC	Endothelial Cells

ECM	Extracellular Matrix
EDTA	Ethylenediaminetetraacetic Acid
ELISA	Enzyme Linked Immunosorbent Assay
ELS	Evaporative Light Scattering
EM	Elastin Mimetic
ePTFE	extended Poly(tetrafluoroethylene)
FITC	Fluorescein Isothiocyanate
Fmoc	Fluorenylmethyloxycarbonyl
G	Glycine
GAPDH	Glyceraldehyde-3-Phosphate Dehydrogenase
GPC	Gel Permeation Chromatography
HBS	HEPES Buffered Saline
HBTU	O-Benzotriazole-N,N,N',N'-Tetramethyl-Uronium-Hexafluoro-Phosphate
HCl	Hydrochloric Acid
HEPES	4-(2-Hydroxyethyl)-1-Piperazineethanesulfonic acid
I	Isoleucine
K	Lysine
LOX	Lysyl Oxidase
MMP	Matrix Metalloproteinase
mRNA	Messenger Ribonucleic Acid
MWCO	Molecular Weight Cut Off
NaOH	Sodium Hydroxide
NVP	<i>N</i> -vinylpyrrolidone
OPD	<i>o</i> -Phenylenediamine
P	Proline

PBS	Phosphate Buffered Saline
PCL	Poly(caprolactone)
PDI	Polydispersity Index
PEG	Poly(ethylene glycol)
PEG-DA	Poly(ethylene glycol) Diacrylate
PEG-NHS	Acrylate-PEG-N-Hydroxysuccinimide
PEG-SVA	Acryloyl- PEG-Succinimidyl Valerate
PGA	Poly(glycolic) Acid
PLGA	Poly(lactic-co-glycolic acid)
PU	Poly(urethane)
R	Arginine
RT-PCR	Reverse Transcriptase Polymerase Chain Reaction
S	Serine
SMC	Smooth Muscle Cells
TCPS	Tissue Cultured Polystyrene
TPPS	5,10,15,20-Tetraphenyl-21,23-Porphine Tetra- Sulfonate
UV	Ultraviolet
UV-vis	Ultraviolet-visible
V	Valine
Y	Tyrosine

## SUMMARY

The growing incidences of coronary artery bypass graft surgeries have triggered a need to engineer a viable small diameter blood vessel substitute. An ideal tissue engineered vascular graft should mimic the microenvironment of a native blood vessel, while providing the adequate compliance post-implantation. Current vascular graft technologies lack the ability to promote vascular ECM deposition, leading to a compliance mismatch and ultimately, graft failure. Hence, in order to engineer suitable vascular grafts, this thesis describes the synthesis and characterization of novel elastin mimetic peptides, EM-19 and EM-23, capable of promoting vascular ECM deposition within a poly(ethylene glycol) diacrylate (PEG-DA) hydrogel. By combining the material properties of a synthetic and bio-inspired polymer, a suitable microenvironment for cell growth and ECM deposition can be engineered, leading to improved compliance.

As such, characterization of EM-19 and EM-23 was conducted in human vascular smooth muscle cell (SMC) cultures, and the peptides self-assembled with a growing elastic matrix. After grafting the peptides onto the surface of PEG-DA hydrogels, EM-23 increased SMC adhesion by 6000% over PEG-RGDS hydrogels, which have been the gold standard of cell adhesive PEG scaffolds. Moreover, EM-23 grafted surfaces were able to promote elastin deposition that was comparable to tissue cultured polystyrene (TCPS) surface even though TCPS had roughly 4.5 times more SMCs adhered. Once translated to a 3D model, EM-23 also stimulated increased elastin deposition and improved the mechanical strength of the scaffold over time. Moreover, degradation studies suggested that EM-23 may serve as a template that not only promotes ECM

deposition, but also allows ECM remodeling over time. The characterization studies in this thesis suggest that this peptide is an extremely promising candidate for improving vascular ECM deposition within a synthetic substrate, and that it may be beneficial to incorporate EM-23 within polymeric scaffolds to engineer compliant vascular grafts.

## **Chapter 1**

### **Introduction**

#### **1.1 Summary**

The American Heart Association estimates that the number of coronary artery bypass graft surgeries is expected to increase significantly in the next 5 years [1]. As such, there has been a heightened demand for an implantable blood vessel substitute capable of depositing vascular extracellular matrix (ECM) while providing the appropriate mechanical properties. Synthetic grafts have found long term success as large diameter arterial replacements; however, they fail significantly when implemented as small diameter substitutes. Therefore, this dissertation will describe and characterize the efficacy of elastin mimetic peptides in promoting vascular ECM deposition when incorporated within a biomaterial. The central hypothesis of the work presented in this thesis is that more compliant vascular grafts can be engineered from a combination of synthetic and bio-inspired materials.

#### **1.2 Cardiovascular Diseases**

Cardiovascular related diseases are the number one cause of patient morbidity in the United States, and the number of patients diagnosed with various cardiovascular diseases is expected to increase in the coming years [1]. Atherosclerosis, narrowing of the blood vessels due to plaque buildup, is the most common form of cardiovascular disease [1, 2]. According to the American Heart Association, the majority of patients diagnosed with a form of atherosclerosis have weakened arterial walls that eventually lead to cardiac arrest [1]. Furthermore, as the disease progresses over time, the blood flow

dynamic within the cardiovascular system changes significantly, causing decreased blood flow and greater arterial wall pressures [2-4].

Patients diagnosed with atherosclerosis undergo coronary artery bypass graft surgery, in which blocked arteries with plaque buildup are rerouted with a substitute saphenous vein or internal mammary artery in order to alleviate the arterial pressure and increase blood flow [5-8]. Furthermore, patients undergoing such a surgery frequently require multiple bypasses, and for many patients, multiple bypasses are not possible because the donor supply of arterial substitutes are diseased themselves or are in a state of trauma due to a previous surgery [2-4, 9]. As a result, there is a significant demand for a viable blood vessel substitute having an internal diameter less than 6 mm [10, 11]. To address this demand, this thesis will investigate a novel material derived from synthetic and bio-inspired sources as a potential candidate for a blood vessel substitute. The central hypothesis of this work lies in engineering suitable vascular grafts by combining the advantages of utilizing materials from synthetic and bio-inspired sources.

### **1.3 Anatomy of a Blood Vessel**

A blood vessel is comprised of three different layers: tunica intima, media, and adventitia (Figure 1.1). The innermost layer, tunica intima, comprises of a monolayer of endothelial cells (ECs) that are in direct contact with blood. The ECs inhibit platelet activation and create a non-thrombotic blood contacting surface by secreting small molecules such as nitric oxide [12, 13]. The medial layer, tunica media, is comprised of smooth muscle cells (SMCs), while the outermost layer, tunica adventitia, is primarily comprised of adventitial fibroblasts [4]. Also, an internal elastic lamina is found between

the intimal and medial layers while an external elastic lamina is found between the medial and adventitial layers. Both elastic laminae provide the adequate compliance necessary for a blood vessel to function properly *in vivo*. Compliance is an important property in characterizing the ability of a material to undergo volumetric changes when subjected to large changes in pressure as the heart pumps blood throughout the body [14]. The SMCs in the tunica media secrete elastin and organize themselves in a circumferential orientation providing the necessary compliance for a blood vessel *in vivo* [5, 15, 16].

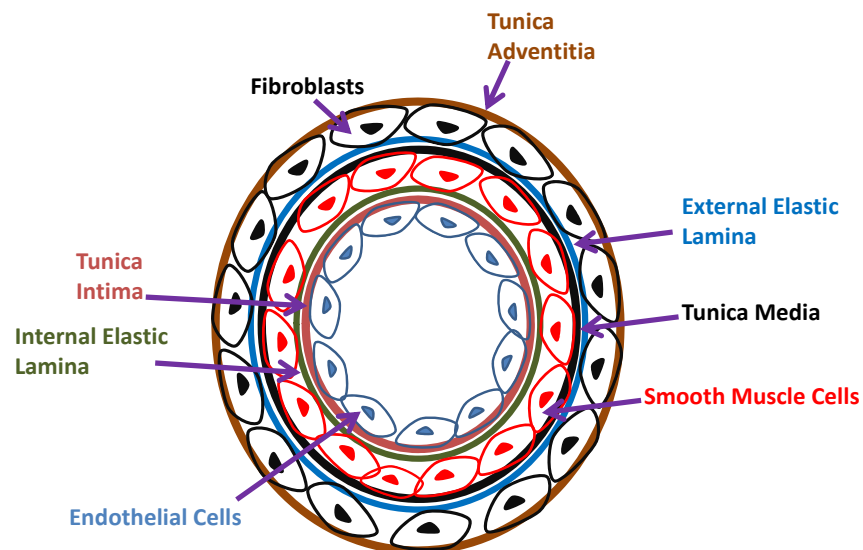


**Figure 1.1.** A blood vessel is comprised of three different layers: tunica intima, media, and adventitia. The intimal layer is in contact with lumen and contains endothelial cells, whereas the medial and adventitial layers contain smooth muscle cells and fibroblasts, respectively. There is an internal elastic lamina between the intimal and medial layer; an external elastic lamina exists between the medial and adventitial layer. Both layers provide adequate elasticity and compliance to a blood vessel.

A significant challenge in vascular graft engineering is the ability to mimic the medial layer of a blood vessel within the synthetic substitute [2, 11]. An ideal biocompatible substitute should not only have a non-thrombotic intimal layer, but also an elastic layer that provides structural compliance while allowing for the development of a functional endothelium [17-19]. Therefore, this thesis investigates a novel material derived from

synthetic and bio-inspired sources that is capable of promoting ECM deposition and may potentially lead to the engineering of more compliant vascular grafts. A poly(ethylene glycol) diacrylate (PEG-DA) hydrogel was chosen as the synthetic polymer for its biocompatible and hydrophilic properties that limit platelet adhesion and thrombosis function. Two different peptides, inspired by elastin, were chosen to help promote vascular ECM deposition within the PEG-DA hydrogels. By combining the strengths of these two materials, a more suitable microenvironment for engineering vascular tissues may be achieved.

#### **1.4 Tissue Engineering of Vascular Grafts**

For the past two decades, the field of tissue engineering has grown considerably and is the most promising alternative for engineering a viable blood vessel substitute. By definition, “the goal of tissue engineering is to repair or replace damaged tissues within the body by providing functional cells and scaffolds to the areas of need” [19]. Tissue engineering combines engineering and life science principles to fabricate viable biological substitutes aimed at repairing or replacing damaged organs or tissues [20-22]. The general approach for tissue engineering lies in seeding autologous cells within a three-dimensional (3D) scaffold *in vitro*, allowing the scaffold to promote ECM deposition *in vivo*, and having the cells completely resorb the 3D scaffold space [4, 5, 23-25].

Indeed the “holy grail” in tissue engineering is the fabrication of a viable vascular graft and in order to be successful, a few design considerations must be implemented [2, 11]. First, an ideal scaffold should be biocompatible and mimic the microenvironment of

a native blood vessel while limiting non-specific protein adsorption, which leads to a reduced inflammatory response post-implantation. The scaffold must also contain proper biochemical cues that allow the encapsulated cells to remodel the scaffold and eventually replace the entire conduit with a natural ECM [26].

Second, the choice of cell types to seed and cell orientation within the scaffold is critically important [27-30]. A native blood vessel is comprised of three different cell types: ECs, SMCs, and fibroblasts [16, 30]. Each cell type has its own distinct function within the blood vessel. For example, ECs line themselves along the lumen, are capable of withstanding greater changes in shear stresses, and provide a non-thrombotic surface. On the other hand, SMCs have a concentric alignment within the medial layer and are responsible for synthesizing the elastin that provides compliance to a blood vessel. Finally, the fibroblasts, found in the outermost layer of a blood vessel, have an axial alignment with the blood vessel and provide structural integrity by secreting vascular collagen [16, 30, 31]. Ideally, an engineered vascular graft should have all three cell types; however, co-culturing these cells within a construct presents a significant challenge.

Further, the mechanical properties of the scaffold should match that of a native blood vessel before implantation. The mechanical strength of a native blood vessel is anisotropic by nature, exhibiting high elasticity at low pressures, yet providing greater stiffness at high pressures [32]. A synthetic polymeric scaffold will allow for better control over the mechanical properties, however, synthetic scaffolds lack the necessary cues to promote a microenvironment mimicking a blood vessel [33]. On the other hand, a

scaffold engineered from naturally occurring polymers such as collagen, although biodegradable, will have compliance that falls short of a native blood vessel [34].

Next, the scaffold must also have easy off-the-shelf availability. A big limitation in engineering vascular grafts is the long processing times required before implantation [30]. For example, Isenburg et al. attempted to engineer ready-to-use vascular grafts in a bioreactor using key ECM components such as elastin. However, the short maturation times yielded grafts that had low mechanical strengths and stability [35]. Regardless of the choice of material or cell type used to fabricate the vascular graft, current technology limits the ability of vascular grafts to have quick off-the-shelf availability. Also, one of the key requirements of an engineered vascular graft is that the final scaffold must be functional as soon as it is implanted [36].

As such, this thesis attempts to address the aforementioned design considerations by engineering scaffolds for vascular grafts using a combination of synthetic (PEG-DA) and bio-inspired (elastin mimetic) materials. By utilizing the strengths of each class of material, scaffolds can be engineered that are not only compliant, but also mimic the microenvironment of a native blood vessel. The rationale behind this work comes from previous studies that have investigated the strengths and weaknesses of different synthetic and natural materials for vascular graft applications.

#### *1.4.1 Synthetic Materials for Engineering Vascular Grafts*

For decades, synthetic vascular grafts engineered from Dacron or extended poly(tetrafluoroethylene) (ePTFE) have found long term success as viable large diameter blood vessel replacements (i.e. >6 mm) [2, 3, 37]. Synthetic materials offer a greater degree of control over intrinsic properties such as molecular weight, porosity, and

mechanical strength [38]. However, these grafts fail significantly when implemented as small diameter replacements due to their inability to provide the necessary cues to support cell adhesion and ECM deposition. Moreover, once implanted, the inability of the synthetic grafts to provide a non-thrombotic surface results in a drastic decrease in graft diameter, leading to, hyperplasia, occlusion and compliance mismatch with native arteries[10, 11, 39-41].

Similarly, poly(glycolic acid) (PGA) is another example of a synthetic material routinely used for engineering vascular grafts. The inherent biocompatibility and biodegradability of PGA makes this polymer highly attractive for engineering vascular grafts [16, 42-47]. However, PGA based scaffolds degrade quickly and secrete acidic byproducts that may have cytotoxic effects over a long period of time. The fast degradation of PGA scaffolds *in vivo* may alter the mechanical properties of the graft too quickly, leading to inadequate burst strengths and compliance [26]. PGA based scaffolds also do not promote ECM deposition over time, a key design criteria for engineering viable blood vessels.

Niklason et al. engineered the first autologous vascular graft made entirely of PGA conditioned in a bioreactor [48]. SMCs were cultured on the PGA scaffold followed by EC seeding on the lumen of the scaffold. The final construct was allowed to mature in physiological flow conditions for 8 weeks after which burst pressures of  $2150 \pm 709$  mm Hg were achieved. In comparison, the burst pressure of saphenous vein is  $1680 \pm 307$  mm Hg. Although promising, the inherent lack of elastin within the scaffold and the long culture time were the major limitations to this system [26].

The first clinical application of a vascular graft engineered from PGA was conducted in 2001 by Shin'oka et al. [49]. Polymeric vascular grafts fabricated from a combination of poly(caprolactone) (PCL) and PGA fused with autologous venous and bone marrow cells were implanted in a 4 year old girl. After a 5 year follow-up study, no complications post-implantation were reported, including no signs of thrombosis and stenosis [25, 50, 51]. However, the use of bone marrow cells within these grafts presents a greater risk of cell differentiation and tumor formation [26]. The grafts were also implanted in low-pressure circulation of 20 mm Hg compared to a high pressure circulation system within the coronary system of 140 mm Hg [11]. Further, long term effects, such as calcification, must also be investigated. Calcification is defined as the deposition of crystalline calcium phosphate that occurs *in vivo*, causing severe deterioration and stiffening, which can lead to graft failure [52].

Alternatively, vascular grafts fabricated from poly(lactic acid) (PLA) have also shown to be promising blood vessel replacements, having slower degradation kinetics than PGA-based scaffolds [26, 53, 54]. The slower degradation of PLA scaffolds allows the final conduit to retain higher mechanical strength over a longer period of time. Kim et al. engineered vascular grafts from a combination for PLA and PGA polymers and conditioned the grafts in a dynamic flow environment [55, 56]. Rat aortic SMCs were seeded within the scaffold under dynamic flow conditions and elastin biosynthesis was quantified, the results showing that the choice of polymer was important in elastin production during the dynamic conditioning of the scaffold. In a different study, Wang et al. electropun PLA/silk fibroin-gelatin composite scaffold and were able to demonstrate burst pressures of  $1596 \pm 20$  mm Hg [57]. However, these grafts lacked elastin

deposition, as PLA-based vascular grafts also lack the ability to promote ECM deposition over time.

Polyurethanes (PUs) are another class of materials routinely used to fabricate small diameter vascular grafts. With its natural elasticity and ease of handling, PU-based vascular grafts have become the current gold-standard for engineering synthetic vascular grafts [10, 33, 58-60]. For example, Jun et al. engineered microporous PU scaffolds with EC adhesive ligands and observed increased endothelialization and decreased platelet aggregation [61]. The scaffolds also showed increased mechanical strength in comparison to microporous PU urea scaffolds without EC adhesive ligands. Further, Rashid et al. modified PU with a fibronectin-like protein and engineered a vascular graft capable of increasing SMC proliferation [62].

Similarly, Ratcliffe et al. successfully engineered a PU based vascular graft under pulsatile flow conditions leading to comparable mechanical strengths to native blood vessels [36]. In a separate study, Grenier et al. pre-coated PU surfaces with fibronectin and observed higher SMCs adhesion and infiltration within the 3D scaffold in comparison to Matrigel-coated PU scaffolds [63]. However, neither condition showed any significant differences in elastin or collagen production. Further, a major drawback and limitation in PU scaffolds is the involvement of toxic precursor, diisocyanates, in the overall synthesis [64].

Although synthetic substitutes offer the advantage of fine-tuning their intrinsic properties, a major disadvantage is the generation of foreign body response over a long period of time [11, 19]. Furthermore, the synthetic materials discussed above are limited as blood vessel substitutes because of their inability to behave as ECM mimics [10, 17,

18, 65, 66]. As an alternative approach, this thesis will investigate the use of PEG-DA hydrogels as the synthetic material for engineering vascular grafts.

Hydrogels are a class of materials that are biocompatible, possess higher water content, are fabricated under mild conditions, and facilitate improved oxygen and essential nutrient transport [67-73]. Although these gels serve as blank slates and lack any biological cues to promote normal cell functions, they can be easily tailored with adhesive peptides that can promote cell attachment, proliferation, and ECM deposition [74]. Hydrogels are an example of 3D systems that are composed of crosslinked networks that behave as ECM mimics and hence, utilizing them as scaffold materials for tissue engineering vascular grafts is highly attractive [75]. Specifically, PEG derivatized hydrogels have shown to be biocompatible, reproducible, and easily allow fine tuning of their mechanical properties [76, 77].

PEG is a well-characterized polymer that is FDA approved for a wide range of biomaterial applications [68, 78-80]. Moreover, PEG hydrogels limit nonspecific protein adsorption while reducing platelet aggregation and thrombosis [81-85]. In addition to being resistant to nonspecific protein adsorption, PEG-DA hydrogels are optically transparent, highly elastic, and their mechanical properties are easily tunable [81]. The intrinsic properties of PEG-DA hydrogels can also be fine-tuned to achieve different elastic responses by varying the molecular weight or polymer concentration in solution [84]. Moreover, hydrogels from diacrylate derivatized PEG (PEG-DA) have shown to be promising models for scaffold materials [82, 84-86]. In the presence of a photoinitiator and UV light, the free acrylate groups on PEG-DA crosslink to form a hydrogel [68, 87, 88]. Also, PEG-DA hydrogels can be tailored with adhesive peptides to drive cell

adhesion for specific cell types [82, 86, 89]. For example, Gobin et al. conjugated the peptide sequence valine-alanine-proline-glycine (VAPG) onto the surface of a PEG-DA hydrogel with a monoacrylate PEG derivative, which facilitated vascular SMC adhesion and spreading [86].

Although PEG-DA is a biocompatible polymer, it is not biodegradable [69, 90]. With protein engineering evolving in the past few years, specific peptide sequences can now provide the cues necessary not only for cell adhesion, proliferation, migration, and matrix deposition, but also for scaffold degradation. The work presented in this thesis discusses different elastin mimetic peptides that can promote vascular ECM deposition within a PEG-DA hydrogel. The elastin mimetic peptides serve as the bioactive moieties intended to increase elastin within the scaffold, whereas the PEG-DA hydrogels serve to provide structural integrity. In comparison, previous studies have also investigated the strengths and weaknesses of vascular grafts engineered from only natural sources such as collagen and these will be discussed in the subsequent section.

#### *1.4.2 Natural Material for Engineering Vascular Grafts*

Many different approaches have been made to engineer vascular grafts from natural polymers. For example, decellularized tissues have gained considerable attention for engineering vascular grafts in which the native ECM is preserved within the final construct [91-95]. Many groups have utilized decellularized small intestinal submucosa as vascular graft constructs, showing high patency rates and feasibility [96-98].

Furthermore, Derham et al. used decellularized porcine aorta as scaffold material for small diameter vascular grafts and observed similar ultimate tensile strength and compliance to native tissues [99]. In another study, decellularized human umbilical

arteries were implanted in rats as small diameter blood replacements [100]. The vascular grafts showed high patency and did not show any signs of thrombosis or stenosis 8 weeks after implantation [101].

However, the source material for decellularized tissues comes from either allogeneic (another animal of the same species) or xenogeneic (an animal of another species) sources. As a result, there lies a great risk of disease transmission and immune response [26]. Furthermore, the harsh conditions used to decellularize tissues could alter the ECM structure, thus making it difficult for large batch preparations [102].

Decellularized tissues show great potential; however, little information is available for their long term stability [19, 33, 101, 103].

On the other hand, previous studies have also investigated engineering vascular grafts from collagen and elastin, the critical ECM components found in a blood vessel [4, 104, 105]. Collagen, for example, gels readily under physiological conditions and has been a primary natural source material for vascular grafts [4, 26, 106, 107]. Weinberg and Bell utilized collagen gels as scaffold materials for vascular grafts; however, the final construct was found to be too weak for use as a blood vessel substitute [108]. The construct also lacked elastin formation, which is critical for graft compliance [19]. This pioneering study, however, led to many different strategies that utilized natural polymers as materials for vascular graft engineering. There have been many attempts to increase the mechanical strength of collagen gels using different strategies such as providing a Dacron support to increase the gel stiffness, glycation to chemically increase collagen stiffness, using degradable meshes as sleeves, and mechanically conditioning the gels [109-116]. Although these techniques have increased the mechanical properties of

collagen, the final constructs still fall short of the required strength for a blood vessel substitute [26]. Furthermore, collagen based vascular grafts also lack the presence of elastin [4, 16].

Elastin is a 70 kDa insoluble protein found in the vascular ECM from which blood vessels derive their high compliance and tensile strengths [117-119]. The protein is an important asset to the overall vascular ECM as it makes up about 50% of its dry weight [104, 105]. Elastin also inhibits dynamic tissue creep and fibrocellular pathology [120, 121]. Finally, elastin is a key factor for promoting SMC proliferation and also helps regulate SMC migration within the medial layer of a blood vessel [122, 123].

Structurally, elastin has alternating hydrophobic and hydrophilic domains [124]. The hydrophobic domain is rich in nonpolar amino acids such as V, P, G, and A. These amino acids are often present as four to six repeating peptides such as GGVP, GVGVP, VGVAPG [125]. The hydrophilic domain, on the other hand, is rich in lysine (K) or alanine. The lysine residues are often interspersed between the alanine residues, playing a significant role in the crosslinking of tropoelastin, a 72 kDa elastin precursor, to form insoluble elastic fibers [126]. Moreover, peptide sequences such as VAPG and VGVAPG have been specifically shown to have chemotactic activity against monocytes, fibroblasts, and tumor cells [127-130]. The hexapeptide sequence VGVAPG interacts with SMCs via the cell surface-bound receptor called the elastin binding protein (EBP), leading to different chemotactic responses from cells such as vasorelaxation and platelet anti-aggregation [127, 130-132]. Elastic fibers have a half-life of 70 years and elastin is one of the most stable proteins found in the vascular ECM [133].

Elastin is a critical component of a blood vessel and many researchers have focused on improving elastin biosynthesis within biomaterials by incorporating various growth factors, providing a mechanical stimuli, or engineering scaffolds from a combination of soluble elastin and collagen [112, 116, 120, 134-137]. Although promising, many elastin mimetic grafts lead to calcification post-implantation [138-141]. As a result, there has been a greater push to engineer elastin-like proteins capable of promoting elastin deposition within a synthetic scaffold [142-145]. For example, Martin et al. chemically crosslinked elastin-like polymers to engineer macroporous 3D constructs for tissue engineering applications and found favorable EC cell adhesion [146]. The study concluded that by controlling the porosity of the construct, more robust scaffolds can be engineered.

Moreover, recombinant elastin block copolymers have also gained considerable attention in engineering 3D constructs that have properties comparable to native elastin [147]. For example, Nagapudi et al. engineered elastin-like polypeptides using recombinant techniques and found similar viscoelastic behavior to native elastin [148]. However, the techniques described above are limited by their long processing times and the high costs associated in engineering the construct. As such, this dissertation describes the synthesis and characterization of novel elastin mimetic peptides capable of promoting vascular ECM deposition within a synthetic scaffold. The use of these peptides provides the advantage of having lower processing times and associated costs.

## 1.5 Synthetic and Natural Polymers for Engineering Vascular Grafts

The different strategies discussed so far lack the ability to promote elastin production within a synthetic or natural material which leads to a compliance mismatch with the native blood vessels post-implantation. As such, to engineer compliant vascular grafts, different elastin mimetic peptides capable of promoting elastin deposition within a PEG-DA hydrogel were investigated in this thesis. The peptides were engineered based on the native structure of elastin as well as its ability to interact with the cells to induce more elastin production.

*In vivo*, elastin is first secreted as tropoelastin by SMCs into the extracellular space. An important property of tropoelastin is the ability to self-assemble under physiological conditions, leading to the proper alignment of elastic fibers post crosslinking [149]. This self-assembly is primarily induced due to the presence of hydrophobic sequences on tropoelastin [150]. Tropoelastin is primarily synthesized in the rough endoplasmic reticulum of SMCs and undergoes posttranslational modification once secreted into the ECM [125]. Intracellularly, tropoelastin first binds to the EBP [149]. Once released from the cell surface, lysine residues on tropoelastin undergo spontaneous oxidative deamination under the presence of lysyl oxidase (LOX), a 50 kDa active enzyme also secreted by SMCs, resulting in tropoelastin aggregates [151, 152]. Four lysine groups from two tropoelastin molecules condense to form desmosine or isodesmosine (Fig. 1.2) [126, 153, 154].

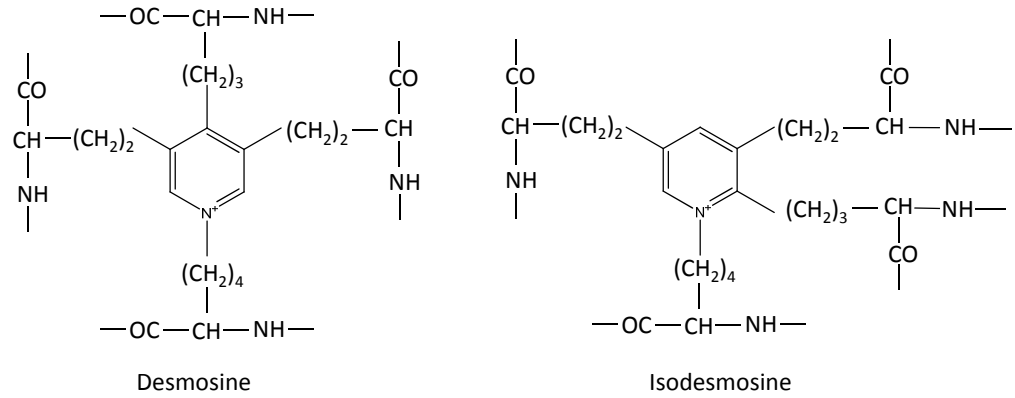


**Figure 1.2.** Structure of desmosine and isodesmosine [126].

The EBP then chaperones the tropoelastin aggregate to adjacent microfibrils in the extracellular space, where the complex binds to galactosugars, causing a simultaneous release of the aggregates from the EBP [126, 149]. Once released, LOX further crosslinks the tropoelastin aggregates to form mature elastin fibers (Figure 1.3). Moreover, recent studies have suggested that tropoelastin may interact with the cell surface-bound integrin  $\alpha_v\beta_3$ , and that this integrin may assist the EBP in elastogenesis [122, 155-158]. Previous studies also have utilized desmosine as an effective marker of to quantify the extent of elastin crosslinking, as 0.9% of total elastin content is comprised of desmosine [159, 160].

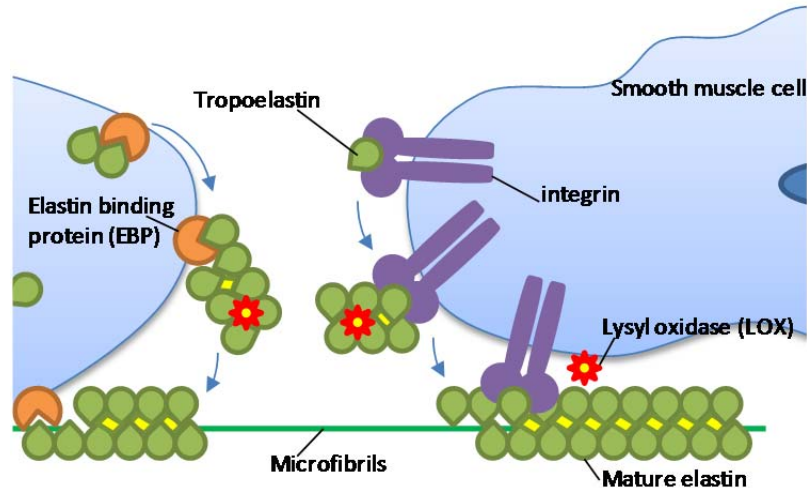


**Figure 1.3.** Elastin production involves a sequence of events involving the secretion of tropoelastin, which binds EBP on cell surfaces. Tropoelastin aggregates are then transported to adjacent microfibrils involved in elastin fiber assembly, and the EBP is recycled. The  $\alpha_v\beta_3$  integrin also binds the C-terminal region of tropoelastin, playing a yet unknown role in the synthesis of mature elastin.

However, a major drawback of elastin is that the protein is very hydrophobic and practically insoluble in aqueous media [161]. Post crosslinking, 75% of elastin is hydrophobic [126]. Furthermore, tropoelastin is hard to isolate due to its spontaneous reactivity to form elastin fibers [126, 162]. It is only after crosslinking that elastin achieves high elasticity, stability, tensile strength, and provides cellular cues for adhesion and proliferation. Incorporating elastin within a biomaterial for vascular graft applications has yielded poor results due to calcification post-implantation [138-141]. Nimni et al. hypothesized that improper fiber alignment of elastin and uncontrolled crosslinking of collagen and elastin within the scaffold could be possible reasons for calcification in constructs implanted *in vivo* [139].

In this work, two different peptides were engineered to serve as elastin mimetics capable of self-assembling with cell-deposited ECM *in vitro*. Once incorporated within a PEG-DA hydrogel, the peptides will serve as templates for promoting vascular ECM deposition, leading to scaffold materials with enhanced biochemical cues and mechanical

properties. The elastin mimetic peptides investigated in this thesis contain the cell adhesion and crosslinking motifs found in native elastin, including a hydrophobic and hydrophilic domain. The central hypothesis is that the incorporation of an elastin mimetic peptide within a 3D scaffold can lead to cell adhesion and elastin crosslinking motifs serving as a template to facilitate an increase in elastin deposition within the scaffold. With increased elastin content, the final scaffold will have an appropriate ECM similar to that of a native blood vessel, leading to a suitable material for engineering compliant vascular grafts.

## <sup>1</sup>Chapter 2

### **Design and Characterization of Elastin Mimetic Peptide Sequences as Potential Templates for Vascular ECM Deposition**

#### **2.1 Summary**

Two different elastin mimetic peptides, EM-19 and EM-23, were engineered to serve as templates for self-assembling with cell-deposited elastin matrix. Both peptides contain the hexapeptide sequence VGVAPG that binds the surface bound EBP receptor and a crosslinking domain, resulting in a sequence that closely mimics the active motifs of tropoelastin. EM-23 also contains an RGDS domain, which has an affinity for cell surface integrins. Preliminary characterization indicated that both peptides have a disordered structure similar to soluble elastin and are able to self-assemble with a growing elastin matrix on a two-dimensional (2D) TCPS surface. The characterization studies also suggested that EM-23 has a higher affinity for integrins than for the EBP, suggesting the possibility that integrins play a significant role in elastin fiber assembly. To further clarify which integrins play a role in elastogenesis, total elastin content was quantified while blocking the activity of specific integrins. The results suggested that the integrin  $\alpha_v\beta_3$  plays a significant, yet unknown, role in elastogenesis.

---

<sup>1</sup> *Work discussed in this Chapter is adapted from:*  
D Patel, R Menon, LJ Taite. "Self-assembly of elastin-based peptides into the ECM: the importance of integrin  $\alpha_v\beta_3$  and the elastin binding protein in elastic fiber assembly." *Biomacromolecules* (2011), 12(2), 432-440.

## 2.2 Introduction

The formation of a suitable ECM within a biomaterial still remains a significant challenge in the field of tissue engineering [73]. The ECM contains important growth factors and enzymes that help regulate cell migration, differentiation, and proliferation throughout the tissue [163]. Moreover, the ECM is comprised of several cell secreted proteins that serve as communication bridges between cells and the extracellular environment. A blood vessel, for example, is comprised of three different layers and each layer contains a unique ECM that provides compliance and structural integrity to the tissue. For example, the tunica intima of a blood vessel contains connective and anchoring filaments of fibrin-containing microfibrils and collagen [15, 164-166]. Tunica media contains a significant amount of elastin providing adequate compliance whereas tunica adventitia is rich in collagen and provides structural integrity to the blood vessel [15, 167-170]. Further, elastin accounts for approximately 50% of the dry ECM weight, and promotes SMC proliferation and migration throughout the intimal layer [104, 122, 123, 133, 171-174].

Elastin interacts with SMCs via a surface-bound receptor called the EBP [175]. The EBP forms a complex with intrinsic membrane proteins sialidase and carboxypeptidase A, and has high affinity for the hexapeptide sequence VGVAPG [130, 176]. The binding of this sequence to the EBP has been shown to influence chemotaxis, vasorelaxation, and inhibit platelet aggregation [127, 172, 177]. Synthesis of elastin is a multi-step process in which tropoelastin is first secreted by SMCs and binds to the EBP [178]. Lysine residues on tropoelastin undergo oxidative deamination in the presence of LOX, forming tropoelastin aggregates. The EBP chaperones the aggregates to adjacent

microfibrils in the extracellular space, where it is proposed to interact with galactosugars on the microfibrils [136, 178-180]. After interacting with galactosugars, the EBP releases the aggregates for further crosslinking to form mature elastin fibers, while forming desmosine or isodesmosine at the crosslink sites [125, 126, 151, 152, 181, 182]. After crosslinking, the EBP is recycled via internalization and can bind with newly synthesized tropoelastin to facilitate further elastin fiber assembly [183]. Although this model has long been accepted as the basis for elastin production, recent evidence has also pointed to integrins playing an active role in elastin fiber assembly. Specifically, the integrin  $\alpha_v\beta_3$  has been shown to interact with the C-terminal GRKRK motif of tropoelastin, alluding to the likelihood of this integrin somehow assisting the EBP in elastogenesis [155].

It is only after crosslinking that elastin achieves such high elasticity, stability, and tensile strength [8, 36, 133, 161, 184]. Moreover, the hydrophobicity of elastin makes it difficult to implement elastin as a biomaterial and as a result, many alternative approaches have been to engineer elastin-like proteins for vascular applications [8, 112, 126, 139, 185-189]. For example, Nagpudi et al. utilized recombinant engineering to synthesize large elastin block copolymers that mimic native elastin [148]. The copolymers demonstrated a viscoelastic behavior similar to native elastin. In a separate study, Lee et al. also utilized recombinant DNA techniques to engineer elastin-like polypeptides capable of mimicking the active domains of elastin [186]. However, engineering protein expression can be costly, arduous, and require high processing times.

This thesis describes the design and synthesis of two different hydrophilic elastin mimetic peptides, EM-19 (AAKAAKVGVAPGAAKAAKK) and EM-23 (AAKAAKVGVAPGRGDSAAKAAKK), that were engineered for use as potential

templates for promoting vascular ECM deposition. Both peptides contain an EBP binding motif and a crosslinking domain that are native to tropoelastin. Furthermore, EM-23 contains an additional integrin-binding domain, and may provide further insight to the role integrins play in elastin fiber assembly [190-193]. This chapter discusses the preliminary characterization of these peptides and investigates the potential role that each peptide may play in elastogenesis.

## **2.3 Materials and Methods**

### *2.3.1 Circular Dichroism Studies*

Circular dichroism (CD) measurements were conducted on EM-19 and EM-23 to characterize the inherent structure of each peptide and compared to soluble human elastin. The measurements were performed by Alliance Protein Laboratories (Camarillo, CA). Peptides were dissolved in water at 0.2 mg/ml and CD measurements were carried out on a Jasco J-715 spectropolarimeter using a 0.1 cm cell at room temperature and 37°C. The temperature was controlled by a PTC-348WI temperature controller and Peltier cell holder. The solvent spectrum was subtracted from the sample spectra and converted to the mean residue ellipticity (CD intensity per amino acid).

### *2.3.2 Peptide Synthesis*

All materials and reagents for peptide synthesis were purchased from Advanced Automated Peptide Protein Technologies (AAPPTec; Louisville, KY). Six different peptides were synthesized using standard O-Benzotriazole-N,N,N',N'-tetramethyluronium-hexafluoro-phosphate (HBTU) coupling and fluorenylmethyloxycarbonyl (Fmoc) protection chemistry on an Apex 396 peptide synthesizer (AAPPTec, Louisville, KY). A 23 amino acid sequence (EM-23; AAKAAKVGVAPGRGDSAAKAAKK),

containing two cell adhesion motifs (VGVAPG and RGDS) as well as lysine rich crosslinking domains, was synthesized along with a 23 amino acid control peptide in which the VAPG sequence is scrambled and the RGDS sequence is left intact (EM-23S; AAKAAKVGVPAGRGDSAAKAAKK). A 19 amino acid sequence (EM-19; AAKAAKVGVAPGAAKAAKK) and a 19 amino acid peptide in which the VAPG sequence is scrambled (EM-19S; AAKAAKVGVPAGAAKAAKK) were synthesized, omitting the RGDS motif completely in order to observe the importance of integrin binding. Both 23 and 19 amino acid sequences containing glycine residues in place of lysine were used to observe the importance of the hydrophilic crosslinking domain (EM-23G; AAGAAGVGVAPGRGDSAAGAAGG; EM-19G, AAGAAGVGVAPGAAGAAGG). Peptides were dialyzed using cellulose ester membrane tubing (MWCO 1000; Spectrum laboratories, Rancho Dominguez, CA). The dialyzed peptides were then frozen and lyophilized overnight. Peptides were characterized using mass spectrometry. RGDS was purchased (American Peptide Company, Sunnyvale, CA) and used as received.

### *2.3.3 Cell Culture and Maintenance*

Human aortic smooth muscle cells (SMCs, passages 3-5; Invitrogen Inc., Carlsbad, CA), were used in this work. SMCs were maintained in Medium 231 (Invitrogen Inc., Carlsbad, CA) supplemented with smooth muscle cell growth supplement (SMGS, Invitrogen Inc., Carlsbad, CA), 2 mM L-glutamine, 1 unit/ml penicillin, and 100 mg/l streptomycin (GPS; Cellgro, Manassas, VA) at 37°C in a 5% CO<sub>2</sub> environment.

#### 2.3.4 Peptide Influence on Elastin and Desmosine Formation

Elastin production and desmosine content were characterized *in vitro* after a 48 hour incubation of each peptide with SMCs. The 48 hour incubation period was chosen after initial experiments confirmed that the protein concentration following incubation with elastin mimetic peptides was well within the range of the commercially available assay used to quantify elastin. A stock solution of 5  $\mu\text{mol/ml}$  of each peptide was made by dissolving in 10 mM HEPES buffered saline (HBS) at pH 7.4. The solution was then sterile-filtered using 0.2  $\mu\text{m}$  pore size nylon filters (Pall Life Sciences, Port Washington, NY). A 24-well plate was seeded with 30,000 SMCs/cm<sup>2</sup>. Peptides were added to the cell suspensions during the seeding procedure at concentrations of 0.01, 0.1, or 1  $\mu\text{mol/ml}$ . Peptides were directly seeded with the SMCs to investigate the efficacy of the peptides to self-assemble with the growing elastin matrix. Moreover, the integrins on the cell surface are utilized as cell adhesion motifs. In order to assess the role integrins play on elastin fiber assembly, it was important to seed the cells simultaneously with the peptides so that each peptide was able to fully interact with integrins before the cells fully adhered onto the TCPS surface.

After 48 hours, the media was removed, the wells were thoroughly washed with phosphate buffered saline (PBS), and the well plates were frozen and lyophilized overnight. The contents of each well were hydrolyzed by adding 0.1 N NaOH and incubated for 1 hour at 100°C. The resulting lysate was centrifuged at 8,000 $\times$ g for 10 mins and the supernatant containing the cell debris and soluble matrix components was removed. The remaining insoluble elastin was suspended in 0.25 N oxalic acid and further hydrolyzed for 48 hours at 100°C. Following the oxalic acid treatment, the

solubilized elastin was purified using Amicon Ultra-0.5 Centrifugal Filters with Ultracel-10 membranes (MWCO 10,000; Millipore, Billerica, MA). A Fastin assay (Accurate Chemical, Westbury, NY) and an enzyme-linked immunosorbent assay (ELISA) were used to quantify elastin and desmosine content, respectively.

### *2.3.5 Peptide Competition with $\alpha$ -Lactose & RGDS*

To elucidate the role integrins play in elastin fiber assembly, studies were conducted in which the EBP or integrins were subjected to competitive binding with EM-19 and EM-23 using  $\alpha$ -lactose or soluble RGDS, respectively. The galactosugar  $\alpha$ -lactose also binds the EBP [175]. However, once  $\alpha$ -lactose binds the EBP, it changes the structural confirmation of the EBP, causing it to be shed from the cell surface [194]. This phenomenon results in less elastin fiber production [195]. Soluble RGDS was used as another competitive control for integrin binding with EM-23. With its high affinity for various integrins, adding RGDS to SMC cultures and quantifying elastin production with or without the elastin mimetic peptides was done to shed more insight on the role integrins play in elastogenesis.

In separate experiments, 30,000 SMCs/cm<sup>2</sup> were incubated with elastin mimetic peptides as well as 10 mM  $\alpha$ -lactose or 1 mM RGDS solution (sterile-filtered using 0.2  $\mu$ m pore size nylon filters; Pall Life Sciences, Port Washington, NY). The elastin mimetic peptides were again added to cell suspensions during the seeding procedure at concentrations of 0.01, 0.1, or 1  $\mu$ mol/ml, this time also in the presence of either  $\alpha$ -lactose or RGDS. After a 48 hour incubation period, cell cultures were washed and the elastin and desmosine isolated as previously described.

### *2.3.6 Fastin Assay for Assessment of Elastin Production*

A Fastin assay was used to quantify elastin deposition after sample hydrolysis. In brief, samples and  $\alpha$ -elastin standards in oxalic acid were treated with an equal volume of elastin precipitation reagent containing trichloroacetic acid and hydrochloric acid (HCl) for 10 mins. Following precipitation of elastin, the mixture was centrifuged at  $10,000\times g$  for 10 mins and the supernatant was discarded. The recovered sample was incubated with 1.0 ml of Fastin dye reagent, containing 5,10,15,20-tetraphenyl-21,23-porphine tetra-sulfonate (TPPS), for 90 mins. TPPS has an affinity for the basic amino acid side chains of elastin. The elastin-dye complex was then separated via centrifugation at  $10,000\times g$  for 10 mins. The supernatant was again discarded, and the dye-elastin complex was dissociated by adding 250  $\mu$ l of dye dissociation reagent, containing guanidine HCl and propan-1-ol. The final dye extract was placed in a 96-well plate and absorbance was read using a Beckman DTX 880 Multimode Plate Reader (Beckman Coulter, Brea, CA) at 513 nm. Concentrations of elastin were calculated by comparison with  $\alpha$ -elastin standards.

### *2.3.7 Desmosine ELISA*

A competitive ELISA was used to quantify desmosine content. First, an ovalbumin-desmosine conjugate (a gift from Dr. Barry Starcher of the University of Texas Health Science Center at Tyler) in 50 mM sodium bicarbonate buffer (pH 8.5) was adsorbed to the wells of a 96-well plate for 1 hour at room temperature. After 1 hour, the wells were washed three times with washing buffer composed of 10 mM PBS with 0.05% Tween 20. The wells were blocked by adding 1% bovine serum albumin (BSA; Sigma, St. Louis, MO) in 10mM PBS for 30 mins at room temperature, then washed three times

with washing buffer. A primary desmosine antibody (Elastin Products Company, EPC, Owensville, MO) in 1% BSA solution (1:1000 dilution) along with either samples or standards was added and allowed to interact for 1 hour at room temperature. After primary antibody interaction, the wells were washed three times with washing buffer. A secondary ant-rabbit IgG conjugated with horseradish peroxidase (1:3500 dilution; Promega, Madison, WI) was then added to each well and incubated for 1 hour at room temperature. The wells were again washed three times and incubated with *o*-phenylenediamine (OPD; Sigma, St. Louis, MO) for 30 mins at room temperature in the dark. The final reaction was quenched by adding 3 M HCl to each well and the absorbance of each sample was read using a Beckman DTX 880 Multimode Plate Reader at 492 nm.

### *2.3.8 Immunofluorescence Staining*

Immunofluorescence staining experiments were conducted to visualize peptide colocalization with the elastin matrix. EM-23, EM-23S, EM-19 and EM-19S were each conjugated to fluorescein isothiocyanate (FITC). 10 mg of each peptide was dissolved in 5 ml deionized water, and FITC (1:1 amine mole ratio) was dissolved in 4 ml 0.1 M sodium bicarbonate buffer (pH 8.5). The dye solution was added to the peptide solution dropwise and allowed to react for 2 hours. After 2 hours, any unreacted dye and peptide were dialyzed using 2000 MWCO dialysis cassettes (Pierce Biotechnology, Rockford, IL) for 2 hours. The dialyzed product was frozen and lyophilized overnight. The conjugated peptide-dye moiety was dissolved in 10 mM HEPES buffer (pH 7.4) such that the final concentration in one 24-well plate would be 1  $\mu$ mol peptide/ml. The solution was sterilized using 0.2  $\mu$ m pore size nylon filters (Pall Life Sciences, Port Washington,

NY). The sterile solution was added to each well plate containing 80,000 SMCs/cm<sup>2</sup> and incubated for 48 hours.

Immunostaining techniques were then utilized to visualize elastin fibers. In brief, each well was washed with 10 mM PBS, and the cells were fixed with 100% methanol for 5 mins. Wells were again washed with 10 mM PBS and a primary elastin antibody (BA-4, Santa Cruz Biotechnology (SCBT), Santa Cruz, CA) at a 1:100 dilution in 10 mM PBS was incubated with cell cultures for 2 hours at room temperature. The wells were washed with 10 mM PBS and incubated with a secondary goat anti-mouse IgG conjugated with Texas Red (SCBT, Santa Cruz, CA) at a 1:400 dilution for 1 hour at room temperature. Elastin fibers, along with peptide-dye moieties, were visualized simultaneously in each well using a Leica DMI 4000B fluorescent microscope (Leica Microsystems, Inc.; Bannockburn, IL).

### *2.3.9 Quantification of Tropoelastin and LOX mRNA Levels*

Quantitative two-step reverse transcriptase polymerase chain reaction (RT-PCR) was conducted after 48 hours of cell culture to elucidate the impact on tropoelastin and LOX mRNA levels by soluble EM-19 and EM-23. Briefly, 1 μmol of EM-19 or EM-23 was first sterile filtered using 0.2 μm pore size nylon filters (Pall Life Sciences, New Port Washington, KY), mixed with media, and simultaneously seeded with SMCs at a density of 30,000 cells/cm<sup>2</sup>. Samples without any peptides were used as positive controls. After 48 hours, the media was aspirated and samples were thoroughly washed with PBS. Cells were then detached through incubation with 0.21% trypsin containing 0.25% ethylenediaminetetraacetic acid (EDTA; Cellgro, Manassas, VA) at 37°C for 4 mins, and resuspended such that each sample contained the same number of cells. Total RNA was

extracted using the Aurum Total RNA Mini Kit (Bio-Rad, Hercules, CA) and RNA quality and concentration were determined by taking the ratio of absorbances at 260 and 280 nm. Complimentary DNA (cDNA) sequences were prepared using the iScript cDNA Synthesis Kit (Bio-Rad, Hercules, CA), utilizing a blend of oligo(dT) and random hexamer primers. cDNA was then subjected to PCR amplification using SSoAdvanced SYBR Green Supermix (Bio-Rad, Hercules, CA) for tropoelastin, LOX and glyceraldehyde-3-phosphate dehydrogenase (GAPDH), which served as an internal control, on an Applied Biosystems StepOne Plus instrument (Applied Biosystems, Carlsbad, CA). Primers used were (forward) 5'-GCTGACGCTGCTGCAGCCTA-3' and (reverse compliment) 5'-CAGCAAAGCTCCACCTACA-3' for tropoelastin and (forward) 5'-GCAGATGTCAGAGATTATGATCA-3' and (reverse compliment) 5'-ATCGCCTGTGGTAGCCATAGT-3' for LOX. Amplification included 40 cycles of denaturation (95°C, 10 s) and annealing/extension (60°C, 30 s). Fluorescence generated during amplification was used to quantify mRNA levels from SMCs over the different conditions.

#### *2.3.10 Blockage of Integrins*

To investigate the importance of specific integrins in elastic fiber assembly, SMCs were first blocked with either anti- $\alpha_v\beta_3$  or anti- $\alpha_5\beta_1$  antibodies and elastin content was quantified after 48 hours in presence or absence of the elastin mimetic peptides. Cells were first allowed to adhere in the wells of a 24-well TCPS plate at a cell density of 30,000 SMCs/cm<sup>2</sup> for 4 hours after which the media was removed and replenished with media doped with either anti- $\alpha_v\beta_3$  (1:1000 dilution, Abcam, Cambridge, MA) or anti- $\alpha_5\beta_1$  (1:1000 dilution, Abcam, Cambridge, MA). Previous work has confirmed that the

integrin  $\alpha_5\beta_1$  interacts with the fibronectin derived sequence RGD, as does  $\alpha_v\beta_3$  [Charo 1990]. Additionally, Bax et al. have shown that the C-terminus of tropoelastin does not interact with  $\alpha_5\beta_1$  and hence this integrin was used as an appropriate comparison to demonstrate the importance of interactions between RGDS and  $\alpha_v\beta_3$  in the mechanism of elastin maturation [155]. Antibodies were incubated with cell cultures for 2 hours, after which the media was removed, wells were washed with 10 mM PBS, and replenished with fresh media. EM-23 and EM-19 (1  $\mu\text{mol/ml}$  in 10 mM HEPES buffer; pH 7.4) were sterile filtered using 0.2  $\mu\text{m}$  pore size nylon filters (Pall Life Sciences, New Port Washington, KY), added to the media, and incubated with cells for 48 hours. The media was then removed, the wells rinsed with PBS, and the well plates were frozen and lyophilized. The contents of each well were hydrolyzed by adding 0.1 N NaOH for 1 hour at 100°C. The resulting lysate was centrifuged at 8,000 $\times g$  for 10 mins and the supernatant containing the cell debris and soluble matrix components was removed. The remaining insoluble elastin was resuspended in 0.25 N oxalic acid and further hydrolyzed for 48 hours at 100°C. Following the oxalic acid treatment, the solubilized elastin was purified using Amicon Ultra-0.5 Centrifugal Filters with Ultracel-10 membranes (MWCO 10,000; Millipore, Billerica, MA). A Fastin assay (Accurate Chemical, Westbury, NY) and an ELISA were used to quantify elastin and desmosine, respectively. Well plates treated only with antibodies served as controls. Separate experiments were conducted to quantify elastin production on TCPS surfaces after 48 hours without any addition of antibodies or media exchange. The data showed that elastin production from this sample set was comparable to elastin production on TCPS surfaces with media exchanged after 4 hours, indicative of minimal cell loss during the media exchange and

no significant changes in cell viability in the presence of the antibodies used in these studies. An isotype control (mouse monoclonal IgG1, Abcam, Cambridge, MA), which was produced against a synthetic hapten not normally present in humans or animals, was also tested in the antibody experiments.

#### *2.3.11 Statistical Analysis*

All experiments were performed minimally in triplicate. Error bars indicate standard deviation, and statistical analysis was performed using a single factor ANOVA;  $p$ -values  $< 0.05$  were considered to be significant.

## **2.4 Results**

### *2.4.1 Circular Dichroism Studies*

CD studies were conducted on EM-19 and EM-23 to characterize the inherent structure and peptide folding in solution (Figure 2.1). Both CD spectra for EM-19 and EM-23 at room temperature and 37°C show a large negative band at 197 nm, indicating a disordered structure like the random coil of native human elastin. The addition of the RGDS domain in EM-23 decreases the intensity of the negative peak, and, at physiological temperature, small yet significant changes were observed between each spectra, indicating a structural transformation with respect to temperature. The CD spectra show that each peptide has the disordered orientation found in soluble elastin and that the peptides behave as elastin mimetics in solution. Furthermore, the CD spectrum of soluble human  $\kappa$ -elastin includes a shoulder at 220 nm, which may be indicative of  $\alpha$ -helical structures and are typical features of noncoacervated solutions of soluble elastin. However, this shoulder was absent from the CD spectra of EM-19 and EM-23.

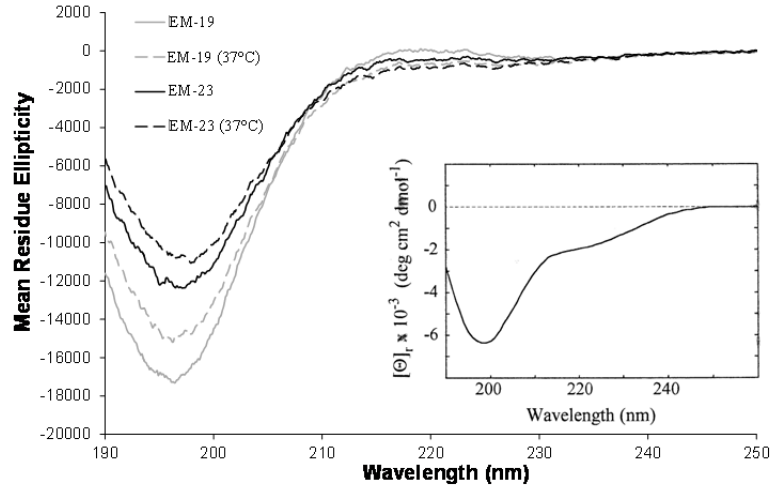


**Figure 2.1.** CD Spectra of EM-19 and EM-23, showing a significant amount of disorder as indicated by the larger negative peak at 190 nm, which is characteristic of random coil structure of human elastin. The inset figure depicts the CD spectra for soluble human  $\kappa$ -elastin [196].

#### 2.4.2 Peptide Influence on Elastin and Desmosine Production

Elastin and desmosine content were quantified in the presence of the elastin mimetic peptides, and their respective controls, by a Fastin assay and a competitive ELISA after 48 hours (Figure 2.2). In the presence of EM-19, elastin production was reduced to  $33 \pm 12\%$ ,  $32 \pm 8\%$ , and  $41 \pm 6\%$  of the TCPS control at 0.01, 0.1, and 1  $\mu\text{mol}$ , respectively (Figure 2.2A). This result suggests that the peptide competes with tropoelastin to bind the EBP. The shorter peptide sequences replace the heavier tropoelastin segments in the maturing elastin fibers, leading to a reduced mass in elastin detected. A similar phenomenon was observed with EM-19S; elastin production was reduced to  $41 \pm 7\%$ ,  $27 \pm 10\%$ , and  $35 \pm 10\%$  of the TCPS control at 0.01, 0.1, and 1  $\mu\text{mol}$ , respectively, even though no binding domains are present in this peptide (Figure 2.2B). This result is likely due to the lysine-rich domains present in EM-19S that are still capable of crosslinking with mature elastin. The desmosine production in the presence of either peptide remained unchanged, indicating the crosslinking activity remained unchanged (Figure 2.2B).

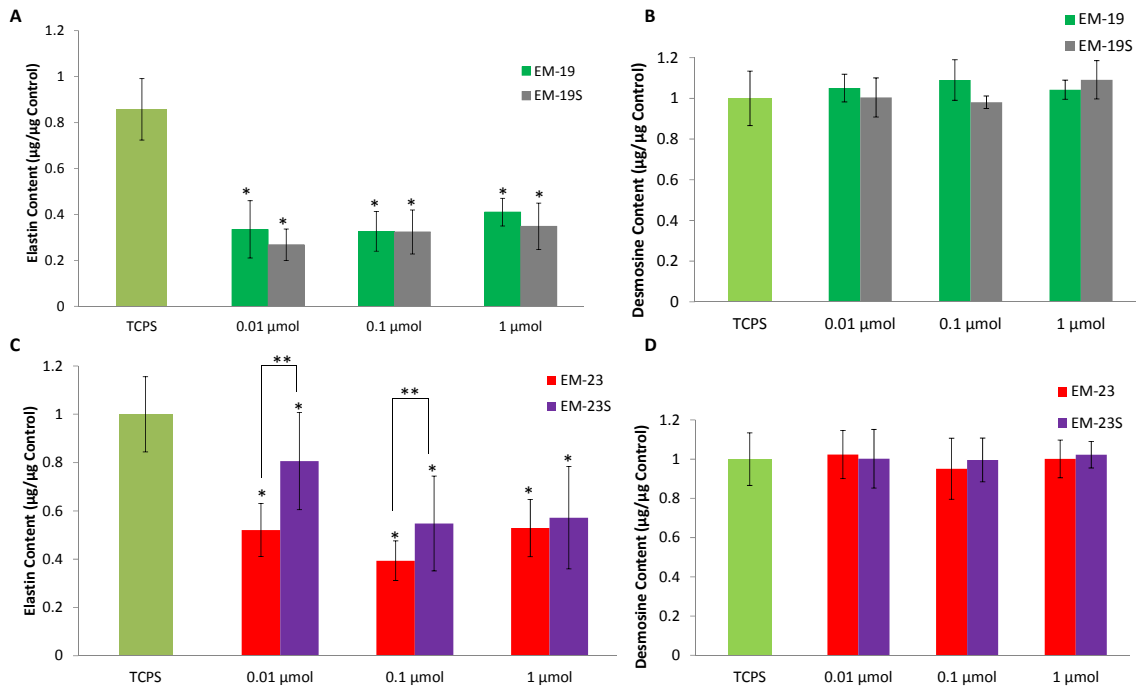


**Figure 2.2.** Elastin and desmosine content in the presence of EM-19, EM-19S, EM-23, and EM-23S. A) EM-19 and EM-19S stimulate decreases in elastin production with increasing peptide concentration. Though only EM-19 can bind to the EBP, both peptides are capable of being crosslinked into the elastin matrix, thus the total mass of tropoelastin being crosslinked is decreased. B) Both EM-19 peptides cause only small fluctuation in desmosine production, indicating that LOX activity is not significantly changed. C) The addition of EM-23 in SMC cultures leads to reduced levels of elastin at lower concentrations, followed by recovery at the highest concentration indicating an added effect of the RGDS domain. D) EM-23 and EM-23S also stimulate only small changes in desmosine production compared to controls ( $n = 7$ ;  $*p < 0.05$  compared to TCPS;  $**p < 0.005$  compared to scrambled sequences; the data taken for elastin deposition for EM-23 at 0.01  $\mu\text{mol}$  and 1  $\mu\text{mol}$  are not significantly different, whereas both conditions are significantly different from 0.1  $\mu\text{mol}$  with  $p < 0.02$ ).

A similar trend is observed with EM-23; elastin production is reduced to  $52 \pm 11\%$  and  $39 \pm 8\%$  of the control at 0.01  $\mu\text{mol}$  and 0.1  $\mu\text{mol}$ , respectively (Figure 2.2C). However, at 1  $\mu\text{mol}$ , elastin deposition is reduced only to  $53 \pm 12\%$  of the TCPS control and recovers to the same amount of the lowest EM-23 concentration. This data suggests that, at higher EM-23 concentrations, the peptide preferentially binds integrins over the EBP and the higher amount of elastin detected is likely due to EM-23 chaperoned via integrins in concert with EBP-bound tropoelastin for crosslinking. The control peptide, EM-23S, undergoes a trend similar to that of EM-23, in which elastin deposition is first reduced to  $81 \pm 20\%$  and  $55 \pm 20\%$  of the TCPS control at 0.01  $\mu\text{mol}$  and 0.1  $\mu\text{mol}$ ,

respectively, but slightly recovers to  $58 \pm 21\%$  at  $1 \mu\text{mol}$  (Figure 2.2C). This data suggests that integrins play a synergistic role with the EBP in elastogenesis. The desmosine crosslinking remained unchanged throughout all the concentrations suggesting LOX activity was unchanged in the presence of EM-23 or EM-23S (Figure 2.2D). As crosslinking controls, desmosine content was quantified after 48 hours in the presence of peptides in which lysine was substituted with glycine (EM-19G and EM-23G; Figure 2.3). The desmosine content remained mostly unchanged throughout all peptide concentrations, indicating that LOX activity remained unperturbed.

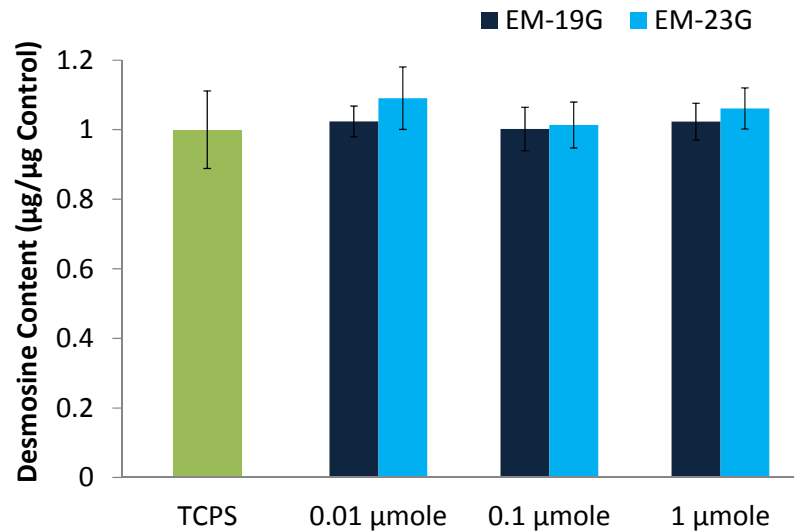


**Figure 2.3.** Desmosine production in the presence of EM-19G and EM-23G. No significant changes were observed in desmosine production across all peptide concentrations indicating LOX activity was remained unchanged ( $n = 5-6$ ).

#### 2.4.3 Peptide Competition with $\alpha$ -lactose

Elastin and desmosine content were quantified in the presence of the elastin mimetic peptides and 10 mM  $\alpha$ -lactose after 48 hours (Figure 2.4). The presence of  $\alpha$ -lactose alone decreases the elastin content to  $120 \pm 9\%$  of the TCPS control (Figure 2.4A). The combination of EM-19 and 10 mM  $\alpha$ -lactose leads to a competitive behavior between the peptide and the galactosugar, and the elastin production recovers with

increasing peptide concentration (elastin deposition decreased by  $103 \pm 16\%$ ,  $46 \pm 7\%$ , and recovered to  $78 \pm 21\%$  of the TCPS control at 0.01, 0.1, and 1  $\mu\text{mol}$ , respectively). Although the data is normalized to TCPS, it is of note that at the highest EM-19 concentration, elastin deposition recovers to  $5.48 \pm 1.81 \mu\text{g}$ , which is only slightly less than the  $7.23 \pm 1.06 \mu\text{g}$  of total elastin production at 1  $\mu\text{mol}$  in the absence of  $\alpha$ -lactose. The control peptide, EM-19S, does not have any active binding sites that will interact with the EBP, and hence does not compete with  $\alpha$ -lactose, leading to similar levels of elastin production as  $\alpha$ -lactose across all concentrations (elastin production decreased by  $120 \pm 11\%$ ,  $123 \pm 4\%$ , and  $126 \pm 5\%$  in comparison to the TCPS control at 0.01, 0.1, and 1  $\mu\text{mol}$ , respectively).

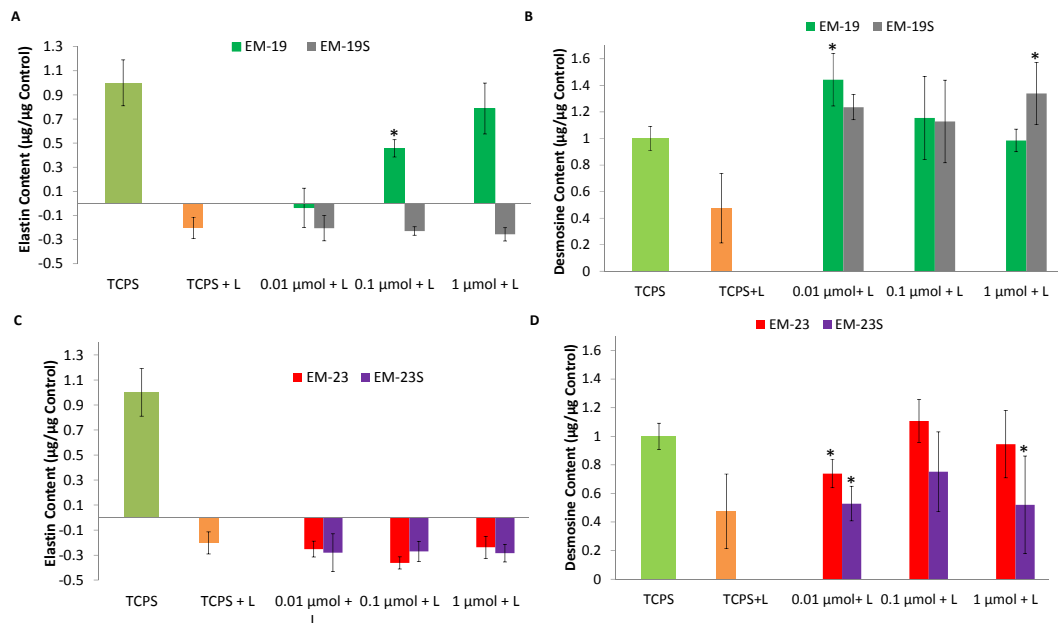


**Figure 2.4.** Elastin and desmosine production as a result of competition between 10 mM  $\alpha$ -lactose (L) and EM-19, EM-19S, EM-23, or EM-23S. A) EM-19 undergoes competition with  $\alpha$ -lactose but elastin levels show signs of recovery at high concentrations due to competition of the VGVAPG sequence with lactose. EM-19S does not compete to bind the EBP and no functional recovery is possible. B) EM-19 and EM-19S stimulate significant increases in desmosine production. C) Elastin levels in the presence of EM-23 and EM-23S remain drastically decreased, suggesting the peptide binds to integrins and cannot stimulate EBP activity. D) EM-23 and EM-23S are able to promote desmosine production, yet not at the levels observed for the EM-19 peptides ( $n = 5$ ;  $*p < 0.05$  compared to TCPS).

Desmosine production further decreased to  $48 \pm 25\%$  of the TCPS control in the presence of  $\alpha$ -lactose alone (Figure 2.4B). Moreover, higher amounts of desmosine in the presence of EM-19 and  $\alpha$ -lactose were detected at the lower concentrations of both EM-19 sequences (an increase of  $44 \pm 20\%$  and  $15 \pm 31\%$  compared to the TCPS control at 0.01 and 1  $\mu\text{mol}$ , respectively), while decreasing to the control levels at 1  $\mu\text{mol}$  ( $98 \pm 8\%$  of the TCPS control). In the presence of EM-19S and  $\alpha$ -lactose, however, desmosine levels were greater than the TCPS control at all concentrations (an increase of  $23 \pm 9\%$ ,  $12 \pm 31\%$ , and  $33 \pm 23\%$  compared to the control at 0.01, 0.1, and 1  $\mu\text{mol}$ , respectively).

On the other hand, elastin production did not recover in the presence of EM-23 and  $\alpha$ -lactose, reinforcing the possibility that EM-23 preferentially binds to integrins instead of the EBP (Figure 2.4C). At each concentration, the elastin levels were comparable to the levels observed in the presence of  $\alpha$ -lactose (reductions of  $125\% \pm 6\%$ ,  $226 \pm 5\%$ , and  $124 \pm 9\%$  compared to the TCPS control at 0.01, 0.1, and 1  $\mu\text{mol}$ , respectively). A similar trend in elastin deposition was also observed in the presence of EM-23S and  $\alpha$ -lactose (reductions of  $128 \pm 15\%$ ,  $12\% \pm 8\%$ , and  $128 \pm 7\%$  compared to the TCPS control at 0.01, 0.1, and 1  $\mu\text{mol}$ ). The desmosine content, on the other hand, increased with increasing EM-23 concentration, although no statistical significance was found between the control and peptide concentrations of 0.1 and 1  $\mu\text{mol}$  (Figure 2.4D). Desmosine content was  $73 \pm 10\%$  and  $94 \pm 23\%$  of the TCPS control at 0.01 and 1  $\mu\text{mol}$ , respectively, whereas it increased by  $11 \pm 15\%$  at a concentration of 0.1  $\mu\text{mol}$  in comparison to the control. In the presence of EM-23S, the desmosine content was  $53 \pm 12\%$ ,  $75 \pm 28\%$ , and  $52 \pm 34\%$  compared to the TCPS control at 0.01, 0.1, and 1  $\mu\text{mol}$ , respectively.

#### 2.4.4 Peptide Competition with Soluble RGDS

To further characterize the role integrins play in elastin fiber assembly, the elastin and desmosine content were quantified after 48 hours in the presence of the elastin mimetic peptides and soluble RGDS (Figure 2.5). The addition of RGDS alone decreased the elastin levels to  $71 \pm 30\%$  of the TCPS control (Figure 2.5A). The presence of EM-19 and RGDS caused a decrease in elastin levels across all concentrations ( $52 \pm 19\%$ ,  $46 \pm 8\%$ , and  $41 \pm 21\%$  compared to the TCPS control at 0.01, 0.1, and 1  $\mu\text{mol}$ , respectively; Figure 2.5A). Desmosine production, on the other hand, remained unchanged throughout the entire spectrum of EM-19 concentrations, indicating that LOX activity also remained unchanged (Figure 2.5B).

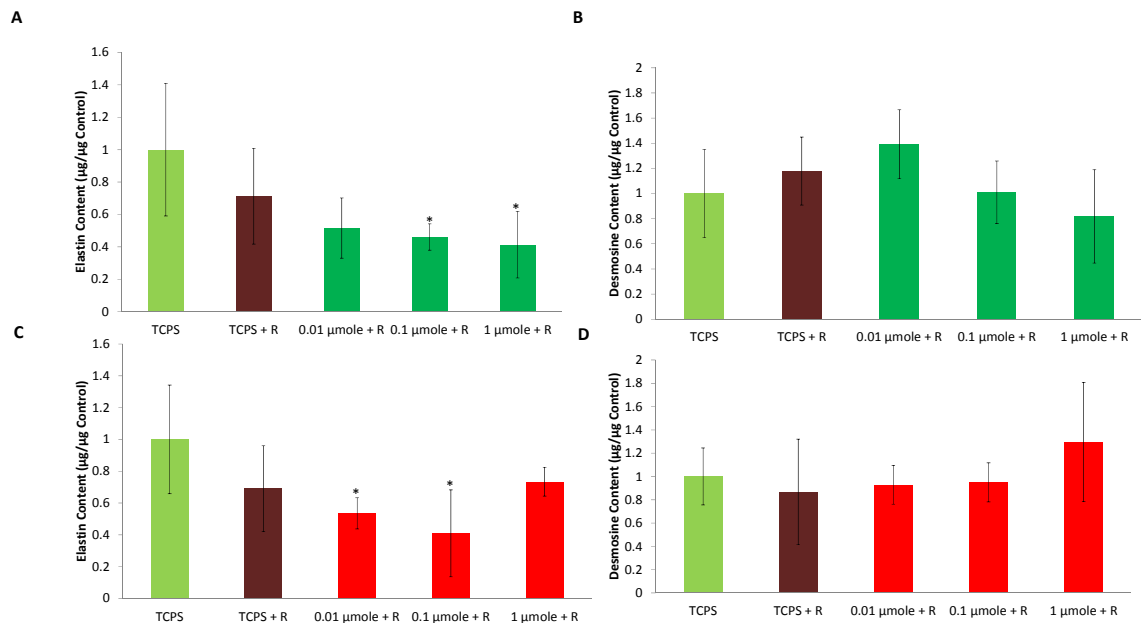


**Figure 2.5.** Elastin and desmosine production stimulated by EM-19 and EM-23 in the presence of 1  $\mu\text{mol}$  RGDS. A) The addition of RGDS alone decreases elastin production in SMC culture, and EM-19 promotes further decreases in elastin levels, suggesting that RGDS plays an important role in elastin production. B) Desmosine production decreases with increasing peptide concentration, a trend similar to that observed in the presence of lactose. C) EM-23 stimulates a similar trend in elastin content as cultures that did not contain RGDS. The data suggests that there is a synergistic interplay between RGDS and VGVAPG on EM-23 that is influencing elastin production. D) Desmosine production from EM-23 only increases marginally at all peptide concentrations ( $n = 5$ ;  $*p < 0.05$  compared to TCPS).

In contrast, elastin production initially decreased at lower EM-23 concentrations and eventually recovered at 1  $\mu\text{mol}$  ( $53 \pm 10\%$ ,  $41 \pm 27\%$ , and  $73 \pm 9\%$  compared to the TCPS control at 0.01, 0.1, and 1  $\mu\text{mol}$ , respectively; Figure 2.5C). The desmosine levels remained unchanged across all EM-23 concentrations, indicating LOX activity was unchanged (Figure 2.5D).

#### 2.4.5 Visualizing Peptide Activity via Immunofluorescence

The bioactivity of the elastin mimetic peptides at 1  $\mu\text{mol}$  was visualized using immunofluorescence techniques (Figure 2.6). Each peptide was tagged with FITC and the elastin fibers were labeled with Texas Red. Strong colocalization of EM-19 and EM-19S was observed around the periphery of the cell membrane (Figure 2.6A and 2.6B, respectively). However, EM-23 and EM-23S showed an even stronger ability to colocalize with the deposited elastin matrix (Figure 2.6C and 2.6D, respectively).

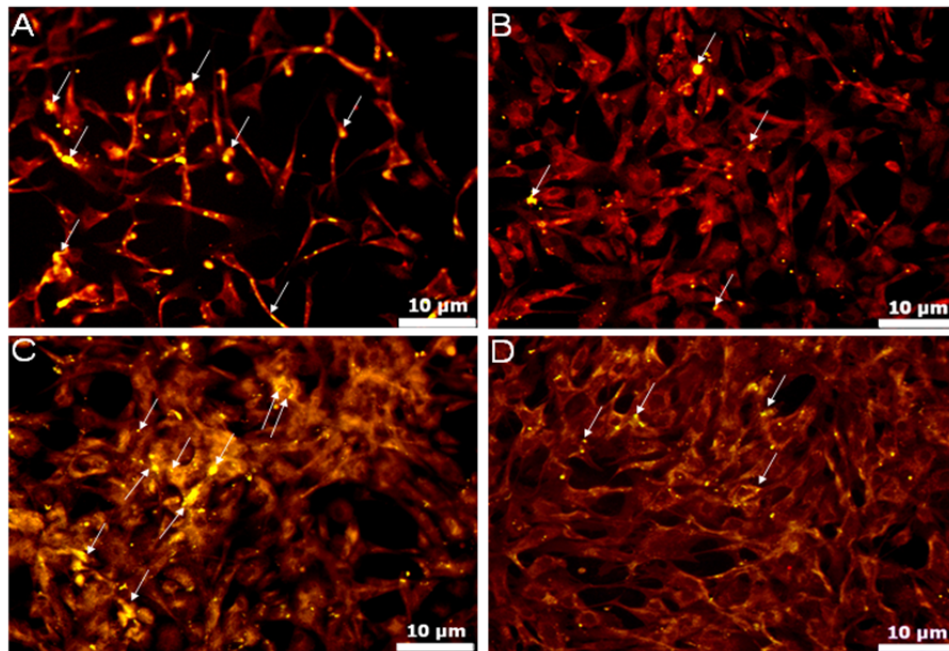


**Figure 2.6.** Immunofluorescent images of peptide activity *in vitro* after 24 hours. Arrows indicate sites of peptide localization with the elastin matrix. EM-19 colocalizes strongly with the elastin matrix (A) whereas with EM-19S there is less peptide incorporated into the matrix due to the scrambling of the EBP-binding sequence (B). Both EM-23 (C) and EM-23S (D) are able to bind the cell surface and greater colocalization is observed compared to the EM-19 peptides.

#### 2.4.6 Tropoelastin and LOX mRNA Levels

Tropoelastin and LOX mRNA levels were quantified in the presence of the elastin mimetic peptides after 48 hours (Figure 2.7). As an internal control, GAPDH mRNA levels were also quantified in the presence of the elastin mimetic peptides and their respective controls. In the presence of EM-19, tropoelastin mRNA level increased by  $7 \pm 2\%$  from the TCPS control samples, and LOX mRNA level decreased by  $3 \pm 6\%$  from the control, however, neither condition was statistically different from the TCPS controls (Figures 2.7A and 2.7B, respectively). Moreover, in the presence of EM-19S tropoelastin mRNA levels decreased by  $3 \pm 4\%$  while the LOX mRNA production increased by  $10 \pm 5\%$  without any statistical difference from TCPS (Figures 2.7A and 2.7B, respectively). Similarly, in the presence of EM-23, tropoelastin and LOX mRNA levels decreased by  $12 \pm 6\%$  and  $11 \pm 15\%$ , respectively, with no statistically significant difference from the TCPS control (Figures 2.7A and 2.7B, respectively).

Furthermore, in the presence of EM-23S, tropoelastin production increased by  $22 \pm 13\%$  while LOX production decreased by  $13 \pm 19\%$  without any significant difference from TCPS (Figures 2.7A and 2.7B, respectively). Additional statistical analysis between samples incubated with EM-19 and EM-23 was also conducted, and no significant differences in any mRNA levels were observed between the different samples. Further, no significant changes in GAPDH mRNA levels were observed between the controls and samples incubated with either EM-19 or EM-23 (GAPDH mRNA levels decreased by  $11 \pm 2\%$  when in the presence of EM-19 whereas GAPDH mRNA levels increased by  $3 \pm 11\%$  in the presence of EM-23, Figure 2.7C). No significance in GAPDH mRNA levels were also observed between TCPS and EM-19S or EM-23S (GAPDH mRNA levels

increased by  $8 \pm 11\%$  when exposed to EM-19S whereas GAPDH mRNA levels increased by  $5 \pm 12\%$  when exposed to EM-23S, Figure 2.7C).

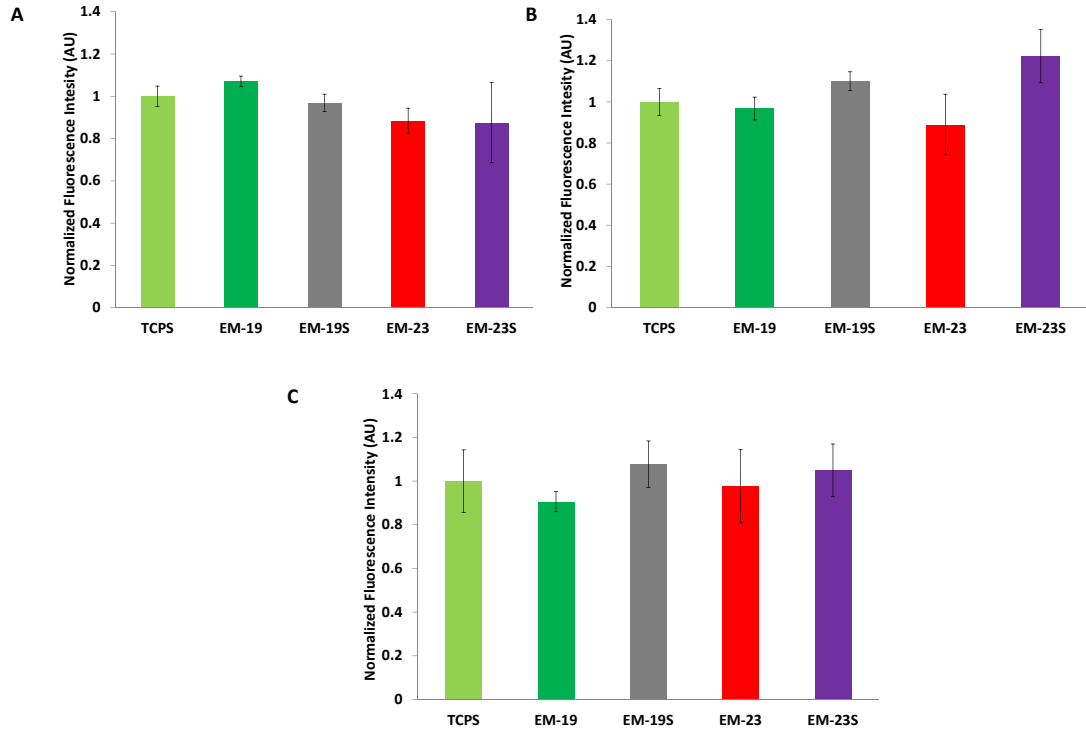


**Figure 2.7.** Tropoelastin (A), LOX (B), and GAPDH (C) mRNA levels in the presence of  $1 \mu\text{mol}$  of the elastin mimetic peptides. No statistical significance in the tropoelastin, LOX, or GAPDH mRNA levels was found between the elastin mimetic peptides and TCPS ( $n = 3-4$ ).

#### 2.4.7 The Role of Integrins in Elastin Fiber Assembly

To further assess the roles integrins play in elastin fiber assembly, the elastin and desmosine content were quantified after 48 hours in the presence of  $1 \mu\text{mol}$  EM-19 or EM-23 while the integrins  $\alpha_v\beta_3$  or  $\alpha_5\beta_1$  were blocked (Figure 2.8). In the presence of the  $\alpha_v\beta_3$  antibody, elastin production reduces to  $68 \pm 10\%$  of the TCPS control, whereas no change in elastin deposition was observed in the presence of the  $\alpha_5\beta_1$  antibody (Figure 2.8A). Moreover, in the presence of EM-19, elastin production reduces to  $48 \pm 3\%$  and  $54 \pm 3\%$  of the control when  $\alpha_v\beta_3$  and  $\alpha_5\beta_1$  are blocked, respectively, whereas in the

presence of EM-23, elastin production reduces to  $82 \pm 7\%$  and increases by  $28 \pm 8\%$  when  $\alpha_v\beta_3$  and  $\alpha_5\beta_1$  are blocked, respectively (Figure 2.8A).

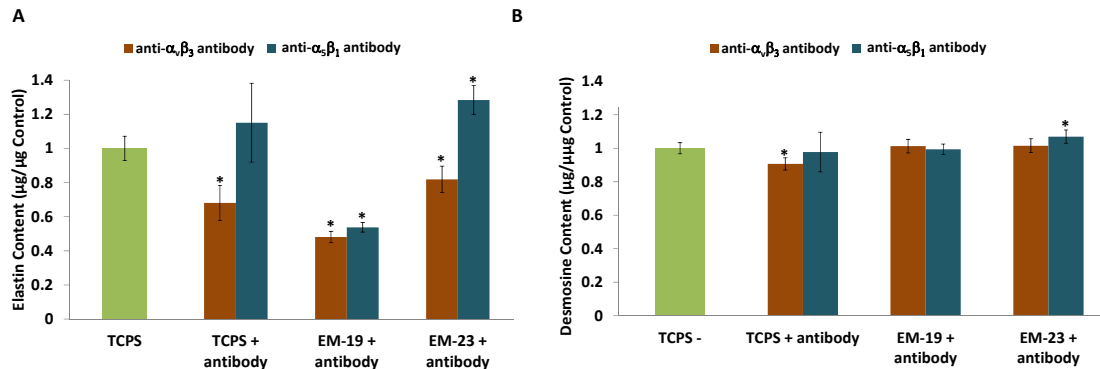


**Figure 2.8.** A) Changes in elastin production are evident in the presence of EM-19 and EM-23 when the activities of two different integrins,  $\alpha_v\beta_3$  and  $\alpha_5\beta_1$ , are blocked. When the activity of  $\alpha_v\beta_3$  is blocked, elastin production decreases significantly, while no change in elastin activity is observed when the activity of  $\alpha_5\beta_1$  is blocked, alluding to the importance of  $\alpha_v\beta_3$  in elastin fiber assembly. EM-19 is still capable of self-assembling with the elastin matrix in the presence of either antibody, suggesting that the binding affinity of EM-19 to the EBP is not affected. However, blocking the activity of  $\alpha_v\beta_3$  significantly reduces the ability of EM-23 to bind to integrins and as a result, elastin levels are still significantly lowered since the peptide is utilizing the EBP. On the other hand, by blocking the activity of  $\alpha_5\beta_1$ ,  $\alpha_v\beta_3$  integrin-bound EM-23 is crosslinked within the elastin matrix in addition to EBP-bound tropoelastin, leading to significantly higher elastin production than in control cultures (n = 3-4; \* $p < 0.05$  compared to TCPS). B) Desmosine production in the presence of EM-19 and EM-23 mirrors the elastin levels when  $\alpha_v\beta_3$  and  $\alpha_5\beta_1$  are blocked. (n = 4-6, \* $p < 0.05$  compared to TCPS).

The desmosine data mirrors that of elastin, in that desmosine production reduces to  $91 \pm 4\%$  of the TCPS control when  $\alpha_v\beta_3$  is blocked (Figure 2.8B). However, no change in desmosine production is observed when  $\alpha_5\beta_1$  is blocked. Similarly, in the presence of EM-19, no change in desmosine is observed when either  $\alpha_v\beta_3$  or  $\alpha_5\beta_1$  is blocked. Although desmosine levels are comparable to TCPS controls in the presence of EM-23 and the  $\alpha_v\beta_3$  antibody, a significant increase of  $7 \pm 4\%$  is observed in the presence of EM-23 and the  $\alpha_5\beta_1$  antibody (Figure 2.8B).

Furthermore, elastin and desmosine production were also quantified in the presence of an isotype control and EM-19 or EM-23 (Figure 2.9). The isotype control was produced against a synthetic hapten not normally present in humans or animals, and

therefore does not react with any antigen of human or animal cells. The addition of the isotype control did not affect the overall elastin production, indicating that the antibody did not have any cross reactivity with the SMCs (Figure 2.9A). Furthermore, in the presence of either EM-19 or EM-23 and the isotype control, the elastin levels remained comparable to the levels observed in Figure 2.2 (elastin production reduced to  $61 \pm 7\%$  and  $57 \pm 8\%$  in comparison to TCPS in the presence of EM-19 and EM-23, respectively). The desmosine production remained unchanged throughout all conditions (Figure 2.9B).

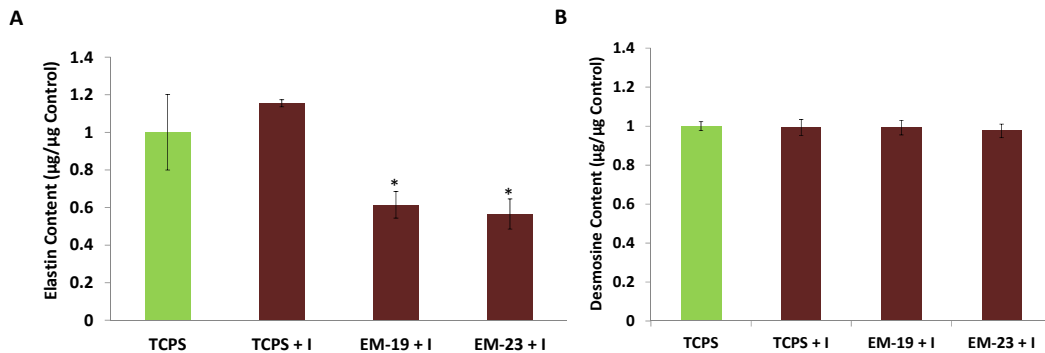


**Figure 2.9.** Elastin (A) and desmosine (B) in the presence of IgG isotype control (I) and EM-19 or EM-23. Elastin production in the presence of the isotype control and EM-19 or EM-23 is comparable to levels observed without the addition of the isotype control, indicating that the antibody does not have any cross reactivity with the SMCs. Desmosine production remained unchanged in the presence of the isotype control and the combination of isotype control and EM-19 or EM-23 ( $n = 3-4$ ,  $*p < 0.05$  compared to TCPS).

## 2.5 Discussion

The ECM is an essential part of any tissue, as it provides the necessary microenvironment for cell growth. Currently available biomaterials for vascular prostheses lack a viable ECM, and hence are not able create a suitable microenvironment for cell growth. For example, elastin is a critical component of vascular ECM yet many vascular prostheses lack the ability to promote elastin production [16]. Although the exact mechanism of elastin fiber assembly is debatable, it is certain that the EBP plays a

dominant role in chaperoning tropoelastin during elastogenesis [178]. Moreover, recent studies have suggested that integrins may assist the EBP in chaperoning tropoelastin for elastogenesis [155-157].

With this mechanism in mind, two different elastin mimetic peptides, EM-19 and EM-23, were engineered to translate the complex mechanism of elastin fiber assembly to a synthetic scaffold. Before the peptides could be implemented as templates that promote ECM deposition, they first were thoroughly characterized *in vitro* and their ability to self-assemble with the growing elastin matrix was evaluated. Further, the role that integrins play in the elastogenesis was also investigated.

As part of the initial peptide characterization, the native structure of each peptide was determined via CD. No significant differences in the CD spectra for EM-19 and EM-23 were found between room temperature and 37°C. Moreover, the lack of negative peaks from 208 to 220 nm in the CD spectra for either peptide suggests the absence of an  $\alpha$ -helical structure. The CD spectra for EM-19 and EM-23 also have a characteristic negative band at 197 nm representing a disordered structure such as the random coil of human elastin [196]. Also, the spectra are directly comparable to that of soluble human elastin suggesting that the peptides are capable of behaving as soluble elastin mimetics [197-202].

Further, elastin and desmosine production were quantified in the presence of the elastin mimetic peptides and their respective controls after 48 hours. The addition of EM-19 reduced the elastin content by almost 50%. A possible explanation for this phenomenon is that the peptide is directly able to compete with native tropoelastin to bind the EBP. Once the smaller peptide chain binds the EBP, it is chaperoned to the

adjacent microfibrils where the cell-secreted enzyme LOX crosslinks the peptide with the elastin matrix. This phenomenon leads to a reduced overall mass of elastin detected (Figure 2.10).

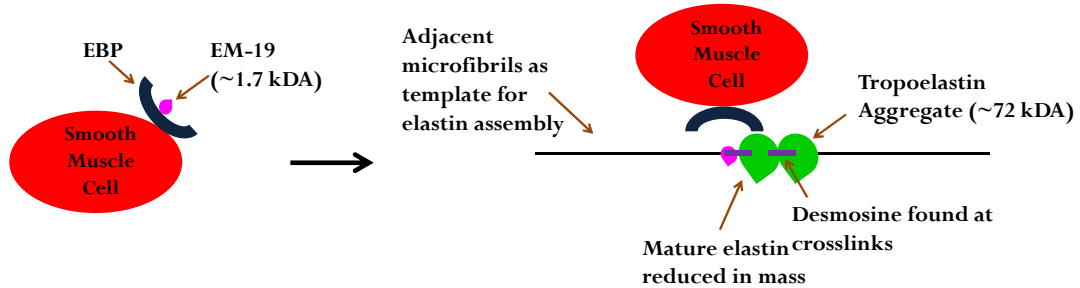


**Figure 2.10.** Proposed mechanism for self-assembly of EM-19 within the elastin matrix. EM-19 readily competes with tropoelastin for EBP binding. Once bound on the EBP, the peptide is chaperoned to the adjacent microfibrils where the cell-secreted enzyme LOX crosslinks the peptide with the elastin matrix, leading to a reduced mass of elastin detected.

This hypothesis was further confirmed by quantifying the desmosine content in the presence of EM-19 after 48 hours. The desmosine content remained unchanged across all EM-19 concentrations, suggesting that the reduced mass of elastin detected in the presence of EM-19 may be a result of the peptide being crosslinked within the elastin matrix. A similar phenomenon was also observed in the presence of EM-19S. Although EM-19S contains no cell binding motifs, it may be possible for the peptide to be crosslinked with the elastin matrix due to the active crosslinking domains, and hence a reduced mass of elastin was detected while having no significant impact on desmosine production.

A similar trend in elastin production was observed in the presence of EM-23; however, the amount of elastin detected significantly recovered at the highest EM-23 concentration. A possible explanation for the recovery of elastin levels is a result of the peptide preferentially binding integrins instead of the EBP. The integrins and the EBP synergistically chaperone the peptide and tropoelastin for crosslinking, resulting in larger

amounts of elastin detected (Figure 2.11). Furthermore, the desmosine content remained the same throughout all EM-23 concentrations, which reinforces the hypothesis that peptide crosslinking occurs through a synergistic mechanism between the EBP and integrins. Similarly, in the presence of the control sequence, EM-23S, which contains the active integrin binding domain, elastin fiber assembly begins to recover at the highest concentration, and the desmosine content remains unchanged throughout all EM-23S concentrations. This data further strengthens the initial hypothesis of integrins playing an integral role in elastogenesis.

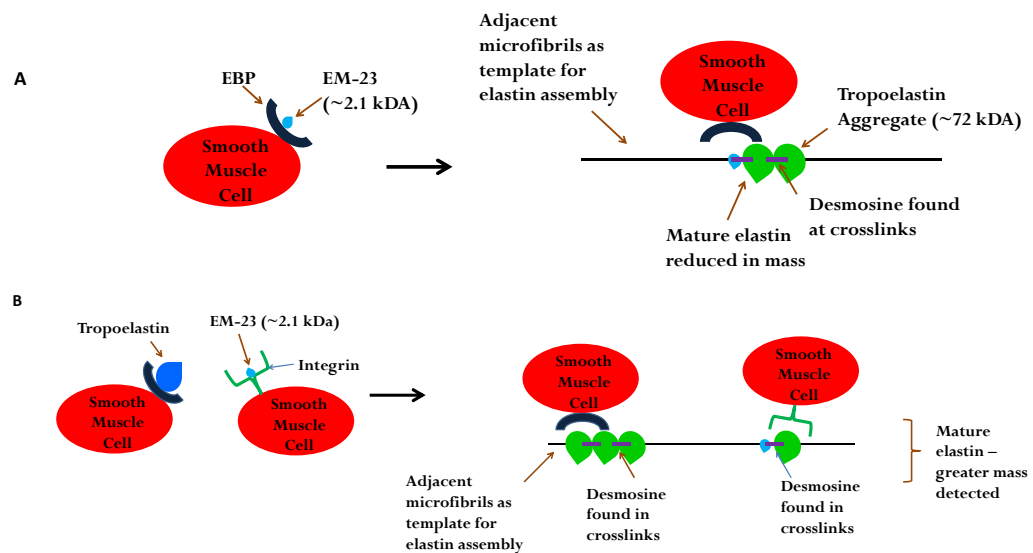


**Figure 2.11.** Proposed mechanism of EM-23 crosslinking with the elastin matrix. At low concentrations, EM-23 competes with and replaces the heavier tropoelastin chain in crosslinking with the elastin matrix leading to a reduced mass of elastin detected (A). However, at the highest concentration, the peptide preferentially binds with integrins which play a synergistic role with the EBP to chaperone the peptide for crosslinking. The final mass of elastin detected is a result of the heavier tropoelastin chains crosslinking with EM-23.

Further control studies were conducted in which the lysine-rich domain in EM-19 and EM-23 was replaced with glycine, yielding EM-19G and EM-23G, respectively, and the desmosine content was quantified in the presence of EM-19G or EM-23G. No change in desmosine content was detected, which suggests that when EM-19G binds to the EBP, the EBP chaperones it to the adjacent microfibrils for crosslinking. However, due to the

absence of crosslinking motifs in EM-19G, the peptide is unable to crosslink with the deposited elastin matrix. The EBP is then recycled back to the SMC surface where it continues to chaperone the heavier tropoelastin chains for crosslinking. Hence, the overall desmosine production remains the same. A similar behavior is also observed with EM-23G, even though the peptide preferentially binds integrins at the higher concentration. The lack of active crosslinking motifs on EM-23G simply allows tropoelastin to crosslink with the elastin matrix, leading to a sustained amount of desmosine content detected at each EM-23G concentration.

Also, to ensure that the peptides do not have any effects on LOX and tropoelastin production, the mRNA levels of LOX and tropoelastin were quantified in the presence of EM-19 and EM-23 along with their respective controls. The tropoelastin and LOX mRNA levels remained consistent with the TCPS control, indicating that the presence of elastin mimetic peptides and their respective controls do not interfere with tropoelastin production and LOX activity. The mRNA levels of an internal control, GAPDH, were also quantified in the presence of the peptides and as expected no changes were observed in the GAPDH mRNA levels.

The preliminary characterization of EM-19 and EM-23 suggested that the peptides can self-assemble with the elastin matrix. However, the role peptides and integrins play in elastogenesis remained unclear. Therefore, competitive studies were conducted in the presence of  $\alpha$ -lactose and soluble RGDS to further assess the roles the peptides and integrins play in elastogenesis. The galactosugar  $\alpha$ -lactose has high affinity for the EBP. However, when  $\alpha$ -lactose binds the EBP, the structural conformation of the EBP changes and it is shed from the cell surface. This results in a drastic reduction of

elastin deposition, since the EBP is unable to transport tropoelastin for elastin crosslinking (Figure 2.12).

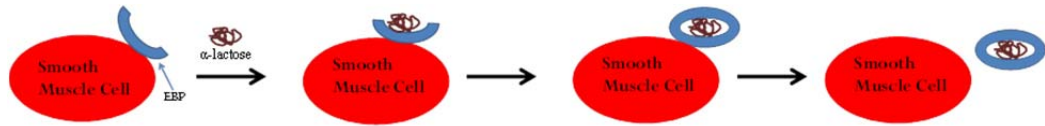


**Figure 2.12.** The binding of the galactosugar  $\alpha$ -lactose causes a structural transformation of the EBP. The EBP is then sheds from the cell surface, leading to a drastic reduction in elastogenesis.

The levels of elastin detected in SMC cultures with  $\alpha$ -lactose were consistent with the mechanism described in Figure 2.12. In the presence of EM-19 and  $\alpha$ -lactose, elastin production almost decreases to the levels observed with only  $\alpha$ -lactose at 0.01  $\mu$ mol. However, elastin production begins to recover as the peptide concentration increases. This result suggests that EM-19 may be competing with  $\alpha$ -lactose for EBP binding, and at the highest peptide concentration, EM-19 is able to efficiently bind to the EBP, causing peptide incorporation into the elastin matrix. Of note, the actual amount of elastin detected was slightly less than the total elastin production at 1  $\mu$ mol in the absence of  $\alpha$ -lactose. This remarkable consistency once again reinforces the hypothesis that EM-19 is able to effectively compete with  $\alpha$ -lactose to bind the EBP. On the other hand, EM-19S, which does not have an EBP binding motif, did not induce any elastin recovery for any of the peptide concentrations. Desmosine content in the presence of EM-19 or EM-19S and  $\alpha$ -lactose varied greatly, showing that the peptides are still able to crosslink due to the lysine rich domains present within the peptides.

On the other hand, elastin production did not recover at the any of the concentrations when SMCs were cultured in the presence of EM-23 and  $\alpha$ -lactose. This result suggests that EM-23 does not compete with  $\alpha$ -lactose and instead preferentially binds to integrins. A similar behavior is also observed with EM-23S, although this result

is to be expected due to the absence of the EBP-binding motif. Desmosine production once again varied greatly with each EM-23 or EM-23S concentration, suggesting that the crosslinking activities are greatly affected when the EBP is completely shed from the cell surface. Overall, the competition studies with  $\alpha$ -lactose suggested that EM-23 preferentially binds to the cell surface integrins instead of the EBP.

To elucidate how the binding of EM-23 and integrins affects elastin production, further competitive studies were conducted in the presence of soluble RGDS and EM-19 or EM-23. Elastin and desmosine content were quantified in the presence of soluble RGDS and the elastin mimetic peptides. The addition of RGDS alone decreases the elastin production by 30%, with EM-19 further reducing the amounts of elastin detected, suggesting that by blocking integrin activity, the mechanism of elastin production is somehow inhibited. Desmosine production decreases in the presence of RGDS and increasing EM-19 concentrations, a trend similar to that found in presence of  $\alpha$ -lactose. Moreover, EM-23 is able to effectively compete with RGDS for integrin binding and is able to maintain similar levels of elastin and desmosine as in cultures without any addition of RGDS.

Integrins are a broad class of receptors and of the 24 different heterodimers of the integrin family, previous work has shown tropoelastin to interact with  $\alpha_v\beta_3$  [155, 203]. Therefore to clarify the role  $\alpha_v\beta_3$  plays in elastogenesis, total elastin content after 48 hours was quantified in the presence of either EM-19 or EM-23 while blocking the activities of  $\alpha_v\beta_3$ . Previous work has also suggested that the integrin  $\alpha_5\beta_1$  does not interact with tropoelastin, though it does bind RGDS, and hence this integrin was used as a control [155, 204]. When the activity of  $\alpha_v\beta_3$  was blocked, elastin production decreased

by almost 40%, while no change in elastin deposition was observed when the activity of  $\alpha_5\beta_1$  was blocked. This result further reinforces that  $\alpha_5\beta_1$  does not play a role in elastin fiber assembly, whereas hindering the ability of tropoelastin to interact with  $\alpha_v\beta_3$  reduces elastin deposition and reaffirms the importance of  $\alpha_v\beta_3$  in elastin fiber assembly. In the presence of EM-19 and anti- $\alpha_v\beta_3$  or anti- $\alpha_5\beta_1$ , elastin production decreases to the levels observed in SMC cultures without the antibodies, suggesting that EM-19 is still able to effectively bind to the EBP. Once bound to the EBP, the peptide is still able to self-assemble with the deposited elastin matrix. No change in desmosine production was observed in the presence of EM-19 and either anti- $\alpha_v\beta_3$  or anti- $\alpha_5\beta_1$ , suggesting that LOX activity was unperturbed and the peptide was able to self-assemble with the elastin matrix.

On the other hand, EM-23 contains VGVAPG and RGDS sequences that bind to the EBP and integrins, respectively. In the presence of anti- $\alpha_v\beta_3$ , elastin production decreased by 25%. This result is in excellent agreement with the competitive experiment with soluble RGDS, in which elastin production was reduced by 30% in the presence of EM-23 and RGDS. Both sets of data suggest that blocking the activity of integrin  $\alpha_v\beta_3$  will inhibit tropoelastin binding to  $\alpha_v\beta_3$ , hindering elastogenesis. In the presence of EM-23 and anti- $\alpha_5\beta_1$ , elastin production increased by 20%. As suggested previously with competition studies in the presence of  $\alpha$ -lactose, EM-23 preferentially binds integrins with higher affinity than the EBP. By blocking the activity of  $\alpha_5\beta_1$ , the interactions between EM-23 and  $\alpha_v\beta_3$  were enhanced. This allowed both the peptide and tropoelastin bound to the EBP to simultaneously crosslink, leading to an increased mass of elastin detected.

Desmosine production mirrored that of elastin production; no change in desmosine content was detected in the presence of EM-23 and anti- $\alpha_v\beta_3$ . A significant increase in desmosine production was observed in the presence of EM-23 and anti- $\alpha_5\beta_1$ , suggesting that the increased crosslinks are a result of both the peptide and tropoelastin incorporation into elastic fibers. Elastin and desmosine production were also quantified in the presence of EM-19 or EM-23 and an isotype control that does not have any cross-reactivity with human SMCs. As expected, elastin and desmosine levels were similar to those observed in SMC cultures without the presence of the isotype control.

Finally, the self-assembly of each elastin mimetic peptide with elastin was also visually evaluated. Each elastin mimetic peptide was conjugated with FITC (green fluorescence) and incubated with SMCs for 48 hours. The deposited elastin matrix was then tagged with Texas Red (red fluorescence) using immunostaining techniques and both tagged moieties were visualized under a fluorescence microscope. EM-19 colocalized well around the periphery of the cell membrane and some colocalization of EM-19S was also observed. This is likely due to the presence of the active crosslinking domains allowing the peptide to self-assemble with the elastin matrix. Qualitatively, stronger localization was observed in the presence of EM-23, which reinforces the initial hypothesis that EM-23 can utilize the two different receptors to self-assemble with the elastin matrix. Although EM-23S colocalizes fairly well around the cell membrane, the observed fluorescence is less than that seen in cultures containing EM-23.

## 2.6 Conclusion

Preliminary characterization studies showed that both engineered peptides were able to self-assemble with a cell secreted elastin matrix. Moreover, the role integrins play in elastogenesis was also investigated and the results suggested that EM-23 preferentially binds with integrins, and the integrin  $\alpha_v\beta_3$  may play a synergistic role with the EBP in elastogenesis. The studies confirmed that the peptides are capable of utilizing the EBP and integrins to self-assemble with a growing elastin matrix. Furthermore, incorporation of these peptides into synthetic scaffolds will serve as templates for promoting elastin production. As such, the next chapter will discuss the efficacy of EM-19 and EM-23 to serve as templates for translating the complex mechanism of elastin fiber assembly once immobilized onto the surface of a synthetic scaffold.

## <sup>2</sup>Chapter 3

### Synthesis and Characterization of PEG-peptide Copolymer Hydrogels

#### 3.1 Summary

This chapter will characterize the ability of each elastin mimetic peptide to facilitate cell adhesion and elastin deposition on the surfaces of PEG-DA hydrogels. Each elastin mimetic peptide was physically immobilized onto hydrogel surfaces and SMC adhesion, proliferation, and viability studies were conducted at various PEG-peptide concentrations. Elastin production was also quantified and compared to cells cultured on a TCPS surface. The results from 2D characterization studies suggested that EM-23 facilitates the highest amounts of cell adhesion, spreading, viability, and elastin production over all peptides, including RGDS.

#### 3.2 Introduction

Immobilizing peptides onto PEG-DA hydrogel surfaces has previously been shown to be a suitable model system for characterizing the efficacy of peptides to promote cell adhesion, proliferation, and ECM deposition on a synthetic construct [82, 85, 205, 206]. Moreover, Hern et al. have shown significant cell adhesion on PEG-DA surfaces modified with the fibronectin-derived sequence RGDS [191]. Additionally,

---

<sup>2</sup> *Work discussed in this chapter is adapted from:*

*D Patel, SE Vandromme, ME Reid, LJ Taite. "Synergistic activity of  $\alpha_v\beta_3$  integrins and the elastin binding protein enhance cell-matrix interactions on bioactive hydrogel surfaces." *Biomacromolecules* (2012), 13(5), 1420-1428.*

Gobin et al. immobilized the elastin-derived sequence VAPG onto the surface of PEG-DA and observed significant cell adhesion [86].

Furthermore, PEG-DA hydrogels limit non-specific protein adsorption, reduce platelet aggregation and thrombosis, and their mechanical properties can be changed by simply changing the molecular weight of the polymer [81-85, 89, 207]. The hydrogels are fabricated under mild conditions in the presence of a photoinitiator, such as 2,2-dimethyl-2-phenyl-acetophenone (DMPAP), and UV light at a wavelength of 365 nm (Figure 3.1) [208]. In this work, PEG-DA hydrogel surfaces were modified with different concentrations of RGDS, EM-19, and EM-23 in order to assess SMC adhesion, spreading, viability, and elastin deposition. Moreover, the 2D surface studies evaluated the efficacy of the peptides to promote ECM deposition onto a synthetic construct and characterized the peptides for potential application towards engineering viable vascular grafts.

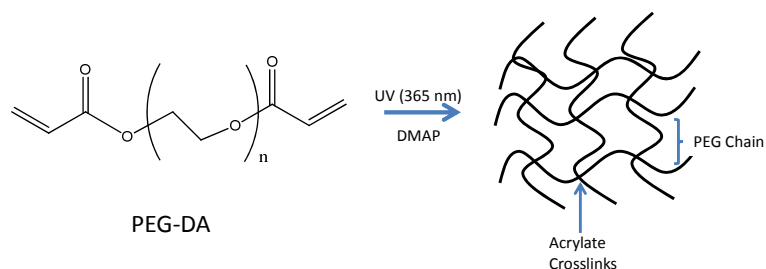


**Figure 3.1.** PEG-DA hydrogel formation. In the presence of UV light and a photoinitiator, the acrylate groups form free radicals and crosslink to generate a swollen hydrogel matrix. The mesh size of the hydrogel is determined by the length of the PEG chain.

### 3.3 Materials and Methods

#### 3.3.1 Peptide Synthesis

All materials and reagents required for peptide synthesis were purchased from AAPPTec (Louisville, KY). Peptides were synthesized using standard solid-phase

peptide synthesis protocols, as previously described [87]. In brief, four different peptides were synthesized using standard HBTU coupling and Fmoc protection chemistry on an Apex 396 peptide synthesizer (AAPPTec; Louisville, KY) using a lysine-conjugated Wang resin. A 23 amino acid sequence (EM-23; AAKAAKVGVAPGRGDSAAKAAKK), containing two cell adhesion motifs (VGVAPG and RGDS) as well as lysine and alanine -rich crosslinking domains, was synthesized along with a 23 amino acid control peptide in which the VGVAPG sequence is scrambled and the RGDS sequence is left intact (EM-23S; AAKAAKVGVPAGRGDSAAKAAKK). A 19 amino acid sequence (EM-19; AAKAAKVGVAPGAAKAAKK) and a 19 amino acid peptide in which the VGVAPG sequence is scrambled (EM-19S; AAKAAKVGVPAGAAKAAKK) were synthesized, omitting the RGDS motif completely to observe the importance of integrin binding. Crude peptides were then cleaved from the resin with cleaving cocktail (95% trifluoroacetic acid, 2.5% water, 2.5% triisopropylsilane) and purified by dialysis using cellulose ester membrane tubing (MWCO 1000; Spectrum laboratories, Rancho Dominguez, CA). The dialyzed peptides were then frozen and lyophilized overnight. Peptides were characterized using mass spectrometry.

### *3.3.2 Cell Culture and Maintenance*

Human aortic smooth muscle cells (SMCs, passages 3-5; Invitrogen Inc., Carlsbad, CA), were used for the remainder of the work discussed in this chapter. SMCs were maintained in Medium 231 (Invitrogen Inc., Carlsbad, CA) supplemented with smooth muscle cell growth supplement (SMGS, Invitrogen Inc., Carlsbad, CA), 2 mM L-

glutamine, 1 unit/ml penicillin, and 100 mg/l streptomycin (GPS; Cellgro, Manassas, VA) at 37°C in a 5% CO<sub>2</sub> environment.

### *3.3.3 PEG-DA Synthesis*

Synthesis of PEG-DA was conducted using well established protocols [81, 86, 209]. PEG-DA was synthesized by dissolving 24 g dry PEG (MW: 10000; Fluka, Milwaukee, WI) in 20 ml anhydrous dichloromethane (DCM) with an equimolar amount of triethylamine and 0.869 g acryloyl chloride (Lancaster Synthesis, Windham, NH) added dropwise. The mixture was stirred under argon for 24 hours, washed with 2M K<sub>2</sub>CO<sub>3</sub>, and separated into aqueous and DCM phases to remove HCl. The mixture was then centrifuged at 2,000×g for 1 hour and the aqueous phase was aspirated and discarded. PEG-DA was then precipitated in diethyl ether, filtered, and dried under vacuum at room temperature overnight. The resulting polymer was dialyzed overnight against DI water with 5 kDa MWCO cellulose ester tubing (Spectrum Laboratories, Rancho Dominguez, CA) to remove any residual salts and impurities. The polymer was also characterized via proton NMR.

### *3.3.4 Conjugation of Peptides to Monoacrylate PEG Derivative*

Peptide sequences (RGDS, EM-19, EM-19S, EM-23 and EM-23S) were conjugated to PEG monoacrylate by reaction with acryloyl-PEG-succinimidyl valerate (PEG-SVA, MW 3400; Laysan Bio Inc., Arab, AL) in 50 mM sodium bicarbonate (pH 8.5) at a 1:1 molar ratio for 2 hours (protected from light and under Argon) to yield a PEG-peptide moiety. The mixture was then dialyzed (3500 MWCO dialysis cassettes; Pierce Biotechnology, Rockford, IL) against deionized water for 2 hours, lyophilized, and stored at -80°C. The final yield for each peptide-conjugated moiety was 82%. The yield

was determined by dividing the moles of the resulting product by the moles of the expected product. UV-Vis spectroscopy and GPC equipped with UV and ELS detectors (Agilent Technologies, Inc., Santa Clara, CA) were used to determine the coupling efficiency.

The number average molecular weight ( $M_n$ ), the weight average molecular weight ( $M_w$ ), and the polydispersity index (PDI) were determined by GPC using polystyrene standards. GPC results showed the expected molecular weights for all of the acrylate-PEG-peptide polymers with low PDIs ( $M_w \approx 5700$ , PDI = 1.02 for acrylate-PEG-EM23 and acrylate-PEG-EM23S;  $M_w \approx 5500$ , PDI = 1.01 for acrylate-PEG-EM19 and acrylate-PEG-EM19S). The low PDIs and consistent molecular weights confirm successful conjugation of the peptides with acrylate-PEG-SVA at the expected molar ratios.

### *3.3.5 PEG-peptide Grafting Efficiencies*

The grafting efficiencies of the monoacrylate PEG-peptide on the PEG-DA surfaces were quantified using the Ninhydrin reagent, which detects amine residues on proteins or peptides [70, 84, 210]. PEG-DA was dissolved in 10 mM HEPES buffer (pH 7.4) at 0.1 g/mL and to this solution, 10  $\mu$ L/mL of the photoinitiator DMAP (Alfa Aesar, Ward Hill, MA) in *N*-vinylpyrrolidone (NVP; 300 mg/mL) was added. This precursor solution was injected between two glass slides separated by a 1.0 mm spacer (C.B.S. Scientific Company, Del Mar, CA) and exposed to UV light (365 nm, 10 mW/cm<sup>2</sup>) to form a thin, flat hydrogel. The top glass slide was then lifted and the hydrogel was rinsed with PBS. A 2 mL solution of PEG-peptide, at 5  $\mu$ mol/mL, containing 10  $\mu$ L/mL DMAP was used to coat the surface and the top glass slide was carefully replaced to distribute

the PEG-peptide solution evenly on the surface. The mold was then exposed to UV light and the monoacrylate PEG peptide was allowed to crosslink to the surface of PEG-DA. Previous work has shown that this method allows for efficient crosslinking of a PEG-peptide to a PEG-DA surface [81, 207]. Residual PEG-peptide solution and DMAP were rinsed away with PBS and 14.3 mm diameter samples were cut.

The samples were then hydrolyzed with 6 N HCl overnight at 100°C, after which the solubilized gels were neutralized, frozen, and lyophilized. The dried gels were then resuspended in 1 ml sodium citrate buffer (pH 5.0) followed by the addition of 1 ml of the Ninhydrin reagent (Spectrum Chemicals, New Brunswick, NJ). The reaction mixture was immersed in boiling water for 15 mins, allowed to cool, and sample absorbances were read at 570 nm. A standard curve comprised of known concentrations of soluble PEG-peptide were used to determine the concentration of the monoacrylate PEG-peptide grafted on the PEG-DA surfaces.

### *3.3.6 Cell Adhesion and Proliferation on PEG-peptide Hydrogels*

SMC cell adhesion and growth on PEG-DA surfaces modified with various concentrations of RGDS, EM-19, EM-19S, EM-23 or EM-23S was determined after culturing cells on hydrogels for 12 hours to assess adhesion or 48 hours to assess proliferation. Different PEG-peptide moieties, at varying concentrations, were grafted onto PEG-DA surfaces in the manner described above, in a sterile environment. After rinsing the residual peptide solution and DMAP from the PEG-DA surface, 14.3 mm diameter gel samples were cut and carefully placed into the wells of a 24 well plate. After a 2 hour incubation with SMC media, the swollen gels were rinsed with PBS and seeded with 30,000 SMCs/cm<sup>2</sup> in fresh media. Cell adhesion and proliferation was

assessed after 12 and 48 hours, respectively, by first removing the media and rinsing the hydrogels with PBS, carefully transferring the rinsed gels to a new 24 well plate, and finally detaching the cells through incubation with 0.21% trypsin containing 0.25% EDTA (Cellgro, Manassas, VA) at 37°C for 4 mins. The dissociated cells were counted using a Beckman Z1 particle counter (Beckman Coulter, Brea, CA).

### *3.3.7 Cell Spreading on PEG-peptide Hydrogels*

Cell spreading was also quantified using different concentrations of PEG-peptide conjugated to hydrogels. Briefly, PEG-peptide (EM-19, EM-23, or RGDS) was immobilized on the surfaces of PEG-DA hydrogels in the manner described above. The gels were allowed to swell in media for 2 hours and then replenished with fresh media. SMCs at 30,000 cells/cm<sup>2</sup> were subsequently seeded and allowed to interact with the peptide modified gel. After 48 hours of incubation, the media was removed and the cells were fixed with 4% formaldehyde solution (AAT Bioquest, Inc., Sunnyvale, CA) for 25 mins. The residual formaldehyde solution was then removed and the gels were rinsed thoroughly with PBS. Images were then collected using a Leica DMI 400B phase contrast microscope (Leica Microsystems Inc., Bannockburn, IL) and cell spreading was evaluated by quantifying cell area using ImageJ software (NIH Scion Image, version 1.6, <http://imagej.nih.gov/ij>).

### *3.3.8 Cell Viability on PEG-peptide Hydrogels*

Cell viability on PEG-peptide modified hydrogels was also assessed using a Live/Dead viability stain (Invitrogen Inc., Carlsbad, CA). In brief, gels with SMCs were prepared with different PEG-peptide concentrations in the manner described above. After 48 hours, the media was removed and the gels were rinsed thoroughly with PBS.

The gels were then incubated with a solution containing 2  $\mu$ M calcein AM and 4  $\mu$ M ethidium homodimer-1 for 20 mins at 37°C. The intracellular enzyme esterase, present in live cells, converts the non-fluorescent calcein AM to green fluorescent calcein. Ethidium homodimer-1 enters dead cells via ruptured membranes and subsequent binding with nucleic acids produces red fluorescence. The wells were then washed thoroughly with PBS and fluorescent images were taken with a Leica DMI 400B fluorescent microscope (Leica Microsystems Inc., Bannockburn, IL). Fluorescence for each condition was also quantified using a Beckman DTX 880 Multimode Plate Reader at 495 nm excitation/523 nm emission and 495 nm excitation/623 nm emission for fluorescent calcein and ethidium homodimer-1, respectively.

### *3.3.9 Biochemical Analysis of PEG-peptide hydrogels*

The amount of elastin deposited on hydrogels was also quantified on PEG-DA surfaces modified with RGDS, EM-19, and EM-23 at 5  $\mu$ mol. Briefly, 5  $\mu$ mol/ml of PEG-peptide was immobilized on the surface of a PEG-DA hydrogel as described above. After swelling in cell culture media for 2 hours, the media was removed, rinsed with PBS, and subsequently seeded with 30,000 SMC/cm<sup>2</sup> in fresh media. After 48 hours, the media was again removed and the hydrogels were rinsed thoroughly with PBS. Immediately after rinsing, the gels were subjected to hydrolysis with 0.1 N NaOH for 24 hours at 37°C. The samples were then transferred to a 100°C oven for 2 hours to further solubilize ECM matrix proteins other than elastin. The digested samples were then centrifuged at 8,000 $\times$ g for 10 min; the resultant pellets were subjected to analysis for elastin content, while the supernatants were discarded.

### *3.3.10 Hydrogel Elastin Content*

The amount of elastin on PEG-DA hydrogels was determined using the Ninhydrin reagent. Initially, a Fastin assay was used to quantify elastin content from the hydrolyzed PEG-DA samples, as done in Chapter 2 of this thesis. However, the PEG chains interfered with the Fastin assay and instead the Ninhydrin reagent was used to quantify the purified elastin (previously separated from all the other proteins). The collected protein pellets were further subjected to acid hydrolysis using 6 N HCl at 100°C for 24 hours. The digested samples were then dried and resuspended in 1 mL sodium citrate buffer (0.1 M, pH 5.0). To this suspension, 1 ml of Ninhydrin reagent (Spectrum Chemicals, New Brunswick, NJ) was added. The reaction mixture was immersed in boiling water for 15 mins, allowed to cool, and sample absorbances were read at 570 nm. A standard curve comprised of known concentrations of soluble  $\alpha$ -elastin in sodium citrate buffer (0.1 M, pH 5.0) was used to determine the elastin content of each sample.

### *3.3.11 Statistical Analysis*

All experiments were performed minimally in triplicate. Error bars indicate standard deviation, and statistical analysis was performed using a single factor ANOVA;  $p$ -values  $< 0.05$  were considered to be significant.

## **3.4 Results**

### *3.4.1 Grafting Efficiencies of Peptides on PEG-DA Surfaces*

A grafting efficiency of  $4.3 \pm 0.11\%$  for was achieved PEG-RGDS (Figure 3.2), and this result was comparable to the values reported by Hahn et al. [82]. Further, grafting efficiencies of  $2 \pm 0.15\%$  and  $1.1 \pm 0.07\%$  were achieved for PEG-EM19 and

PEG-EM23, respectively. The lower grafting efficiencies of PEG-EM19 and PEG-EM23 are likely due to their longer peptide chain lengths and coiled formations reducing the grafting efficiency.

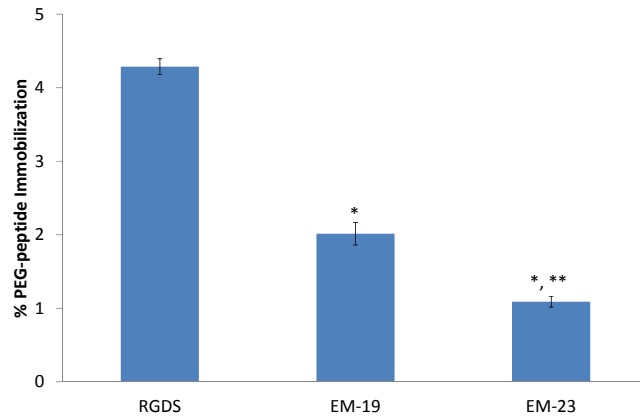


**Figure 3.2.** Grafting efficiencies of PEG-EM19 and PEG-EM23 in comparison to PEG-RGDS. Grafting efficiencies of PEG-EM19 and PEG-EM23 were significantly lower than PEG-RGDS, suggesting that the longer peptide chains may be sterically hindered in the immobilization of the peptide onto the PEG-DA surface. (n = 3-5; \* $p < 0.05$  from PEG-RGDS; \*\* $p < 0.05$  from PEG-EM19).

### 3.4.2 Cell Adhesion on PEG-peptide Hydrogels

SMC adhesion after 12 hours increased to  $1280 \pm 139\%$ ,  $632 \pm 23\%$ ,  $7065 \pm 301\%$ , and  $1287 \pm 134\%$  on PEG-RGDS, PEG-EM19, PEG-EM23, and PEG-EM23S modified surfaces at  $5 \mu\text{mol}$  in comparison to unmodified PEG-DA hydrogels, respectively (Figure 3.3). As expected, no significant differences were observed in cell adhesion over PEG-EM19S modified surfaces in comparison to PEG-DA gels.

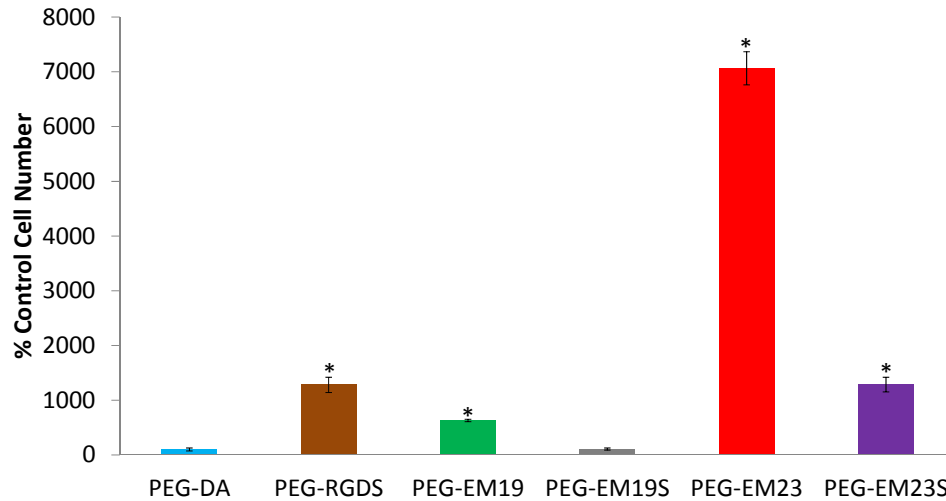


**Figure 3.3.** SMC adhesion on PEG-peptide surface at 5  $\mu\text{mol}$  after 12 hours. All conditions except for EM-19S were able to significantly increase SMC adhesion over PEG-DA. (n = 3-5; \* $p < 0.05$  compared to PEG-DA).

After 48 hours, all PEG-peptide moieties except EM-19S were able to significantly increase SMC adhesion compared to PEG-DA hydrogels (Figure 3.4). PEG-RGDS grafted surfaces increased SMC adhesion to  $424 \pm 17.7\%$ ,  $649 \pm 52\%$ ,  $835 \pm 235\%$ , and  $437 \pm 254\%$  in comparison to PEG-DA hydrogels at 0.01, 0.1, 1, and 5  $\mu\text{mol}$ , respectively. SMC adhesion on PEG-EM23S modified surfaces were comparable to PEG-RGDS at lower concentrations, measuring  $484 \pm 37\%$  and  $492 \pm 52\%$  in comparison to PEG-DA hydrogels at 0.01 and 0.1  $\mu\text{mol}$ , respectively. At the higher PEG-EM23S concentrations, SMC adhesion increased to  $1142 \pm 84\%$  and  $836 \pm 56\%$  in comparison to PEG-DA hydrogels at 1 and 5  $\mu\text{mol}$ , respectively. SMC adhesion between PEG-RGDS and PEG-EM23S was not statistically significant except the highest peptide concentration (i.e. 5  $\mu\text{mol}$ ).

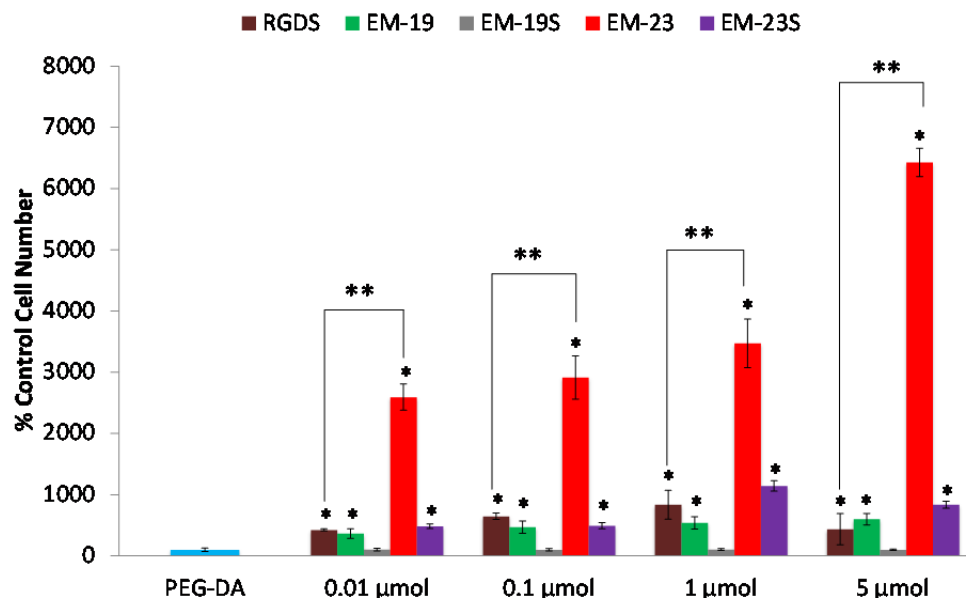


**Figure 3.4.** The number of adherent SMCs on PEG hydrogels grafted with RGDS, EM-19, EM-19S, EM-23, and EM-23S at various concentrations was observed 48 hours after seeding cells. All PEG-peptide moieties were able to significantly increase SMC adhesion at all concentrations when compared to PEG-DA. PEG-EM23, which utilizes both the  $\alpha_v\beta_3$  and the EBP binding motifs, had the highest impact on SMC adhesion even at lower concentrations ( $n = 3-5$ ;  $*p < 0.05$  compared to PEG-DA,  $**p < 0.0002$  compared to PEG-RGDS).

In the presence of PEG-EM19, SMC adhesion increased to  $365 \pm 78\%$ ,  $470 \pm 100\%$ ,  $540 \pm 101\%$ , and  $600 \pm 93\%$  in comparison to PEG-DA hydrogels at 0.01, 0.1, 1, and 5  $\mu\text{mol}$ , respectively. PEG-EM19S, on the other hand, did not stimulate any increases in SMC adhesion at any concentrations. Remarkably, PEG-EM23 had the most impact on SMC adhesion at all concentrations grafted onto the PEG-DA surface. SMC adhesion increased to  $2600 \pm 214\%$ ,  $2914 \pm 352\%$ ,  $3471 \pm 396\%$ , and  $6427 \pm 235\%$  in comparison to PEG-DA hydrogels at 0.01, 0.1, 1, and 5  $\mu\text{mol}$ , respectively.

### 3.4.3 SMC Spreading on PEG-peptide Surfaces

For all three peptides, cell spreading was a function of peptide concentration, and SMC spreading increased with increasing PEG-peptide concentration (Figure 3.5). On PEG-RGDS modified hydrogel surfaces, SMC spreading increased to  $11 \pm 2\%$ ,  $54 \pm 8\%$ ,  $72 \pm 9\%$ , and  $99 \pm 4\%$  of the TCPS control at 0.01, 0.1, 1, and 5  $\mu\text{mol}$ , respectively. On

the other hand, PEG-EM19 facilitated SMC spreading to  $40 \pm 4\%$ ,  $63 \pm 4\%$ ,  $77 \pm 5\%$ , and  $95 \pm 6\%$  of the TCPS control at 0.01, 0.1, 1, and 5  $\mu\text{mol}$ , respectively. Similarly, PEG-EM23 also facilitated SMC spreading to  $42 \pm 5\%$ ,  $74 \pm 4\%$ ,  $85 \pm 6\%$ , and  $97 \pm 5\%$  of the TCPS control at 0.01, 0.1, 1, and 5  $\mu\text{mol}$ , respectively.

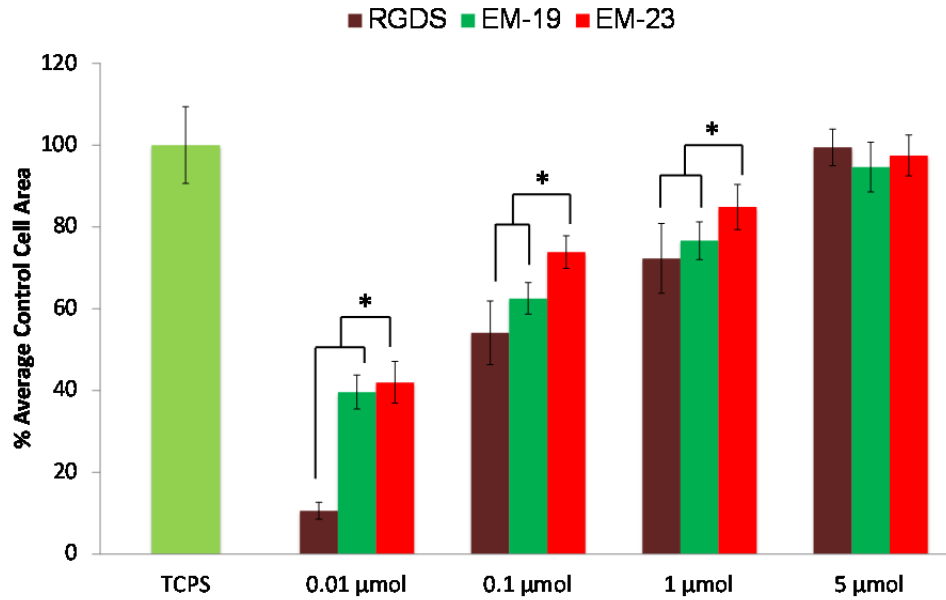


**Figure 3.5.** SMC spreading on PEG hydrogels grafted with RGDS, EM-19, and EM-23 at different concentrations was also observed after 48 hours. PEG-EM19 and PEG-EM23 both had significant impacts on cell spreading in comparison to PEG-RGDS at lower concentrations. In all cases, cell spreading increased to the levels of TCPS at the highest PEG-peptide concentration ( $n = 8$ ;  $*p < 0.05$  compared to PEG-RGDS).

#### 3.4.4 Quantifying and Visualizing Cell Viability on PEG-peptide Surfaces

Cell viability was also a function of peptide concentration; increasing the PEG-peptide concentration grafted onto the hydrogel surface increased the SMC viability (Figure 3.6A). For all peptides, the 5  $\mu\text{mol}$  condition gave the highest cell viability, with  $87.6 \pm 3.6\%$ ,  $92.1 \pm 1.9\%$ , and  $94 \pm 1.7\%$  of the TCPS values for PEG-RGDS, PEG-EM19, and PEG-EM23 respectively. Furthermore, the amounts of cell adhesion, spreading, and viability were visually confirmed in Figure 3.6B. EM-23 at 5  $\mu\text{mol}$  showed the most

significant amounts of SMC adhesion, spreading, and viability compared to the other peptides.

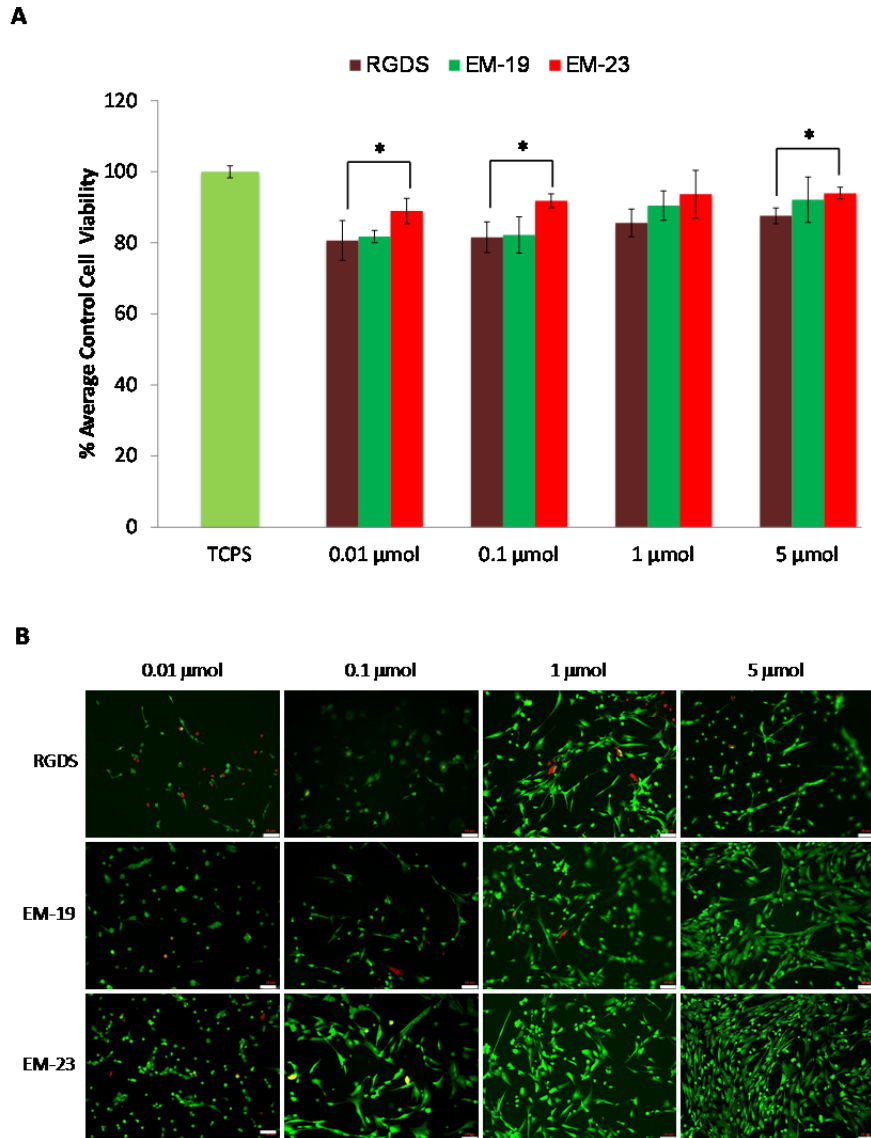


**Figure 3.6.** A) Quantitative assessment of SMC viability on PEG hydrogels grafted with RGDS, EM-19, and EM-23 at various concentrations was observed using a fluorescent Live/Dead viability stain. Cell viability increased with increasing PEG-peptide concentration; the highest viability for each PEG-grafted peptide was achieved at the 5  $\mu\text{mol}$  concentration ( $n = 4-5$ ;  $*p < 0.05$  compared to PEG-RGDS). B) Fluorescent images of SMC adhesion on different PEG-DA hydrogels grafted with RGDS, EM-19, and EM-23 show the extent of cell viability adhesion and spreading. Green fluorescence is indicative of viable cells, whereas red fluorescence is indicative of dead cells. Cells were fully spread to the levels of the control at the highest PEG-peptide concentration with PEG-EM23 showing the greatest amount of SMC adhesion, viability, and spreading. Scale bar represents 10  $\mu\text{m}$ .

### 3.4.5 Quantifying Elastin Deposition over PEG-peptide Surfaces.

PEG-RGDS, PEG-EM19, and PEG-EM23S stimulated elastin production to approximately  $64 \pm 12\%$ ,  $69 \pm 10\%$ ,  $45 \pm 11\%$  of the TCPS control, respectively (Figure 3.7). However, PEG-EM23 was able to promote comparable elastin deposition to TCPS, even though TCPS had  $\sim 4.5$  more cells adhered than PEG-EM23 (elastin production increased by  $35 \pm 28\%$  compared to TCPS).

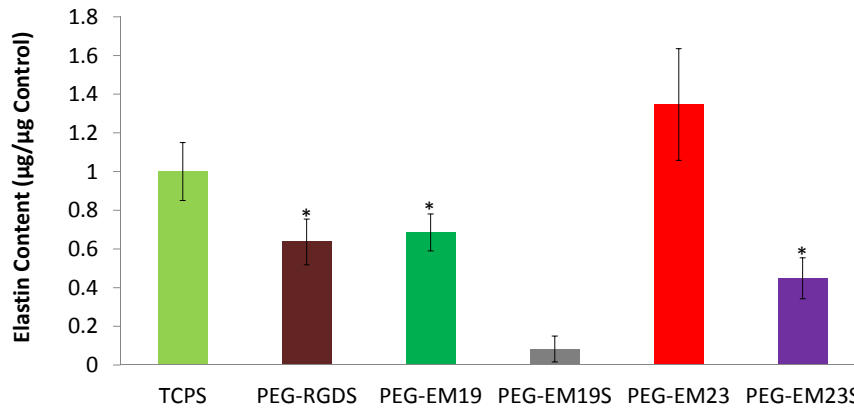


**Figure 3.7.** Elastin content from different PEG-peptides grafted on PEG hydrogels at 5  $\mu\text{mol}$ . PEG-EM23 had comparable elastin deposition as TCPS suggesting the ability of the peptide to utilize importance the two binding motifs for  $\alpha_v\beta_3$  and the EBP in elastin fiber assembly. PEG-EM19S and PEG-EM23S had elastin and desmosine levels comparable to PEG-DA and PEG-RGDS, respectively (n = 3-4; \* $p < 0.05$  compared to TCPS).

## 3.5 Discussion

The next step in characterizing the elastin mimetic peptides was to physically immobilize them onto the surface of a PEG-DA hydrogel and evaluate the efficacy of the peptides to promote SMC adhesion, spreading, viability, and elastin deposition on the synthetic substrate. In order to immobilize a peptide onto the surface of the hydrogel, the peptides were first reacted with a monoacrylate PEG derivative to yield an acrylate-PEG-peptide moiety. The monoacrylate group on the PEG-peptide copolymer reacts with

the free acrylates present on the surface of the PEG-DA hydrogel, conjugating the peptide onto the surface.

For the studies discussed in this chapter, PEG-SVA at 3400 g/mol was used as the conjugating polymer. The succinimide ester on PEG-SVA is highly reactive and under basic conditions (pH 8.5), the ester group reacts with nucleophiles, such as free amines on peptides, to form an acylated product (Figure 3.8) [191].

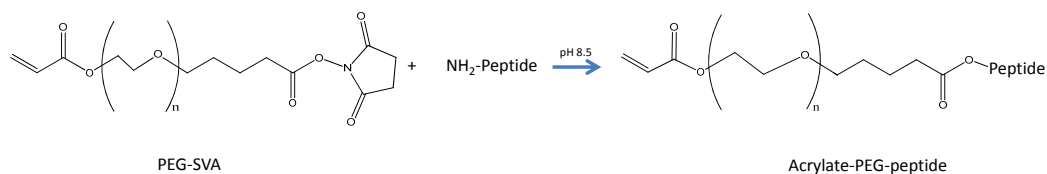


**Figure 3.8.** Reaction of PEG-SVA with a peptide bearing a free amine. The succinimide ester on PEG-SVA undergoes a substitution reaction with a free amine on the peptide giving a monoacylated-PEG-peptide moiety.

Reactions with either primary or secondary amines on peptides create stable amide linkages that do not readily break down [191, 211]. Previous work has suggested that the PEG spacer at 3400 g/mol allows the conjugated peptide on the PEG-peptide moiety to move flexibly, permitting cell spreading and adhesion [191, 211].

After PEG-SVA was conjugated to the elastin mimetic peptides, the grafting efficiency of different PEG-peptide moieties on the surfaces of PEG-DA hydrogels was determined using the Ninhydrin reagent. The amount of PEG-EM19 and PEG-EM23 grafted onto hydrogels was significantly lower than that of PEG-RGDS. Grafting efficiencies of PEG-EM19 and PEG-EM23 were likely lower due to the longer peptide chains causing steric hindrance during the grafting procedure. Moreover, each elastin mimetic peptide has more than one free amine that could react with PEG-SVA. However, GPC results suggested that coupling of PEG-SVA with the peptide occurred at a 1:1 mole

ratio and no side reactions occurred during the coupling process (see Appendix, Figures A.1 and A.2).

SMC adhesion was quantified after 12 hours on different PEG-peptide modified surfaces at 5  $\mu\text{mol}$  over PEG-DA hydrogels. PEG-RGDS served as a positive control. All of the peptides except EM-19S were able to significantly increase SMC adhesion over PEG-DA hydrogels. EM-23, on the other hand, had the highest impact on SMC adhesion. A similar trend in SMC adhesion was also observed after 48 hours; although higher amounts of cell adhesion were observed after 12 hours on PEG-RGDS, PEG-EM23, and PEG-EM23S grafted surfaces. This result suggests that the peptides may primarily serve as cell adhesion motifs, while not promoting cell proliferation.

As expected, all of the peptides besides PEG-EM19S were able to significantly increase SMC adhesion after 48 hours compared to PEG-DA hydrogels. SMC adhesion on PEG-EM23S surfaces was comparable to PEG-RGDS, suggesting that the longer peptide chains do not interfere with cell adhesion. More importantly, PEG-EM23 had the highest impact on SMC adhesion even though the conjugation efficiency was four times lower than that of PEG-RGDS and approximately half that of PEG-EM19. This dramatic increase in cell adhesion and growth is indicative of a highly synergistic relationship between the EBP and  $\alpha_v\beta_3$  integrins in facilitating cell adhesion to the PEG-DA hydrogel. Bax et al. have shown that the C-terminus of tropoelastin interacts with the  $\alpha_v\beta_3$  integrin and numerous other studies have also confirmed this phenomenon (Figure 3.9) [122, 130, 155, 176]. Through EM-19, specific cell adhesion on a PEG-DA surface was tailored via the interaction between the EBP and VGVAPG. However, the results suggested that more

significant cell adhesion on a hydrogel surface was achieved by utilizing both the RGDS and VGVAPG domains to interact with the  $\alpha_v\beta_3$  integrin and the EBP, respectively.

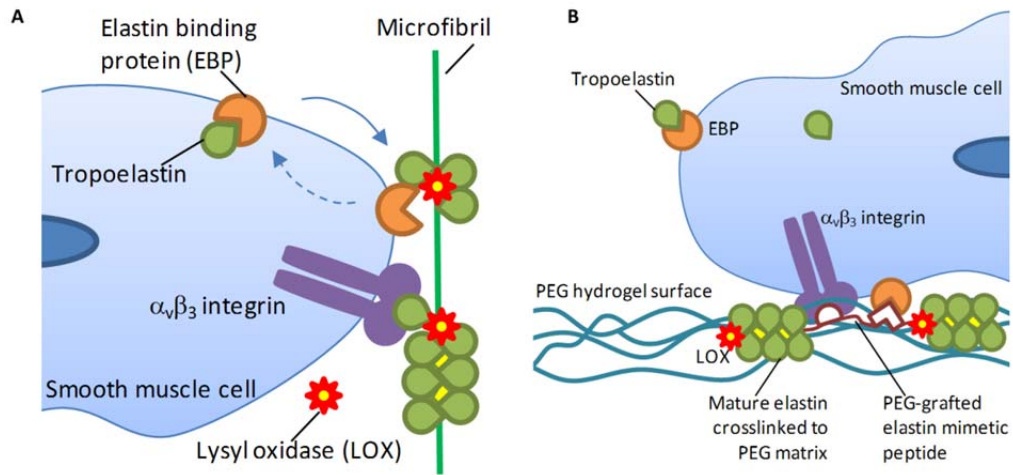


**Figure 3.9.** A ) Elastic fiber assembly is a complex mechanism involving intracellular transport of tropoelastin to the cell surface receptor known as EBP. The EBP transports the protein to adjacent microfibrils for crosslinking by cell-secreted LOX after which the EBP is recycled to repeat the process. Recent discoveries have shown that the C-terminus of tropoelastin interacts with the integrin  $\alpha_v\beta_3$  which also plays an important, yet unknown role in elastin fiber assembly [155-158]. B) PEG-DA hydrogels tailored with bioactive peptides which utilize the  $\alpha_v\beta_3$  and the EBP binding motifs approximates the complex mechanism for elastin fiber assembly occurring in vivo. This direct translation results in mature elastin crosslinked to the PEG matrix from a network of cell secreted tropoelastin and PEG-grafted elastin mimetic peptide.

Moreover, increased SMC adhesion was observed on EM-23 grafted surfaces compared to previously published results which have shown SMC adhesion to a lesser extent on different synthetic substrates. For example, Mann et al. modified glass surfaces with VGVAPG and found a 200% increase in SMC adhesion over unmodified glass surfaces [212]. Further, Rashid et al. fabricated vascular grafts from PUs and fibronectin and observed an increase in SMC attachment by 11% in comparison to bare PU grafts after 8 hours [62]. In a separate study, Miller et al. modified poly(lactic-co-glycolic-acid) (PLGA) with NaOH for vascular graft applications and observed a 16% increase in SMC adhesion after 3 days over untreated PLGA scaffolds [213]. The results suggest that EM-

23, which showed a 6000% increase in SMC adhesion over the controls, may be an extremely promising candidate for engineering vascular grafts.

Furthermore, cell spreading on PEG-RGDS, PEG-EM19, and PEG-EM23 grafted surfaces was quantified using ImageJ software. For all three peptides, cell area was a function of peptide concentration, and an increase in PEG-peptide concentration resulted in an increase in cell area. Although all peptides were able to stimulate cell spreading comparable to TCPS, EM-23 at the lowest concentration had a more significant impact on cell spreading than PEG-RGDS and PEG-EM19. This result suggests that the VGVAPG and the RGDS sequence in EM-23 synergistically serve to promote SMC spreading.

Fluorescence staining was also used to quantify cell viability and visually characterize cell adhesion, spreading, and viability at different PEG-peptide concentrations. Cells on PEG-DA gels did not show any spreading and the staining protocol left no visible cells intact on the hydrogel surface. Cell viability was again found to have a similar trend when compared to cell spreading; an increase in PEG-peptide concentration increased the SMC viability. Visually depicting cell adhesion, viability, and spreading reconfirmed the initial characterization studies in which PEG-EM23 was found to have the most impact on the aforementioned phenomenon. This result is also consistent with previous work in which Gobin et al. achieved highest SMC spreading on a PEG-DA hydrogel surface modified with the VAPG peptide sequence at 5  $\mu\text{mol/mL}$  of PEG-peptide solution [86].

Elastin deposition was quantified after 48 hours on PEG-DA surfaces modified with PEG-RGDS, PEG-EM19, PEG-EM19S, PEG-EM23, and PEG-EM23S at 5  $\mu\text{mol}$ .

Desmosine production was also quantified after 48 hours; however, the PEG chain heavily interfered with the desmosine ELISA (protocol discussed in Chapter 2), showing no feasible results. PEG-RGDS, PEG-EM19, and PEG-EM23S slightly increased elastin deposition while PEG-EM23 had comparable elastin deposition to TCPS. This result suggested that by utilizing the  $\alpha_v\beta_3$  integrins and the EBP receptors, EM-23 may be able to translate the complex mechanism of elastin fiber assembly to the PEG-DA surface.

### **3.6 Conclusion**

The work in this chapter suggests that the synergy between  $\alpha_v\beta_3$  and the EBP in elastin fiber assembly may be translated and utilized in promoting SMC adhesion, spreading, viability, and elastin deposition on a synthetic substrate. These results further suggest that EM-23 may be a potential candidate for engineering viable vascular grafts because of its efficacy in increasing cell adhesion and elastin deposition. By utilizing key receptors, EM-23 is able to surpass an RGDS-based cell adhesive material to stimulate elastin production and may be a promising alternative scaffold for engineering vascular tissues.

## Chapter 4

### EM-23 as a 3D Template for Promoting Vascular ECM Deposition

#### 4.1 Summary

This chapter characterizes the capability of EM-23 to serve as a 3D template for promoting elastin production. EM-23 was conjugated to acrylate-PEG-*N*-hydroxysuccinimide (PEG-NHS) to yield an acrylate-PEG-EM23-PEG-acrylate (PEG-23-PEG) copolymer. The copolymer was crosslinked in the presence of a photoinitiator and UV light to form hydrogels comprised entirely of EM-23. Moreover, a degradable sequence, (DS; AAAAAAAAAAK), was also engineered and conjugated to PEG-NHS to allow for matrix remodeling over time in the presence of SMCs. Characterization studies were conducted on various combinations of PEG-23-PEG, PEG-DS-PEG, and PEG-DA. The 3D characterization discussed in this chapter suggested that EM-23 is a promising template for promoting elastin production in 3D over time, while also allowing scaffold remodeling and increased mechanical properties. Chapters 2 and 3 of this thesis discussed in detail the efficacy of EM-23 to promote and translate the complex mechanism of elastin fiber assembly to a synthetic construct.

#### 4.2 Introduction

Hydrogels are a swollen network of polymer crosslinks that serve as 3D ECM mimics, and tailoring them with a bioactive moiety can provide a suitable microenvironment for cell growth [67, 73]. Specifically, PEG-DA hydrogels were chosen as the synthetic material for vascular graft applications because of their ability to fine-tune their mechanical properties by simply changing the molecular weight of the PEG

chains [23, 82, 84-86, 214]. Although, PEG-DA hydrogels lack the capabilities to promote ECM deposition, they can be easily tailored with bioactive moieties that promote ECM deposition and cell growth [82, 86, 206]. Previous work has also shown that PEG-DA (MW 10 kDa) at a concentration of 10 wt% in solution possesses the correct mesh size for vascular graft applications [81]. As such, hydrogels comprised of EM-23 were engineered to assess the ability of the peptide to promote ECM deposition in 3D. Preliminary characterization suggested that EM-23 may serve as a potential template for promoting vascular ECM deposition in 3D and the results are indicative in suggesting EM-23 as a promising candidate for vascular graft applications.

## **4.3 Materials and Methods**

### *4.3.1 Peptide Synthesis*

All materials and reagents required for peptide synthesis were purchased from AAPPTec (Louisville, KY). Peptides were synthesized using standard solid-phase peptide synthesis protocols [87, 88]. Briefly, four different peptides were synthesized using standard HBTU coupling and Fmoc protection chemistry on an Apex 396 peptide synthesizer (AAPPTec; Louisville, KY) using a lysine-conjugated Wang resin. A 23 amino acid sequence (EM-23; AAKAAKVGVAPGRGDSAAKAAKK), containing two cell adhesion motifs (VGVAPG and RGDS) as well as lysine and alanine -rich crosslinking domains, was synthesized along with a 23 amino acid control peptide in which the VGVAPG sequence is scrambled and the RGDS sequence is left intact (EM-23S; AAKAAKVGVPAGRGDSAAKAAKK). Two additional control sequences were also engineered where the RGDS motif on EM-23 was changed to RGES (EM-23SR;

AAKAAKVGVAPGRGESAAKAAKK) and the VGVAPG and RGDS motifs were collectively scrambled and changed to VGVPAG and RGES, respectively (EM-23X; AAKAAKVGVPAGRGESAAKAAKK). All control sequences, EM-23S, EM-23SR, and EM-23X, were engineered to evaluate the importance of VGVAPG and RGDS to promote elastin fiber assembly in 3D. Moreover, a degradable sequence (DS; AAAAAAAAAAK) was also engineered to help remodel the hydrogel matrix. Crude peptides were then cleaved from the resin with cleaving cocktail (95% trifluoroacetic acid, 2.5% water, 2.5% triisopropylsilane) and purified by dialysis using cellulose ester membrane tubing (MWCO 1000; Spectrum laboratories, Rancho Dominguez, CA). The dialyzed peptides were then frozen and lyophilized overnight. Peptides were characterized using mass spectrometry.

#### *4.3.2 Cell Culture and Maintenance*

Human aortic smooth muscle cells (SMCs, passages 3-5; Invitrogen Inc., Carlsbad, CA), were used. SMCs were maintained in Medium 231 (Invitrogen Inc., Carlsbad, CA) supplemented with smooth muscle cell growth supplement (SMGS, Invitrogen Inc., Carlsbad, CA), 2 mM L-glutamine, 1 unit/ml penicillin, and 100 mg/l streptomycin (GPS; Cellgro, Manassas, VA) at 37°C in a 5% CO<sub>2</sub> environment.

#### *4.3.3 PEG-DA Synthesis*

Synthesis of PEG-DA was conducted using well established protocols [81, 87, 88, 209, 215]. PEG-DA was synthesized by dissolving 24 g dry PEG (MW: 10000; Fluka, Milwaukee, WI) in 20 ml anhydrous DCM with an equimolar amount of triethylamine and 0.869 g acryloyl chloride (Lancaster Synthesis, Windham, NH) added dropwise. The mixture was stirred under argon for 24 hours, washed with 2M K<sub>2</sub>CO<sub>3</sub>, and separated into

aqueous and DCM phases to remove HCl. The mixture was then centrifuged at  $2,000\times g$  for 1 hour and the aqueous phase aspirated and discarded. PEG-DA was then precipitated in diethyl ether, filtered, and dried under vacuum at room temperature overnight. The resulting polymer was dialyzed overnight against DI water with 5 kDa MWCO cellulose ester tubing (Spectrum Laboratories, Rancho Dominguez, CA) to remove any residual salts.

#### *4.3.4 Synthesis of PEG-peptide Copolymers*

Each peptide was conjugated to acrylate-PEG-*N*-hydroxysuccinimide (PEG-NHS, MW 5 kDa; Jenkem Technology, Allen, TX) in 50 mM sodium bicarbonate buffer (pH 8.5) at a 1:2 mole ratio for 2 hours (protected from light and under Argon) to yield a PEG-peptide-PEG copolymer. The final molecular weight of the copolymer was approximately 12 kDa. The mixture was then dialyzed (10000 MWCO dialysis cassettes; Pierce Biotechnology, Rockford, IL) against deionized water for 2 hours, lyophilized, and stored at  $-80^{\circ}\text{C}$ . UV-Vis spectroscopy and GPC equipped with UV and ELS detectors (Agilent Technologies, Inc., Santa Clara, CA) were used to determine the coupling efficiency. The final PEG-peptide-PEG moiety was also characterized via mass spectrometry.

Control peptides, EM-23S, EM-23SR, and EM-23X, were also reacted at a 1:2 mole ratio with PEG-NHS in the manner described above. The control peptides have different binding motifs that are scrambled and were included to observe the importance of VGVAPG and RGDS in promoting elastin fiber assembly in 3D. Mass spectrometry results indicated that one mole of PEG-NHS reacted with DS or EM-23S while no detectable reaction occurred between the polymer and EM-23SR, or EM-23X (See

Appendix, Figures A.4, A.5, A.6, and A.7). A possible explanation for this observation is that the abundant alanine domains in DS and scrambled domains in the control peptides may be forcing the peptide to fold into different conformations while in solution.

Although a reaction between PEG-NHS and the control peptides may be occurring to a certain extent, but to a lesser degree than EM-23.

#### *4.3.5 Hydrogel Degradation Studies*

Hydrogels with different combinations of PEG-23-PG, PEG-DS-PEG, and PEG-DA were synthesized, and their ability to degrade in the presence of elastase, one of many enzymes that cleave elastin, was evaluated. Four different polymer combinations were made and are listed in Table 4.1. The first polymeric gel, A, consisted entirely of PEG-23-PEG while the second combination, B, consisted of an even mixture of PEG-23-PEG and PEG-DS-PEG. The third, C, and fourth, D, polymer combinations consisted of different ratios of PEG-23-PEG, PEG-DS-PEG, and PEG-DA. The different polymeric combinations were kept at 10 wt% in solution.

Each combination was dissolved in 10 mM HEPES buffer (pH 7.4) followed by the addition of 10  $\mu$ l/mL of the photoinitiator DMAP (Alfa Aesar, Ward Hill, MA) in NVP (300 mg/mL). This precursor solution was added to FlexWell incubation chambers (Grace Bio-Labs, Bend, OR) and subsequently polymerized via UV light for 1 min (365 nm, 10 mW/cm<sup>2</sup>), yielding gels that were 6.8 mm wide and 3 mm thick.

**Table 4.1.** Four different hydrogel formulations were made comprised of varying ratios of PEG-23-PEG, PEG-DS-PEG, and PEG-DA. The final copolymer concentration was kept at 10 wt%.

Formulation	Ratios of Each Polymer		
	PEG-23-PEG	PEG-DS-PEG	PEG-DA
<b>A</b>	100	0	0
<b>B</b>	50	50	0
<b>C</b>	50	30	20
<b>D</b>	50	10	40

The polymerized hydrogels were carefully transferred to glass vials and their initial weights were measured. Different concentrations of porcine pancreatic elastase (Elastin Productions Company, Owensville, MO) in PBS at 0.1, 1, and 2 mg/ml were added to the samples and placed in a 37°C incubator. After each time point, the enzyme solution was aspirated, the gels were rinsed thoroughly with PBS, and the hydrogel weight was measured. The gels were again replenished with fresh enzyme solution. As controls, each polymer combination was incubated with only PBS and the hydrogel weights were measured in a similar manner described above.

#### *4.3.6 Cell Encapsulation*

Each polymeric gel formulation was dissolved in 10 mM HEPES buffer (pH 7.4) and sterile-filtered using 0.2- $\mu$ m pore size nylon filters (Pall Life Sciences, Port Washington, NY). To these solutions, SMCs at a concentration of 250,000 cells/mL were added, followed by the addition of 10  $\mu$ l/mL of the photoinitiator DMAP (Alfa Aesar, Ward Hill, MA) in NVP (300 mg/mL). These precursor solutions were added to FlexWell incubation chambers (Grace Bio-Labs, Bend, OR) and subsequently

polymerized via UV light for 1 min (365 nm, 10 mW/cm<sup>2</sup>), yielding gels that were 6.8 mm wide and 3 mm thick. The gels were thoroughly rinsed with PBS and carefully transferred to a 24 well plate and incubated with media. SMC media was replenished every 2 days. Rat tail type I collagen (BD Biosciences, San Jose, California) was used as a positive control. The acidic collagen solution was neutralized using sterile 1 M NaOH and combined with enough SMC media and PBS such that the final collagen concentration would be at 2 mg/mL. To this solution, SMCs at 250,000 cells/mL were added and the collagen gel was allowed to polymerize for 1 hour in a 37°C incubator, which physically encapsulated the SMCs. SMC media was added after the collagen gelled completely and the media was replenished every 2 days. Similar polymeric gel formulations with the control PEG-peptide-PEG copolymers were also made. However, the control copolymers, PEG-23S-PEG, PEG-23SR-PEG, and PEG-23X-PEG, only gelled at the last polymer combination (i.e. the 50:10:40 ratio), and hence this formulation was used for all control experiments. PEG-DA gels as well as SMC encapsulated PEG-DA gels further served as controls.

#### *4.3.7 Biochemical Analysis of PEG-peptide-PEG hydrogels*

After 2, 7, 14, and 21 days, elastin and collagen content were quantified. At each time point, the media was removed and rinsed with PBS. The gels were hydrolyzed with 0.1 N NaOH for 24 hours in a 37°C incubator. The samples were then transferred to a 100°C oven for 2 hours to further solubilize ECM matrix proteins other than elastin. The digested samples were centrifuged at 8,000×g for 10 min; the resultant pellets and supernatant were subjected to analysis for elastin and collagen content, respectively.

The amount of elastin in the resulting pellet after the initial hydrolysis was determined using the Ninhydrin reagent. The collected protein pellets were further subjected to acid hydrolysis using 6 N HCl at 100°C for 24 hours. The digested samples were then neutralized, freeze-dried, and resuspended in 1 mL sodium citrate buffer (0.1 M, pH 5.0). To this suspension, 1 ml of Ninhydrin reagent (Spectrum Chemicals, New Brunswick, NJ) was added. The reaction mixture was immersed in boiling water for 15 mins, allowed to cool, and sample absorbances were read at 570 nm. A standard curve comprised of known concentrations of soluble  $\alpha$ -elastin in sodium citrate buffer (0.1 M pH 5.0) was used to determine the elastin content of each sample.

The resulting supernatant from the digested samples were subjected to further hydrolysis with 6 N HCl at 110°C for 24 hours. The hydrolyzed samples were neutralized, freeze-dried, and resuspended in 1 mL deionized water. Each sample was then reacted with 69 mM chloramine-T-hydrate (Sigma, St. Louis, MO) at room temperature for 20 mins. The reaction was quenched with 1.17 M (4-dimethylamino)benzaldehyde (Sigma, St. Louis, MO) for 30 mins at 60°C and allowed to cool to room temperature. Sample absorbances were read at 570 nm and hydroxyproline (Sigma, St. Louis, MO) served as a positive control. Total collagen content can be indirectly estimated as 1 mg of hydroxyproline is equivalent to 8 mg of collagen [216].

#### *4.3.8 Hydrogel Compression Testing*

Compression testing on each gel formulation was also conducted over a period of 21 days. Initially, the gels were made into 1 mm thick molds intended for tensile tests. However, due to the inherent weakness of the 100% PEG-23-PEG gel, it could not be mounted properly to conduct tensile tests. Hence, thicker gels were made and the

compressive modulus was determined over a course of 21 days. Gel formulations A, B, and C were chosen for compression testing as they had the greatest effect on stimulating elastin production. The control gel, EM-23X-D, was also included in compression tests because this gel showed elastin production even though no adhesive sequences are present on the peptide sequence.

Each gel formulation was made in the manner described previously in 10 mM HEPES buffer (pH 7.4), and sterile-filtered using 0.2- $\mu$ m pore size nylon filters (Pall Life Sciences, Port Washington, NY). To this solution, SMCs at a concentration of 250,000 cells/mL were added, followed by the addition of 10  $\mu$ l/mL of the photoinitiator DMAP (Alfa Aesar, Ward Hill, MA) in NVP (300 mg/mL). This precursor solution was transferred to a 48 well plate and subsequently polymerized under UV light for 1 min (365 nm, 10 mW/cm<sup>2</sup>). The gels were then rinsed thoroughly with PBS, transferred to a 24 well plate, and incubated with SMC media. The media was replenished every 2 days. Collagen gels served as a positive control and SMCs were encapsulated within the collagen gels in the manner described previously.

After each time point, the gels were rinsed with PBS and mounted on a BOSE EnduraTEC ELF 3200 Axial Testing System (EnduraTEC Systems Corporation, Minnetonka, MN). The gels were then subjected to compression with a load cell of 4.9 N at a compression rate of 0.25 mm/sec until failure. A stress-strain curve for each gel was generated using the following correlations:

$$\varepsilon = \frac{l-l_0}{l_0} \quad (1)$$

$$\sigma = \frac{F}{A_0} \quad (2)$$

The strain ( $\varepsilon$ ) generated for each sample was determined by taking the difference in initial ( $l_0$ ) and final ( $l$ ) thickness and dividing it by the initial thickness (Equation 1). The stress, on the other hand, was determined by taking the force ( $F$ ) generated at each displacement and dividing it by the initial surface area ( $A_0$ ) of each gel (Equation 2). The stress and strain corresponding to each displacement and force was tallied and a stress-strain curve was generated for each gel. From each curve, the slope of the linear portion was determined to be the compressive modulus.

#### 4.3.9 Cell Viability

Cell viability in gel formulations A, B, C, and EM-23X-D was also assessed using a Live/Dead assay (Invitrogen Inc, Carlsbad, CA) after 7 and 21 days. Each gel formulation was made in the manner described above in 10 mM HEPES buffer (pH 7.4) and sterile-filtered using 0.2- $\mu$ m pore size nylon filters (Pall Life Sciences, Port Washington, NY). To this solution, SMCs at a concentration of 250,000 cells/mL were added followed by the addition of 10  $\mu$ l/mL of the photoinitiator DMAP (Alfa Aesar, Ward Hill, MA) in NVP (300 mg/mL). This precursor solution was injected between two glass slides separated by a 400- $\mu$ m spacer (Thermo Scientific, Asheville, NC) and subsequently polymerized via UV light (365 nm, 10 mW/cm<sup>2</sup>). The top glass slide was carefully lifted, the polymerized gel sheet was rinsed thoroughly with PBS, and 10 mm diameter gel samples were carefully cut and transferred to a 24 well plate. SMC media was then added and replenished every 2 days.

After days 7 and 21, the media was removed, and gels were rinsed with PBS. The gels were then incubated with a solution containing 2  $\mu\text{M}$  calcein AM and 4  $\mu\text{M}$  ethidium homodimer-1 for 25 mins at 37°C. The gels were then mounted onto a cover slide and imaged using a Zeiss LSM 510 VIS confocal microscope (Carl Zeiss Microscopy, Thornwood, NY). Initially a 200- $\mu\text{m}$  spacer was utilized to make thin flat gels for confocal microscopy. However, the 100% PEG-23-PEG gels were extremely weak and fell apart. As a result, gels were made using the 400- $\mu\text{m}$  spacer.

#### *4.3.10 Statistical Analysis*

All experiments were performed minimally in triplicate. Error bars indicate standard deviation, and statistical analysis was performed using a single factor ANOVA;  $p$ -values  $< 0.05$  were considered to be significant. Moreover, to determine statistical significance between sample sets for the compression data, a Kruskal-Wallis nonparametric ANOVA test was used. The nonparametric test does not assume the data to be normally distributed and the test is instead performed on ranked data. This allows for an accurate comparison between sample sets that have one nominal variable and one measureable variable.

## **4.4 Results**

### *4.4.1 Gel Degradation in the Presence of Elastase*

In the absence of elastase, each hydrogel formulation continued to swell well past 10 hours (Figure 4.1). However, the different types of gels degraded at different rates in the presence of elastase. Gel formulation A completely degraded within 24 hours for each elastase concentration, whereas gel formulation B showed faster degradation kinetics by

completely degrading within 10 hours. On the other hand, gel formulations C and D did not degrade at any elastase concentration and instead swelled over time. This result suggests that elastase is only able to breakdown the EM-23 and DS components within gels C and D, while the PEG-DA component remained intact. As the peptides are degraded in these gels, more water diffuses into the construct, causing increased swelling.

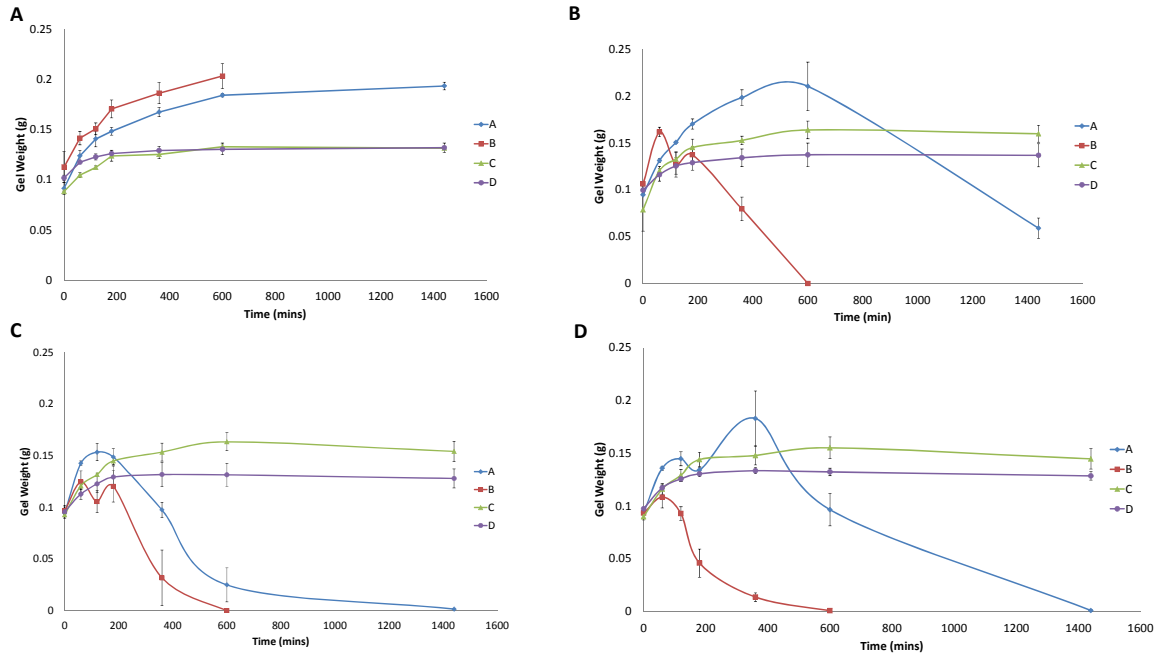


**Figure 4.1.** Gel degradation curves in the presence of elastase at 0 (A), 0.1 (B), 1 (C), and 2 (D) mg/ml. Gel formulation B degrades the most out of all the other formulations at each enzyme concentration (n = 3).

#### 4.4.2 Elastin Content in Peptide Polymerized Hydrogels

In the presence of collagen gels, levels of elastin detected were  $78 \pm 27$ ,  $43 \pm 24$ ,  $38 \pm 27$ , and  $208 \pm 56$   $\mu\text{g}$  at days 2, 7, 14, and 21, respectively (Figure 4.2). Gel formulation A had levels of  $42 \pm 7$ ,  $42 \pm 8$ ,  $99 \pm 16$ , and  $219 \pm 21$   $\mu\text{g}$  at days 2, 7, 14, and 21, respectively. Similarly, gel formulation B had elastin levels of  $44 \pm 7$ ,  $53 \pm 14$ ,  $85 \pm 6$ , and  $192 \pm 26$   $\mu\text{g}$  at days 2, 7, 14, and 21, respectively. Gel formulation C had elastin levels of  $30 \pm 8$ ,  $67 \pm 8$ ,  $105 \pm 3$ , and  $165 \pm 14$   $\mu\text{g}$  at days 2, 7, 14, and 21, respectively.

Finally, in the presence of gel formulation D, elastin levels detected were  $18 \pm 5$ ,  $25 \pm 2$ ,  $139 \pm 11$ , and  $142 \pm 14 \mu\text{g}$  at days 2, 7, 14, and 21, respectively.

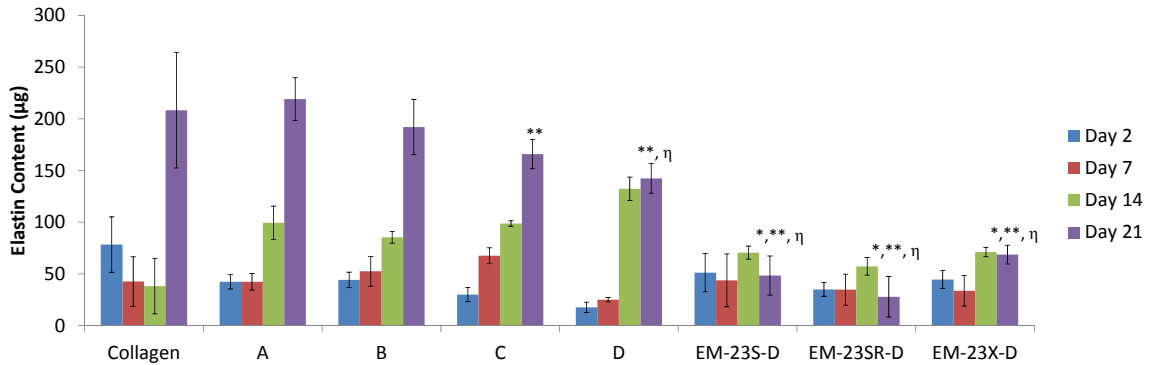


**Figure 4.2.** Elastin content over the course of 21 days in the presence of different PEG-peptide-PEG hydrogels. Gel formulations A, B, C, and D showed comparable elastin production to the positive control of collagen gels after 21 days. The control peptides did not have comparable elastin production to collagen nor the experimental conditions after 21 days. (n=3-5, \* $p < 0.05$  from Collagen; \*\* $p < 0.05$  from gel formulation A;  $\eta p < 0.05$  from gel formulation B).

No statistical significance in elastin production was found between collagen gels at day 21 from gels of A, B, C, and D. However, elastin production was statistically significant between gel A and gels C as well as D. Moreover, elastin production from gels B and D were also statistically significant. Also, from the data presented in Figure 4.1A, the weight of each gel can be approximated to be 0.2 g. Therefore, for each hydrogel, the total elastin content can also be estimated in terms of  $\mu\text{g}$  of elastin per mg of scaffold where after 21 days, elastin content per mg of scaffold is approximately  $1 \pm 0.1$ ,  $1 \pm 0.13$ ,  $0.8 \pm 0.07$ , and  $0.6 \pm 0.3 \mu\text{g}$  elastin/mg of scaffold in gel formulations A, B, C, and D respectively.

Further, the control gel formulations EM-23S-D, EM-23SR-D, and EM-23X-D, had elastin production of only  $48 \pm 19$ ,  $27 \pm 20$ , and  $69 \pm 9 \mu\text{g}$  after 21 days. Elastin production was still observed in gels comprised of EM-23X, although no adhesive motifs are present in the peptide. This phenomenon may be a result of SMCs being trapped within the EM-23X-D gel, which could trigger the cells to secrete ECM proteins.

Previous work has suggested that the least cell adhesive sequence grafted onto the surface of a PEG-DA hydrogel yields the highest ECM deposition, and this phenomenon may translate to this 3D model [205].

#### 4.4.3 Hydroxyproline Content

For each PEG-peptide-PEG gel, the overall hydroxyproline content decreased over time, suggesting collagen degradation by SMCs (Figure 4.3). Quantifying total hydroxyproline content is an indirect estimation of total collagen content, as 1 mg of hydroxyproline is equivalent to 8 mg of collagen. In the presence of gel formulation A, hydroxyproline content detected at days 2, 7, 14, and 21 were  $0.06 \pm 0.01$ ,  $0.17 \pm 0.03$ ,  $0.18 \pm 0.02$ , and  $0.12 \pm 0.03$   $\mu\text{g}$ , respectively. Hydroxyproline content at days 14 and 21 were not significant from each other even though the hydroxyproline levels detected decreased by  $\sim 0.05$   $\mu\text{g}$ . Gel formulation B contained  $0.22 \pm 0.02$ ,  $0.18 \pm 0.05$ ,  $0.21 \pm 0.04$ , and  $0.14 \pm 0.003$   $\mu\text{g}$  of hydroxyproline at days 2, 7, 14, and 21, respectively.

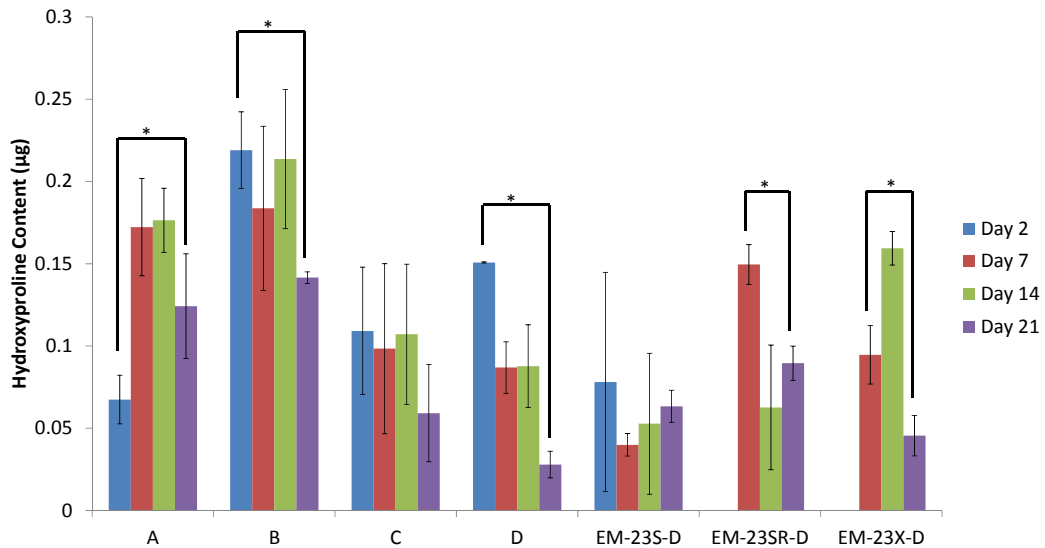


**Figure 4.3.** Hydroxyproline content in the presence of PEG-peptide-PEG hydrogels. Total collagen content can be indirectly calculated by dividing the amount of hydroxyproline content by 0.13. In each hydrogel formulation, hydroxyproline content decreased over time, suggesting collagen degradation. (n = 3-5; \* $p < 0.05$  from days 2 and 21).

A similar trend was also observed with gel formulation C; total hydroxyproline content detected was  $0.11 \pm 0.04$ ,  $0.10 \pm 0.05$ ,  $0.17 \pm 0.04$ , and  $0.06 \pm 0.03$   $\mu\text{g}$  at days 2, 7, 14, and 21, respectively. Finally, gel formulation D had a large increase of  $0.15 \pm 0.004$   $\mu\text{g}$  hydroxyproline observed at day 2 and the levels of hydroxyproline continuously decreased at days 7, 14, and 21 (hydroxyproline levels detected were  $0.09 \pm .016$ ,  $0.09 \pm 0.03$ , and  $0.03 \pm 0.008$   $\mu\text{g}$  after days 7, 14, and 21, respectively). Hydroxyproline levels detected at day 2 and 21 were statistically significant from each other in all gel formulations except C (although gel C shows a similar trend of decreasing hydroxyproline content over time).

The control gel formulations also showed a similar trend as the experimental conditions. In the presence of the EM-23S-D gel formulation, hydroxyproline levels detected were  $0.08 \pm 0.07$ ,  $0.04 \pm 0.006$ ,  $0.05 \pm 0.04$ , and  $0.06 \pm 0.01$   $\mu\text{g}$  at days 2, 7, 14, and 21, respectively. On the other hand, no hydroxyproline content was detected at day 2 for either EM-23SR-D or EM-23X-D gel formulation. In the presence of EM-23SR-D, total hydroxyproline detected was  $0.15 \pm 0.01$ ,  $0.06 \pm 0.04$ , and  $0.09 \pm 0.01$   $\mu\text{g}$  at days 7, 14, and 21, respectively. Finally, hydroxyproline content in the presence of EM-23X-D gels was  $0.09 \pm 0.02$ ,  $0.16 \pm 0.02$ , and  $0.04 \pm 0.01$   $\mu\text{g}$  at days 7, 14, and 21, respectively.

#### *4.4.4 Estimating the Compressive Modulus of Different PEG-peptide-PEG Hydrogels*

The compressive modulus of blank 10 kDA PEG-DA at 10 wt% was determined to be  $106 \pm 5$  kPa (Figure 4.4). Collagen gels, which served as a positive control, showed an increased in compressive Young's Modulus over a course of 21 days (the compressive Young's Modulus calculated was  $7 \pm 2$ ,  $7 \pm 0.2$ ,  $7 \pm 1$ ,  $12 \pm 2$ , and  $13 \pm 2$  kPa at days 0, 2, 7, 14, and 21, respectively).

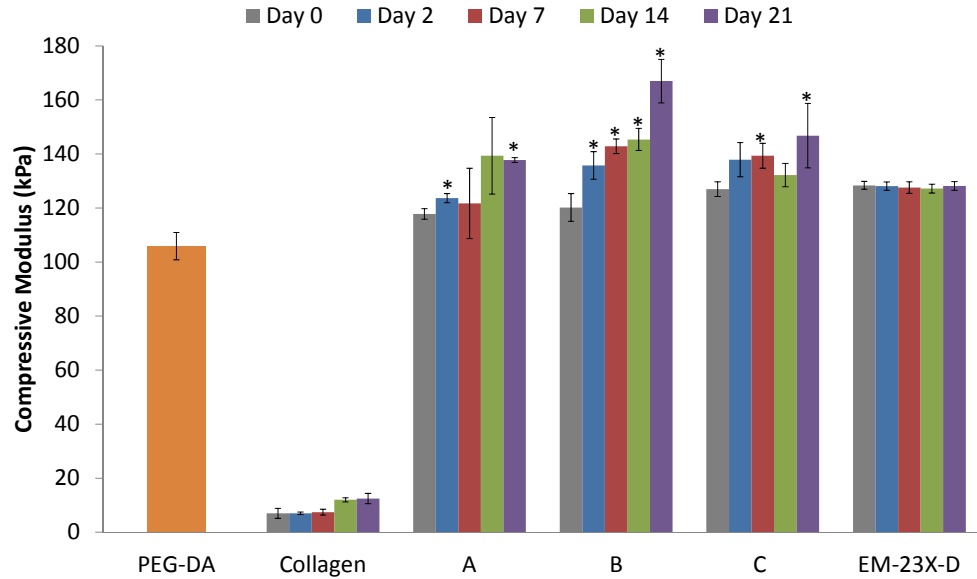


**Figure 4.4.** Estimated compressive modulus of different gel combinations over a course of 21 days. After 21 days of SMC culture, the linear Young's Modulus of each gel combination except EM-23X-D significantly increased from day 0. (n = 3-4; \* $p < 0.05$  from day 0 of each condition).

The compressive modulus for gel formulation A was  $118 \pm 2$ ,  $124 \pm 2$ ,  $122 \pm 13$ ,  $139 \pm 14$ , and  $138 \pm 1$  kPa at days 0, 2, 7, 14, and 21, respectively. Similarly, the compressive modulus for gel formulation B increased over time and was determined to be  $120 \pm 5$ ,  $136 \pm 5$ ,  $143 \pm 3$ ,  $146 \pm 4$ , and  $167 \pm 8$  kPa at days 0, 2, 7, 14, and 21, respectively. Finally, the compressive modulus for gel formulation C was  $127 \pm 3$ ,  $137 \pm 6$ ,  $139 \pm 5$ ,  $132 \pm 4$ , and  $147 \pm 12$  kPa at days 0, 2, 7, 14, and 21 respectively. Gel C showed a higher elastin production than D and hence was chosen for compression testing over gel D (Figure 4.2). The compressive modulus for gel A, B, C, and collagen were statistically significant from day 0 and 21.

The compressive Young's Modulus for the control gel formulation, EM-23X-D, was  $128 \pm 1$ ,  $128 \pm 2$ ,  $127 \pm 2$ ,  $127 \pm 2$ , and  $128 \pm 2$  kPa at days 0, 2, 7, 14, and 21 respectively. No significant difference was observed in the compressive modulus from

day 0 and days 2, 7, 14, and 21 suggesting that the presence of elastin in this control gel may be a result of cells being trapped inside the gel, triggering some ECM formation.

#### 4.4.5 Cell Viability in PEG-peptide-PEG Hydrogels

After 7 and 21 days, SMC viability within the hydrogel formulations of A, B, and C were visually confirmed (Figure 4.5). Visual confirmation of SMC viability over time suggests that the different gel formulations are capable of providing a suitable microenvironment for cell adhesion over time. The control sequence, EM-23X-D, on the other hand did not contain viable cells, which was confirmed by only red fluorescence.

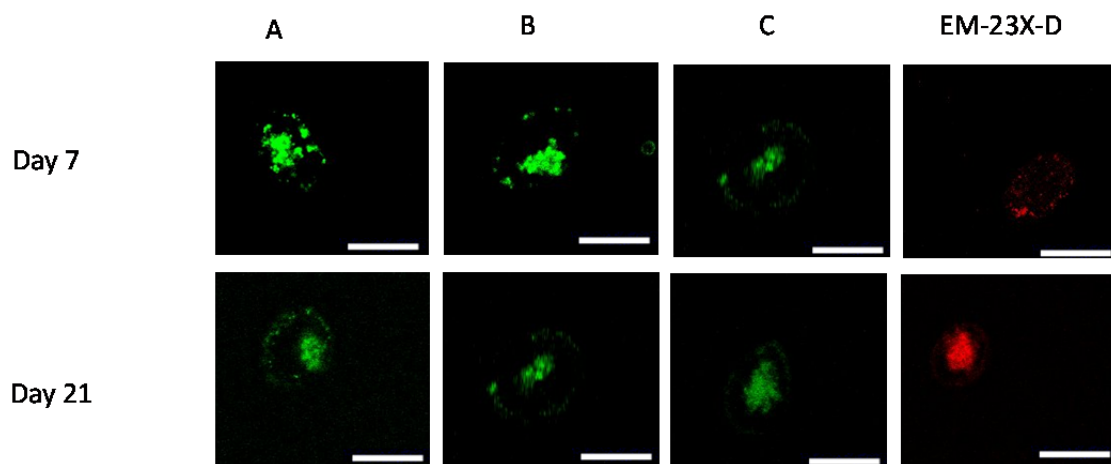


**Figure 4.5.** SMC viability in the presence of different gel formulations at days 7 and 21. Gel formulations A, B, and C had live cells at days 7 and 21 whereas the control gel, EM-23X-D did not show any cell viability at either time point. Scale bar represents 20  $\mu\text{m}$ .

## 4.5 Discussion

The studies detailed in this chapter evaluate the efficacy of EM-23 to promote vascular ECM deposition within a 3D construct for potential vascular graft applications. As such, EM-23 was reacted at a 1:2 mole ratio with PEG-NHS to yield a diacrylated PEG-23-PEG copolymer. The acrylate groups on either end of the copolymer crosslinked to form a 3D hydrogel comprised entirely of EM-23. Moreover, PEG-NHS at 5 kDa was

chosen in order to ensure that the final molecular weight of the copolymer would be close to 10 kDa. Previous studies have confirmed that 10 kDa PEG-DA hydrogels fabricated at 10 wt% are optimum for vascular graft applications [23, 214].

Munoz-Pinto et al. achieved the highest amounts of elastin and collagen production in the presence of SMCs encapsulated with RGDS and 10 kDa PEG-DA hydrogels at 10 wt% in comparison to 20 and 30 wt% [84]. Several other studies have also shown that 10 kDa PEG-DA hydrogels at 10 wt% possess the optimum mesh size for nutrient transport [81, 214]. Therefore, EM-23 was reacted with PEG-NHS at a 1:2 mole ratio to yield a diacrylated product that would be close to 10 kDa (although mass spectrometry analysis suggested that the actual molecular weight was closer to 12 kDa; see Appendix, Figure A.3). A degradable sequence, DS (AAAAAAAAAK), was also reacted with PEG-NHS at a 1:2 mole ratio to yield a PEG-DS-PEG copolymer. This specific sequence is an elastase cleavable sequence, and hence incorporating this copolymer within the 3D construct would be beneficial to allow for ECM remodeling over time [73, 206].

Four different gel formulations were made that consisted of varying amounts of PEG-23-PEG, PEG-DS-PEG, and PEG-DA. The first formulation, A, consisted entirely of PEG-23-PEG whereas the second formulation, B, consisted of an even mixture of PEG-23-PEG and PEG-DS-PEG. The third formulation, C, consisted of a 50:20:30 ratio of PEG-23-PEG:PEG-DS-PEG:PEG-DA while the last formulation, D, consisted of a 50:10:40 ratio of PEG-23-PEG:PEG-DS-PEG:PEG-DA. All of the aforementioned formulations were maintained such that the final copolymer concentration would be at 10 wt%.

Different gel formulations were investigated for their ability to degrade over time in the presence of the cell secreted enzyme elastase. The ability of the gel to degrade can be indicative of how well the cell-deposited ECM can be remodeled during long-term culture. Hence, degradation rates for each gel formulation were determined in the presence of different elastase concentrations. Of note, the elastase concentrations used for this study were much higher than physiological concentrations [217]. However, the higher concentrations allowed for rapid investigation of hydrogel behavior. Gel formulation A, which consisted entirely of PEG-23-PEG, completely degraded in the presence of elastase within 24 hours. Elastase has been shown to cleave a di-alanine amino acid block (i.e. AA) and hence the enzyme was able to cleave EM-23 due to the presence of abundant di-alanine amino acid blocks in the crosslinking moieties of EM-23 [218, 219]. This result also suggests that hydrogels comprised entirely of EM-23 can degrade in addition to promoting vascular ECM deposition. Further, gel formulation B degraded completely within 10 hours in the presence of each elastase concentration. This phenomenon is likely due to the abundance of di-alanine blocks available in the DS and EM-23 sequences.

On the other hand, gel formulations C and D did not degrade and instead showed an increased swelling behavior over time. A possible explanation lies in the ability of elastase to cleave EM-23 and DS, but not the PEG-DA chains. The data suggests that in both C and D gel formulations, the structural integrity of the gels remained intact due to the presence of PEG-DA. As more PEG-23-PEG and PEG-DS-PEG chains degraded, the mesh size of the hydrogel increased, allowing for increased diffusion of water into each construct. This phenomenon resulted in hydrogel swelling instead of degradation, and the

data further suggested that the swelling occurs until equilibrium is reached. Moreover, this data may also imply that ECM remodeling by cells encapsulated within gels C and D could reach a threshold at which PEG-DA chains become the dominant copolymer within the construct.

Further, elastin content in the presence of SMCs was also quantified within the four different gel formulations over a course of 21 days. Rat tail collagen type I was used as a positive control. Elastin content in collagen gels decreased from days 2 to 14, while steeply increasing at day 21. SMCs secrete matrix metalloproteinase-2 (MMP-2) and MMP-9 which actively degrade collagen gels [220-222]. For example Kanda et al. demonstrated SMC invasion through collagen type I lattice by degrading the collagen fibers via MMP-2 and MMP-9 [223]. The current data suggests that once SMCs were encapsulated, the cells degraded the collagen, compacting it over time and the SMCs eventually migrated from the gel to the TCPS surface. Hence, elastin production at days 7 and 14 was lower in comparison to day 2. At day 21, however, most of the gel was completely degraded and a majority of the cells had migrated from the gel and adhered to TCPS. The elastin levels detected likely resulted from all the cells adhered to TCPS; elastin content was also quantified for SMCs seeded on TCPS over 21 days and the total elastin content at day 21 was similar to elastin content from the degraded collagen gels at day 21.

Moreover, gel formulations A, B, C, and D continuously increased elastin deposition over a course of 21 days, and elastin content at day 21 was comparable to elastin content in collagen gels. These results suggest that the gel formulations are able to promote elastin deposition over long culture times. In comparison, Ramamurthi et al.

engineered hyaluronic hydrogels to promote elastin deposition over time. After 4 weeks of static culture, the hyaluronic gels promoted elastin levels that were similar to TCPS, however, a majority of the elastin detected was uncrosslinked and immature [224]. Similarly, Venkataram et al. attempted to stimulate elastin deposition in hyaluronic gels with the addition of transforming growth factor-beta1 (TGF- $\beta$ 1). However, the gels showed poor elastin deposition over the course of 3 weeks [225]. The studies detailed in this chapter suggest that hydrogels comprised of EM-23 can promote elastin deposition over time without the addition of different growth factors. Also, Lee et al. reported values of approximately 90  $\mu$ g of elastin per mg of carotid artery tissue [226]. As an approximation, the results suggested in this chapter indicate that the total elastin content measured was only 1% of the total elastin content found in a native artery. However, the increase in elastin production over 21 days in gels containing EM-23 is highly indicative of the peptide's ability to promote elastin deposition.

The control gel formulations contained elastin levels of approximately half of the total elastin content detected at day 21 in gel formulations A, B, C, and D. The gel formulation EM-23X-D showed elastin production over 21 days even though no cell adhesive motifs are present in EM-23X. This result may be due to SMC entrapment within the gel and in an effort to adhere inside the gels, the cells may be secreting ECM proteins, causing elastin detection.

Hydroxyproline content was also quantified over a course of 21 days in the different gel formulations, including the control copolymers. The amount of hydroxyproline decreased over time within all gel formulations suggesting that significant collagen remodeling may be occurring. As mentioned above, SMCs secrete

active MMP-2 and MMP-9 that continuously degrade collagen and this phenomenon may further help support the decrease in total hydroxyproline content over time. Moreover, in comparison to elastin, collagen is more susceptible to degradation and this effect may be manifesting within the different gels [227].

As further characterization, the compressive modulus for gel formulations A, B, C, and EM-23X-D was determined over a course of 21 days. Collagen gels were again used as the positive control. Initially, the hydrogels were made in 1 mm thick molds intended for tensile tests. However, the gels were too weak and compressive testing was instead done on thicker gels. It should be noted that compressive testing is not as accurate as tensile testing because as the material is compressed, the surface area of that material changes and becomes a function of the force applied on the material. However, previous studies have confirmed that the compressive modulus of 10 kDa PEG-DA hydrogels at 10 wt% is similar to the measured tensile modulus [79, 84]. This result is likely due to the elastic nature of the PEG-DA hydrogels in the strain regime [79]. In addition, cells induce a significant amount of contractile forces during ECM remodeling, and compressive strength is an accurate estimation to determine the mechanical forces experienced by the cells over time [84].

The compressive modulus for 10 kDa PEG-DA hydrogels at 10 wt% was in excellent agreement with previously published results [84, 228, 229]. Collagen gels showed poor compressive modulus until days 14 and 21. The sharp increase in modulus after day 7 is likely a result of collagen degrading and compacting the final scaffold into a stiffer construct. All gel formulations except EM-23X-D showed a significant increase in the compressive modulus after 21 days. This phenomenon suggests that the increase in

compressive modulus could be a result of increased ECM deposition over time [83, 230]. As expected, no change in compressive modulus was observed in the control gel formulation, suggesting that the elastin detected within this gel type may be a result of cell entrapment, which triggers some ECM secretion. Comparatively, gel B had a larger compressive modulus increase between 0 and 21 days suggesting that increased ECM remodeling and deposition may be occurring within this gel.

Moreover, the work presented in this chapter was conducted in static cultures. Previous studies have confirmed large differences in ECM deposition within scaffolds when subjected to static and dynamic conditioning [214, 221, 230]. For example, Song et al. fabricated vascular grafts from poly(trimethylene carbonate) scaffolds and dynamically conditioned them under physiological flow conditions resulting in a maximum tensile strength of  $0.47 \pm 0.06$  MPa (compared to the tensile strength of a native artery of  $1.55 \pm 0.21$  MPa) [231]. Moreover, Gao et al. fabricated vascular grafts from poly(glycerol sebacate) and after dynamically conditioning the grafts for 2 weeks, elastin and collagen deposited were visually comparable to native arteries, although no quantification of elastin content was reported [232]. In a separate study, Syedain et al. fabricated vascular grafts from fibrin, and after dynamically conditioning the grafts, significant improvement was found in mechanical strength over statically cultured grafts [233]. However, the compressive modulus observed for the different gels, except for EM-23X-D, increased by almost 20% after 21 days in comparison to PEG-DA, suggesting the ability of EM-23 to facilitate ECM deposition over time. The increase in elastin production over time, in addition to the increase in compressive modulus over time, suggests that EM-23 is a promising candidate for vascular graft applications.

Cell viability within gel formulations A, B, C, and EM-23X-D was also visualized at days 7 and 21. As expected, cells were viable in gel formulation A, B, and C whereas EM-23X-D gels supported no viable cells. This result is in excellent agreement with the compression data and further reinforces the initial hypothesis of cell-secreted ECM in EM-23X-D hydrogels due to entrapment. The viability data also confirm that formulation A, B, and C can support cell adhesion while providing a suitable microenvironment over time.

#### **4.6 Conclusion**

The engineered elastin mimetic peptide, EM-23, was further characterized as a 3D template for promoting vascular ECM deposition. The studies in this chapter indicate that EM-23 is capable of promoting ECM deposition in a 3D scaffold. Moreover, degradation studies suggested that hydrogels comprising of EM-23 can remodel over time, which further reinforces the ability of the peptide to serve as an ECM promoting and a matrix remodeling template.

## Chapter 5

### Conclusions

#### 5.1 Results and Implications

The work outlined in this thesis investigates the use of novel elastin mimetic peptides, EM-19 and EM-23, in promoting vascular ECM deposition for potential vascular graft applications. Step-by-step characterization studies were conducted on the peptide sequences to elucidate how each peptide interacted with SMC cultures, as well as the impact the peptides had on vascular ECM production. Moreover, the peptides were grafted on top of PEG-DA hydrogel surfaces, and EM-23 stimulated significant cell adhesion and comparable elastin production in comparison to TCPS. Furthermore, 3D hydrogels comprised of EM-23 were able to promote elastin deposition over time. The detailed conclusions will be discussed in the subsequent sections.

##### *5.1.1 EM-23 is a Promising Candidate for Vascular Graft Applications*

Various characterization studies were conducted on different elastin mimetic peptides that could be used as templates for promoting vascular ECM deposition within a synthetic scaffold. The studies suggested that EM-23, containing an EBP binding motif and an integrin binding domain, is a promising candidate for vascular graft applications. The *in vitro* characterization of the peptides suggested that a synergistic mechanism may exist between the EBP and integrins in elastin fiber assembly. Specifically, the integrin  $\alpha_v\beta_3$  was suggested to play the synergistic role with the EBP in elastogenesis and it is beneficial to have the integrin binding domain in EM-23 to help translate the complex mechanism of elastin fiber assembly to a synthetic construct.

Once grafted onto the surfaces of PEG-DA hydrogels, EM-23 was able to facilitate significant SMC adhesion on PEG-DA in comparison to EM-19 and RGDS-grafted surfaces. Moreover, EM-23 promoted elastin deposition comparable to TCPS, suggesting that the peptide may be utilizing the two different binding motifs to promote significant cell adhesion and elastin deposition on PEG-DA surfaces. The studies indicated that EM-23 is an extremely promising candidate for vascular graft applications.

As further characterization, different hydrogels comprised of EM-23, including an enzymatically cleavable sequence, DS, were also able to promote elastin deposition over time. Hydrogels containing only EM-23 degraded in the presence of elastase, suggesting that this peptide may serve as a remodeling and an ECM promoting template. To engineer a suitable vascular graft, it is important that the scaffold have the necessary cues that promote ECM deposition and remodeling over time. This allows the scaffold to create a suitable microenvironment for cell growth while providing adequate structural integrity to the scaffold. In addition, hydrogels with different ratios of EM-23, DS, and PEG-DA demonstrated gel swelling instead of degradation, a phenomenon caused likely due to water diffusing into the construct as EM-23 and DS are continuously degraded. The study further suggested that hydrogels comprised of EM-23, DS, and PEG-DA may reach a threshold in ECM remodeling over time. Moreover, a significant increase in the compressive strength was also observed in hydrogels containing EM-23 in comparison to PEG-DA hydrogels. The increase in mechanical strength was likely a result of increased ECM production and further reinforces the candidacy of EM-23 as a suitable substitute for engineering vascular grafts.

Current vascular graft technologies lack the ability to promote a viable vascular ECM leading to graft failure post implantation. The characterization studies described in this thesis suggest that EM-23 is a potential candidate to bridge the gap in ECM production within the engineered grafts. Although more studies are warranted, it is clear that EM-23 is a promising candidate for addressing the ongoing demands for engineering a suitable vascular graft substitute. As such, future characterization work will be discussed in the subsequent sections.

## **5.2 Future Work**

The following sections detail possible future work in further characterizing the ability of EM-23 to translate the complex mechanism of elastin fiber assembly to a 3D scaffold intended for vascular grafts.

### *5.2.1 Further Characterization of EM-23 as a 3D template*

As outlined in Chapter 4 of this thesis, EM-23 was conjugated with PEG-NHS at a 1:2 mole ratio to yield a diacrylated PEG-EM23-PEG copolymer. However, mass spectrometry results indicated that only 30% of the final product was the diacrylated moiety while the rest was comprised of the monoacrylated product. Hence, it is suggested that the reaction be conducted in a more controlled environment in which 2 moles of PEG-NHS are reacted with every mole of peptide. A controlled environment can be achieved within the peptide synthesizer, which conjugates peptides from the carboxyl to amine terminus (C- to N-terminus), used in the work for this thesis (Figure 5.1).

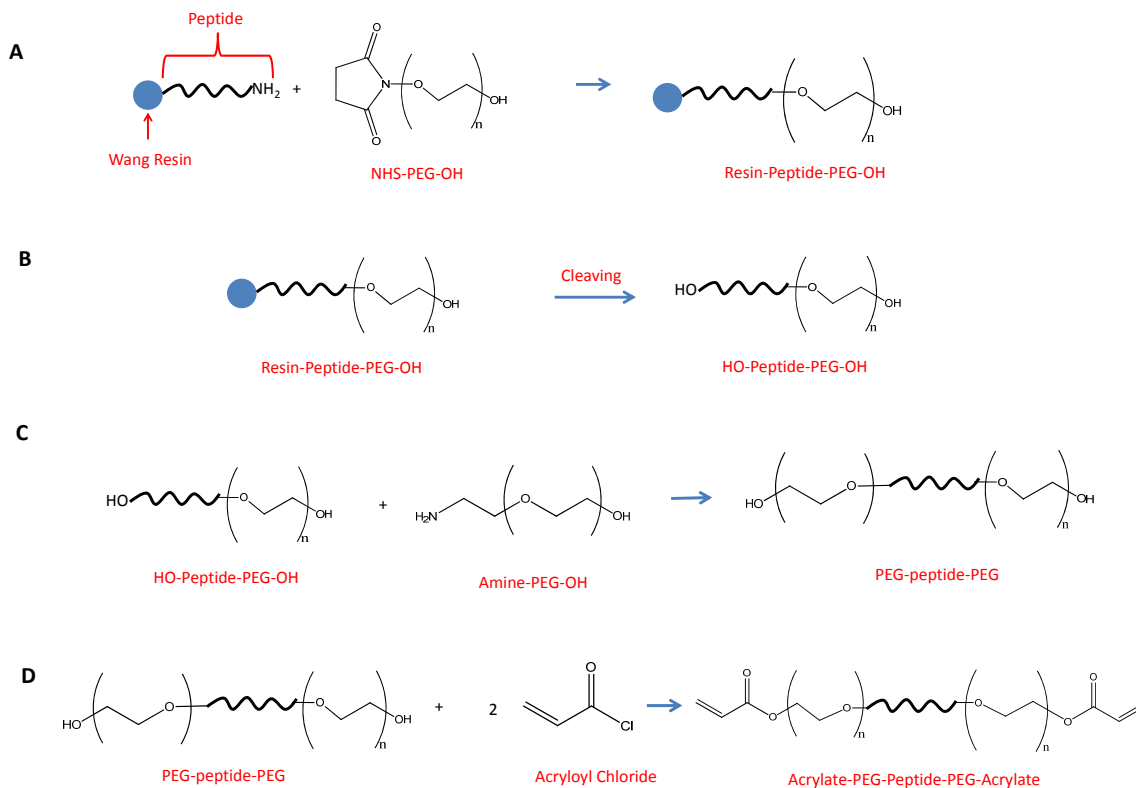


**Figure 5.1.** A proposed mechanism for fabricating a PEG-23-PEG moiety in a controlled manner. The N-terminus of a peptide already coupled to a resin can be conjugated with PEG-NHS (A). After cleaving (B), the resulting product can be further conjugated with an amine based PEG moiety (C), where the product can then be reacted with 2 moles of acryloyl chloride to yield a diacrylated PEG-peptide copolymer (D).

The N-terminus of the peptide conjugated to the resin can be coupled directly with one mole of PEG-NHS that does not bear an acrylate moiety. After cleaving the peptide off of the resin, the peptide-PEG copolymer can be reacted with an additional mole of PEG-NH<sub>2</sub> yielding a di-PEG peptide moiety. Acrylate groups can then be attached to either end of the PEG chains to yield a diacrylate moiety. Although optimization of the reaction conditions must be conducted, this protocol outlines the general procedure for controlling the diacrylation of peptides.

Further, the 3D hydrogel results suggested that constructs made from EM-23 and the proteolytically cleavable peptide sequence, DS, may serve to be the ideal templates for promoting vascular ECM deposition. However, more in depth experiments must be done order to make mechanistic arguments about how EM-23 plays an active role in

translating elastin fiber assembly to a 3D construct. For example, in order to investigate the impact each gel formulation has on elastin crosslinking, tropoelastin and LOX mRNA levels should be quantified. Moreover, quantifying total DNA content within the gels can also help elucidate how much elastin is produced on a per cell basis. The results from these two experiments should reveal further insights on the mechanistic phenomenon of elastin fiber assembly in a 3D scaffold.

### *5.2.2 Dynamic Mechanical Stimulation*

The experiments in Chapter 4 of this thesis were all conducted under static culture. However, to fully investigate the ability of the different 3D templates to serve as potential vascular grafts, dynamic experiments that mimic physiological conditions must be conducted. Numerous studies have confirmed that large differences lie in ECM production and mechanical strength within synthetic constructs when subjected to a static or dynamic environment [81, 221, 230]. Physiological conditions can be mimicked by a bioreactor that simulates flow and culturing conditions of a biologically active environment (Figure 5.2). Along with providing the adequate environment, a bioreactor is also capable of delivering flow-mediated stresses to constructs, allowing for cell culture and growth in different mechanical conditions [234].

Therefore, it is suggested that similar constructs to the ones discussed in Chapter 4 be engineered in a tubular format with encapsulated SMCs and subjected to dynamic stimulation that mimics physiological conditions over a course of 21 days. For example, Syedain et al. fabricated vascular grafts from fibrin gels by developing a bioreactor and conditioning the constructs with physiological flow conditions over time [233]. After 9 weeks of culture, the grafts were significantly remodeled and were able to achieve burst

pressures and compliance comparable to native arteries. However, the grafts lacked elastin deposition and did not have the circumferential cell alignment characteristic of the medial layer of a blood vessel.

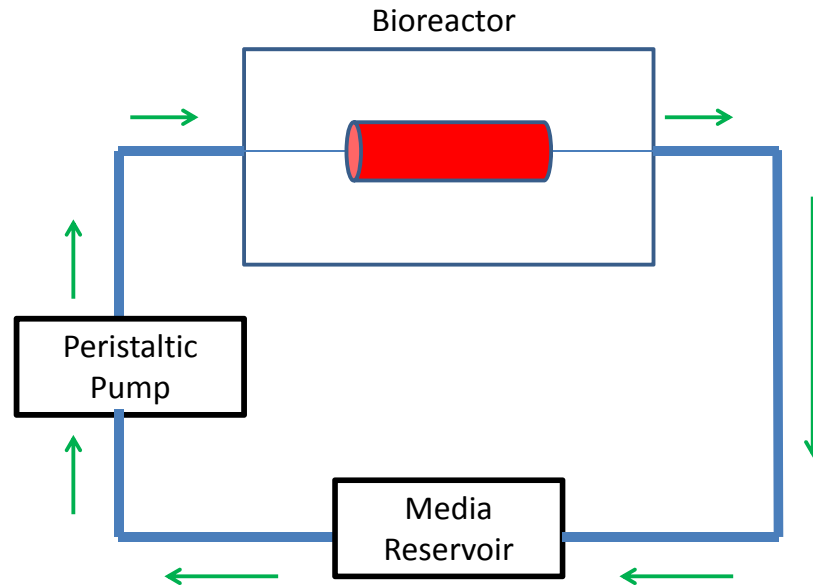


**Figure 5.2.** An example of a bioreactor that could be engineered in order to induce mechanical stimulations.

Cell alignment within the different 3D templates is also another key factor to consider for further studies. Within the medial layer of a blood vessel, SMCs and elastin fibers are circumferentially aligned, which synergistically provide the optimal compliance [3, 15]. Moreover, dynamic mechanical stimulation on synthetic grafts has been found to control the orientation of cells and the ECM deposited [230, 233, 235, 236]. Therefore, in addition to dynamic conditioning of the different gel formulations containing EM-23, it is also suggested to design experiments that control cell alignment within the constructs. Constructs without conditioning or random cell orientation should be used as the appropriate controls. Furthermore, the inherent weakness of the hydrogels could limit the efficacy of engineering the constructs in a tubular format. Hence the investigation of alternative materials that have stronger mechanical properties and

modifying them with EM-23 in order to engineer robust tubular scaffolds is also suggested.

### *5.2.3 Alternative Materials and Techniques for Engineering Vascular Grafts*

Although PEG-DA hydrogels have been suggested to be the ideal material for vascular graft applications, their use is limited due to poor mechanical strength. Polyurethanes are an alternative class of material that have gained much interest in the past few years for vascular graft applications [10, 61, 63]. PU-based materials have been modified with bioactive moieties to facilitate cell adhesion and improve mechanical properties [26, 36, 62]. For example, Punshon et al. chemically combined PU with a nanocomposite fabricated from polyhedral oligomeric silsesquioxane and observed viscoelastic properties similar to native arteries [237]. Moreover, Jun et al. modified microporous PU scaffolds with PEG and a endothelial cell specific bioactive sequence, YIGSR (tyrosine-isoleucine-glycine-serine-arginine) and demonstrated increased endothelialization and improved mechanical properties [61]. As such, it is suggested that similar characterization studies that were conducted in this thesis be done on PU based materials modified with EM-23 and the results directly compared to the PEG based materials modified with EM-23.

Also, PLA and PGA are another class of materials routinely used for vascular graft applications [11, 26]. PLA materials allow for slower degradation rates whereas PGA based materials are highly biocompatible and biodegradable [42, 43, 53, 54]. For example, Kim et al. engineered vascular grafts from PLA based materials and found a significant improvement in elastin production after dynamically conditioning the grafts [56]. In a separate study, Niklason et al. engineered vascular grafts from PGA based

materials and found comparable burst pressures to saphenous veins after dynamically conditioning the grafts, although the grafts lacked the presence of elastin [48]. Combining either material with EM-23 can serve to bridge the gap in elastin production within these materials and potentially lead to engineering more compliant vascular grafts.

Additionally, electrospinning has gained considerable attention in the past five years as an alternative strategy in engineering vascular grafts [67, 238-242].

Electrospinning allows for precise control over fiber orientation and diameters, and allows for a higher area to volume ratio for cell attachment [33, 60, 241]. Combining different polymers such as PU, PLA, and PGA with EM-23 and electrospinning the copolymer solution into a tubular construct may assist in controlling cell adhesion and alignment in a specific manner, while achieving precise fiber orientation within the construct. The fabricated graft should further be mechanically conditioned under physiological flow and long term studies on ECM deposition and mechanical strengths of the graft should be investigated.

Although further characterization studies are clearly warranted, the work presented in this thesis describes the synthesis and characterization of a novel elastin mimetic peptide capable of promoting ECM deposition for vascular graft applications. Current vascular graft technologies lack the capability to promote ECM deposition. With the goal to engineer compliant vascular grafts, this thesis described the initial steps in designing and characterizing a suitable material that can promote vascular ECM deposition within a synthetic scaffold. The future work suggested will further assess the capability of EM-23 to translate the complex mechanism of elastin fiber assembly to an optimum 3D scaffold and move one step closer in engineering compliant vascular grafts.

## APPENDIX

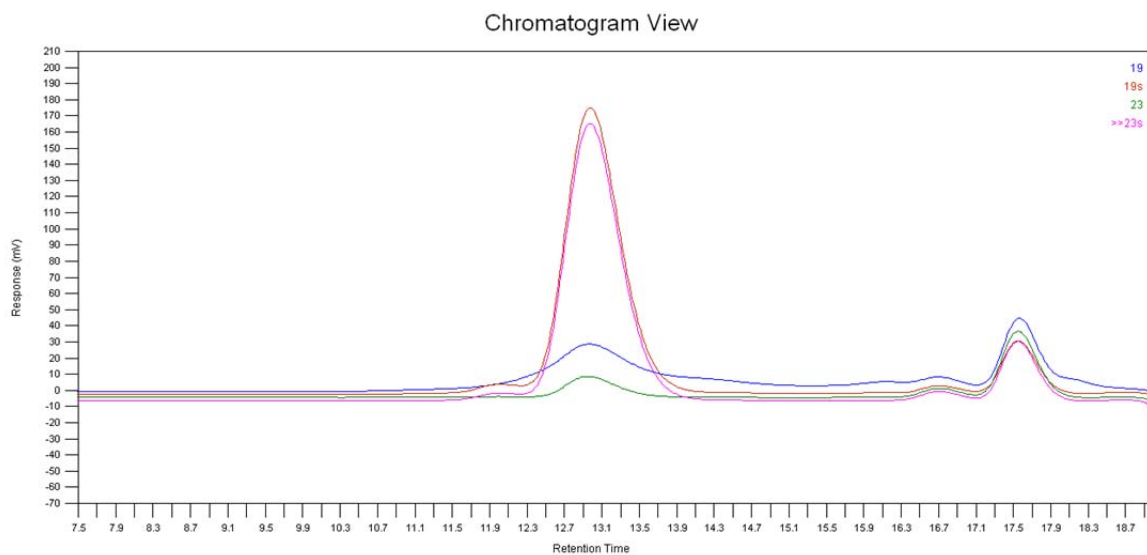


**Figure A.1.** Elution times of various PEG-peptide copolymers. A characteristic tetrahydrofuran solvent peak was eluted for all conditions at 17.75 mins.

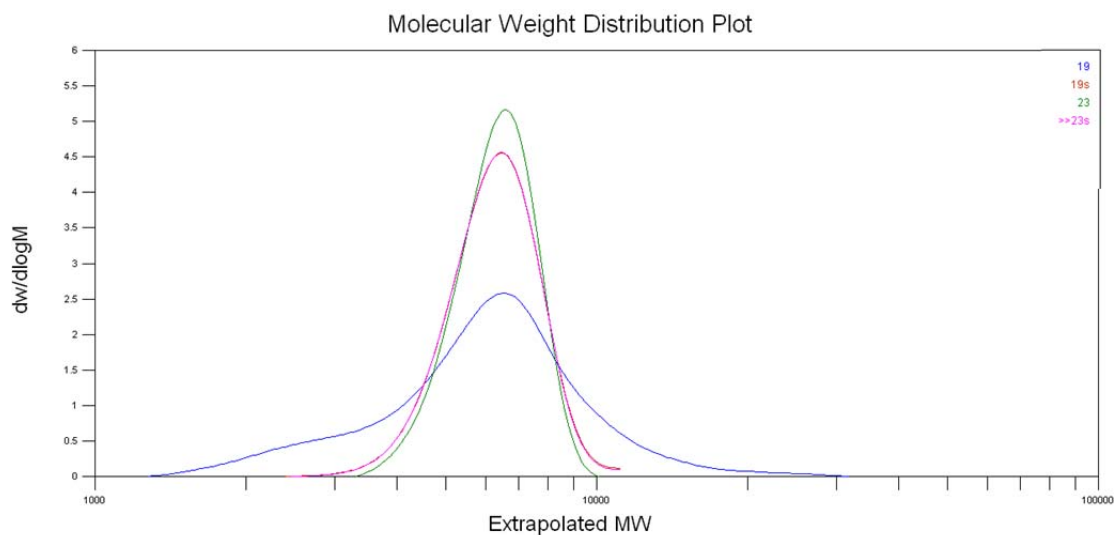


**Figure A.2.** Extrapolated molecular weights for the different PEG-peptide copolymers. The determined molecular weight for PEG-EM19 and PEG-EM19S was 5500 Da while PEG-EM23 and PEG-EM23S has a molecular weight of 5700 Da. These molecular weights confirm successful conjugation of the peptide with acrylate-PEG-SVA at 1:1 mole ratio.

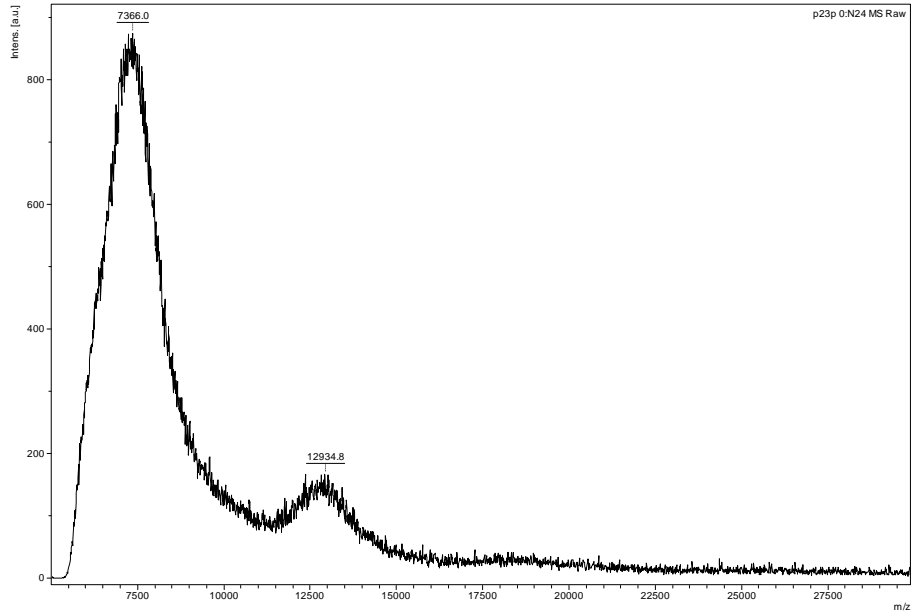


**Figure A.3.** Mass spectrometry results of conjugating EM-23 with PEG-NHS at a 1:2 mole ratio. Only 30% of the total final product showed the expected molecular weight.

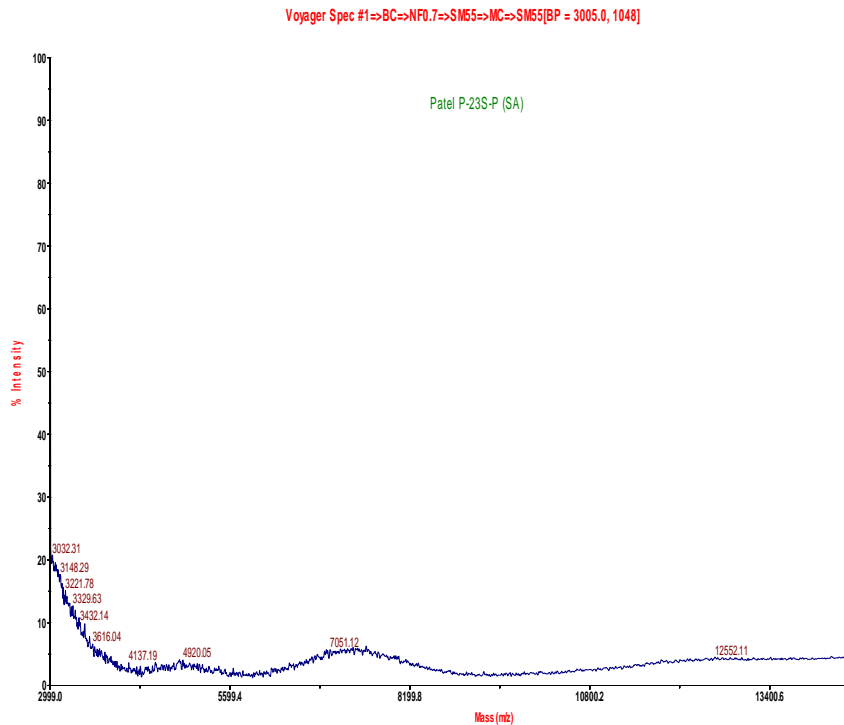
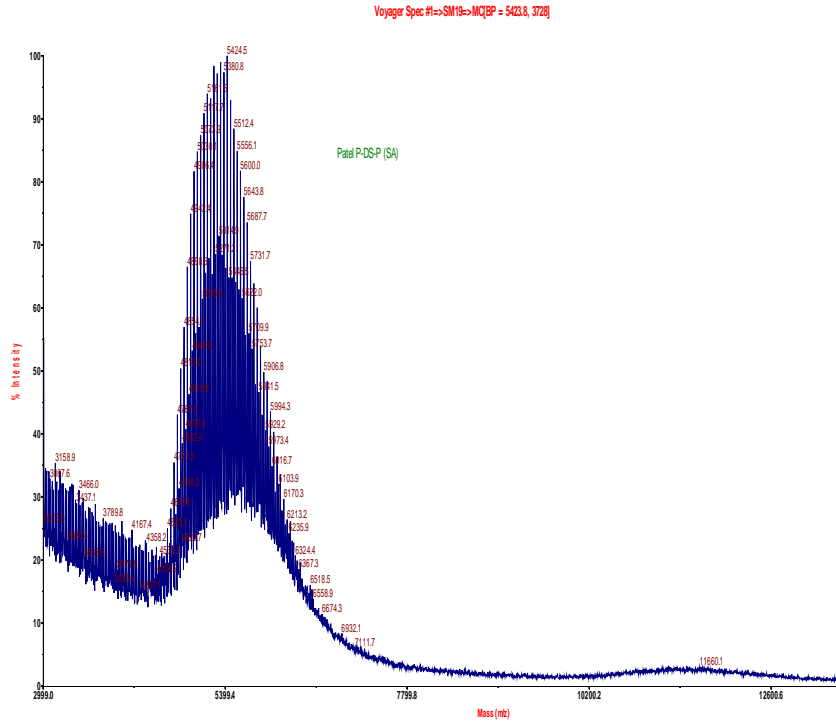


**Figure A.4.** Mass spectrometry results of conjugating EM-23S with PEG-NHS at a 1:2 mole ratio showing trace amounts of the expected product.



Voyager Spec #1=>BC=>NF0.7=>SM55=>MC=>SM55[BP = 3006.4, 814]

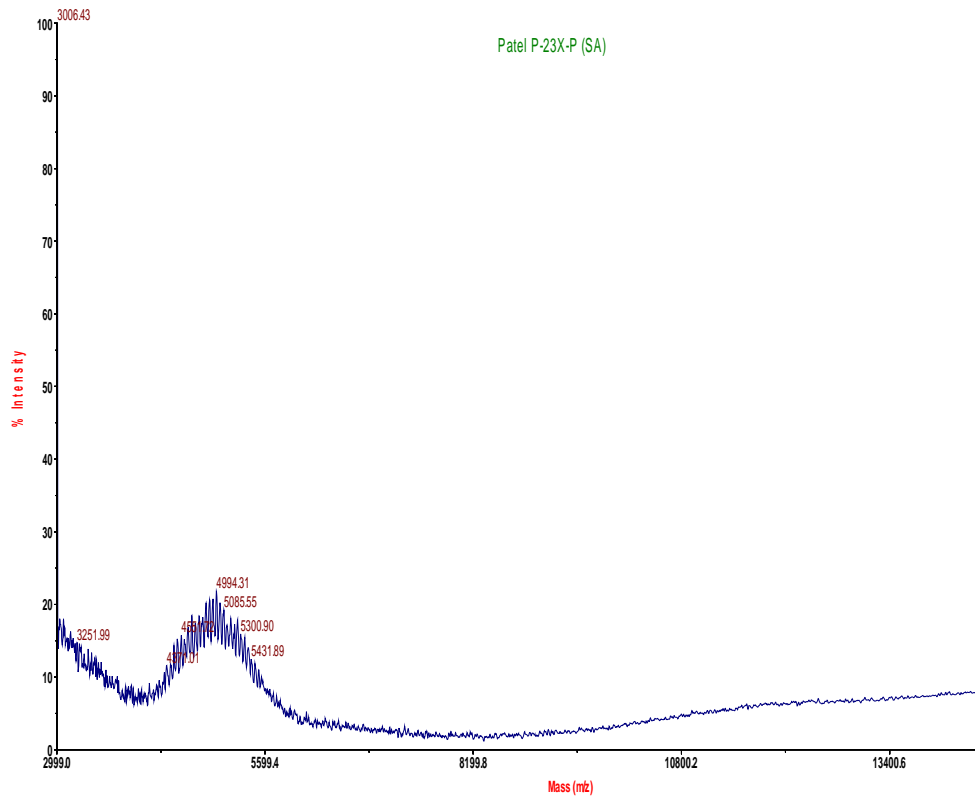


Figure A.7. Mass spectrometry results of conjugating EM-23X with PEG-NHS at a 1:2 mole ratio.

## REFERENCES

1. Association, A.H., www.heart.org, 2012.
2. Conte, M.S., *The ideal small arterial substitute: a search for the Holy Grail?* Faseb Journal, 1998. **12**(1): p. 43-45.
3. Nerem, R.M. and D. Seliktar, *Vascular tissue engineering*. Annual Review of Biomedical Engineering, 2001. **3**: p. 225-243.
4. Zhang, W.J., et al., *Tissue engineering of blood vessel*. Journal of Cellular and Molecular Medicine, 2007. **11**(5): p. 945-957.
5. Nerem, R.M., *Vascular tissue engineering: challenges and opportunities*. Journal of Molecular and Cellular Cardiology, 2004. **37**(1): p. 325-326.
6. Favalaro, R.G., *SAPHENOUS VEIN GRAFT IN SURGICAL TREATMENT OF CORONARY ARTERY DISEASE - OPERATIVE TECHNIQUE*. Journal of Thoracic and Cardiovascular Surgery, 1969. **58**(2): p. 178-&.
7. Kolessov, V.I., *MAMMARY ARTERY-CORONARY ARTERY ANASTOMOSIS AS METHOD OF TREATMENT FOR ANGINA PECTORIS*. Journal of Thoracic and Cardiovascular Surgery, 1967. **54**(4): p. 535-&.
8. Kielty, C.M., et al., *Applying elastic fibre biology in vascular tissue engineering*. Philosophical Transactions of the Royal Society B-Biological Sciences, 2007. **362**(1484): p. 1293-1312.
9. Collins, P., et al., *Radial artery versus saphenous vein patency randomized trial - Five-year angiographic follow-up*. Circulation, 2008. **117**(22): p. 2859-2864.
10. Zilla, P., D. Bezuidenhout, and P. Human, *Prosthetic vascular grafts: Wrong models, wrong questions and no healing*. Biomaterials, 2007. **28**(34): p. 5009-5027.
11. Isenberg, B.C., C. Williams, and R.T. Tranquillo, *Small-diameter artificial arteries engineered in vitro*. Circulation Research, 2006. **98**(1): p. 25-35.
12. Ross, R., *THE PATHOGENESIS OF ATHEROSCLEROSIS - A PERSPECTIVE FOR THE 1990S*. Nature, 1993. **362**(6423): p. 801-809.
13. Bohl, K.S. and J.L. West, *Nitric oxide-generating polymers reduce platelet adhesion and smooth muscle cell proliferation*. Biomaterials, 2000. **21**(22): p. 2273-2278.
14. Tozzi, P. and D. Hayoz, *Definition of arterial compliance*. American Journal of Physiology-Heart and Circulatory Physiology, 2000. **278**(4): p. H1407-H1407.

15. Wagenseil, J.E. and R.P. Mecham, *Vascular Extracellular Matrix and Arterial Mechanics*. *Physiological Reviews*, 2009. **89**(3): p. 957-989.
16. Patel, A., et al., *Elastin biosynthesis: The missing link in tissue-engineered blood vessels*. *Cardiovascular Research*, 2006. **71**(1): p. 40-49.
17. Greisler, H.P., *Interactions at the Blood/Material Interface*. *Annals of Vascular Surgery*, 1990. **4**(1): p. 98-103.
18. Gozna, E.R., et al., *NECESSITY FOR ELASTIC PROPERTIES IN SYNTHETIC ARTERIAL GRAFTS*. *Canadian Journal of Surgery*, 1974. **17**(3): p. 176-&.
19. Campbell, G.R. and J.H. Campbell, *Development of tissue engineered vascular grafts*. *Current Pharmaceutical Biotechnology*, 2007. **8**(1): p. 43-50.
20. Nerem, R.M. and A. Sambanis, *Tissue engineering: from biology to biological substitutes*. *Tissue Eng*, 1995. **1**(1): p. 3-13.
21. Langer, R. and J.P. Vacanti, *TISSUE ENGINEERING*. *Science*, 1993. **260**(5110): p. 920-926.
22. Vacanti, J.P. and R. Langer, *Tissue engineering: the design and fabrication of living replacement devices for surgical reconstruction and transplantation*. *Lancet*, 1999. **354**: p. SI32-SI34.
23. Jimenez-Vergara, A.C., et al., *Approach for Fabricating Tissue Engineered Vascular Grafts with Stable Endothelialization*. *Annals of Biomedical Engineering*, 2010. **38**(9): p. 2885-2895.
24. Mann, B.K. and J.L. West, *Tissue engineering in the cardiovascular system: Progress toward a tissue engineered heart*. *Anatomical Record*, 2001. **263**(4): p. 367-371.
25. Matsumura, G., et al., *Successful application of tissue engineered vascular autografts: clinical experience*. *Biomaterials*, 2003. **24**(13): p. 2303-2308.
26. Pankajakshan, D. and D.K. Agrawal, *Scaffolds in tissue engineering of blood vessels*. *Canadian Journal of Physiology and Pharmacology*, 2010. **88**(9): p. 855-873.
27. Hashi, C.K., et al., *Antithrombogenic property of bone marrow mesenchymal stem cells in nanofibrous vascular grafts*. *Proceedings of the National Academy of Sciences of the United States of America*, 2007. **104**(29): p. 11915-11920.
28. DiMuzio, P. and T. Tulenko, *Tissue engineering applications to vascular bypass graft development: The use of adipose-derived stem cells*. *Journal of Vascular Surgery*, 2007. **45**: p. 99A-103A.

29. de Mel, A., et al., *In situ endothelialisation potential of a biofunctionalised nanocomposite biomaterial-based small diameter bypass graft*. *Bio-Medical Materials and Engineering*, 2009. **19**(4-5): p. 317-331.
30. Sarkar, S., et al., *Achieving the ideal properties for vascular bypass grafts using a tissue engineered approach: a review*. *Medical & Biological Engineering & Computing*, 2007. **45**(4): p. 327-336.
31. Nerem, R.M., *Development of vascular substitutes*, in *Biomedical Materials-Drug Delivery, Implants and Tissue Engineering*, T. Neenan, M. Marcolongo, and R.F. Valentini, Editors. 1999. p. 293-296.
32. Shadwick, R.E., *Mechanical design in arteries*. *Journal of Experimental Biology*, 1999. **202**(23): p. 3305-3313.
33. Rathore, A., et al., *Development of tissue engineered vascular grafts and application of nanomedicine*. *Wiley Interdisciplinary Reviews-Nanomedicine and Nanobiotechnology*, 2012. **4**(3): p. 257-272.
34. Zilla, P., M. Deutsch, and J. Meinhart, *Endothelial cell transplantation*. *Seminars in vascular surgery*, 1999. **12**(1): p. 52-63.
35. Isenburg, J.C., D.T. Simionescu, and N.R. Vyavahare, *Elastin stabilization in cardiovascular implants: improved resistance to enzymatic degradation by treatment with tannic acid*. *Biomaterials*, 2004. **25**(16): p. 3293-3302.
36. Ratcliffe, A., *Tissue engineering of vascular grafts*. *Matrix Biology*, 2000. **19**(4): p. 353-357.
37. Larsen, C.C., et al., *A biomimetic peptide fluorosurfactant polymer for endothelialization of ePTFE with limited platelet adhesion*. *Biomaterials*, 2007. **28**(24): p. 3537-3548.
38. Rabkin, E. and F.J. Schoen, *Cardiovascular tissue engineering*. *Cardiovascular Pathology*, 2002. **11**(6): p. 305-317.
39. Hoenig, M.R., et al., *Tissue-engineered blood vessels - Alternative to autologous grafts?* *Arteriosclerosis Thrombosis and Vascular Biology*, 2005. **25**(6): p. 1128-1134.
40. Heydarkhan-Hagvall, S., et al., *Production of extracellular matrix components in tissue-engineered blood vessels*. *Tissue Eng*, 2006. **12**(4): p. 831-842.
41. Walles, T., et al., *Influence of scaffold thickness and scaffold composition on bioartificial graft survival*. *Biomaterials*, 2003. **24**(7): p. 1233-1239.

42. Iwasaki, K., et al., *Bioengineered three-layered robust and elastic artery using hemodynamically-equivalent pulsatile bioreactor*. *Circulation*, 2008. **118**(14): p. S52-S57.
43. Brennan, M.P., et al., *Tissue-engineered vascular grafts demonstrate evidence of growth and development when implanted in a juvenile animal model*. *Annals of Surgery*, 2008. **248**(3): p. 370-376.
44. Roh, J.D., et al., *Small-diameter biodegradable scaffolds for functional vascular tissue engineering in the mouse model*. *Biomaterials*, 2008. **29**(10): p. 1454-1463.
45. Lopez-Soler, R.I., et al., *Development of a mouse model for evaluation of small diameter vascular grafts*. *Journal of Surgical Research*, 2007. **139**(1): p. 1-6.
46. Kim, B.S., et al., *Optimizing seeding and culture methods to engineer smooth muscle tissue on biodegradable polymer matrices*. *Biotechnology and Bioengineering*, 1998. **57**(1): p. 46-54.
47. Ferguson, T., Zund, and C. Muneretto, *Tissue engineering: A new approach in cardiovascular surgery; Seeding of human fibroblasts followed by human endothelial cells on resorbable mesh - Conference discussion*. *European Journal of Cardio-Thoracic Surgery*, 1998. **13**(2): p. 164-164.
48. Niklason, L.E., et al., *Functional arteries grown in vitro*. *Science*, 1999. **284**(5413): p. 489-493.
49. Shin'oka, T., Y. Imai, and Y. Ikada, *Transplantation of a Tissue-Engineered Pulmonary Artery*. *New England Journal of Medicine*, 2001. **344**(7): p. 532-533.
50. Shin'oka, T., et al., *Midterm clinical result of tissue-engineered vascular autografts seeded with autologous bone marrow cells*. *Journal of Thoracic and Cardiovascular Surgery*, 2005. **129**(6): p. 1330-1338.
51. Hibino, N., et al., *Late-term results of tissue-engineered vascular grafts in humans*. *Journal of Thoracic and Cardiovascular Surgery*, 2010. **139**(2): p. 431-U233.
52. Park, J.C., et al., *Calcification comparison of polymers for vascular graft*. *Yonsei Medical Journal*, 2001. **42**(3): p. 304-310.
53. Uchida, T., et al., *Development of biodegradable scaffolds based on patient-specific arterial configuration*. *Journal of Biotechnology*, 2008. **133**(2): p. 213-218.
54. Naito, Y., et al., *Vascular tissue engineering: Towards the next generation vascular grafts*. *Advanced Drug Delivery Reviews*, 2011. **63**(4-5): p. 312-323.

55. Kim, B.S., et al., *Cyclic mechanical strain regulates the development of engineered smooth muscle tissue*. Nature Biotechnology, 1999. **17**(10): p. 979-983.
56. Kim, B.S. and D.J. Mooney, *Scaffolds for engineering smooth muscle under cyclic mechanical strain conditions*. Journal of Biomechanical Engineering-Transactions of the Asme, 2000. **122**(3): p. 210-215.
57. Wang, S., et al., *Fabrication and Properties of the Electrospun Polylactide/Silk Fibroin-Gelatin Composite Tubular Scaffold*. Biomacromolecules, 2009. **10**(8): p. 2240-2244.
58. El-Kurdi, M.S., et al., *Transient elastic support for vein grafts using a constricting microfibrillar polymer wrap*. Biomaterials, 2008. **29**(22): p. 3213-3220.
59. Sarkar, S., et al., *Manufacture of small calibre quadruple lamina vascular bypass grafts using a novel automated extrusion-phase-inversion method and nanocomposite polymer*. Journal of Biomechanics, 2009. **42**(6): p. 722-730.
60. McMahon, R.E., et al., *Hydrogel-Electrospun Mesh Composites for Coronary Artery Bypass Grafts*. Tissue Engineering Part C-Methods, 2011. **17**(4): p. 451-461.
61. Jun, H.W. and J.L. West, *Endothelialization of microporous YIGSR/PEG-modified polyurethaneurea*. Tissue Eng, 2005. **11**(7-8): p. 1133-1140.
62. Rashid, S.T., et al., *Cellular engineering of conduits for coronary and lower limb bypass surgery: Role of cell attachment peptides and pre-conditioning in optimising smooth muscle cells (SMC) adherence to compliant poly(carbonate-urea)urethane (MyoLink(TM)) scaffolds*. European Journal of Vascular and Endovascular Surgery, 2004. **27**(6): p. 608-616.
63. Grenier, S., M. Sandig, and K. Mequanint, *Smooth Muscle alpha-Actin and Calponin Expression and Extracellular Matrix Production of Human Coronary Artery Smooth Muscle Cells in 3D Scaffolds*. Tissue Engineering Part A, 2009. **15**(10): p. 3001-3011.
64. Ma, P.X., *Biomimetic materials for tissue engineering*. Advanced Drug Delivery Reviews, 2008. **60**(2): p. 184-198.
65. Whittemore, A.D., et al., *WHAT IS THE PROPER ROLE OF POLYTETRAFLUOROETHYLENE GRAFTS IN INFRAINGUINAL RECONSTRUCTION*. Journal of Vascular Surgery, 1989. **10**(3): p. 299-305.
66. Faries, P.L., et al., *A comparative study of alternative conduits for lower extremity revascularization: All-autogenous conduit versus prosthetic grafts*. Journal of Vascular Surgery, 2000. **32**(6): p. 1080-1090.

67. Saha, K., et al., *Designing synthetic materials to control stem cell phenotype*. Current Opinion in Chemical Biology, 2007. **11**(4): p. 381-387.
68. Nguyen, K.T. and J.L. West, *Photopolymerizable hydrogels for tissue engineering applications*. Biomaterials, 2002. **23**(22): p. 4307-4314.
69. Lutolf, M.P. and J.A. Hubbell, *Synthetic biomaterials as instructive extracellular microenvironments for morphogenesis in tissue engineering*. Nature Biotechnology, 2005. **23**(1): p. 47-55.
70. Butcher, J.T. and R.M. Nerem, *Porcine aortic valve interstitial cells in three-dimensional culture: Comparison of phenotype with aortic smooth muscle cells*. Journal of Heart Valve Disease, 2004. **13**(3): p. 478-485.
71. Eyrich, D., et al., *Long-term stable fibrin gels for cartilage engineering*. Biomaterials, 2007. **28**(1): p. 55-65.
72. Azab, A.K., et al., *Crosslinked chitosan implants as potential degradable devices for brachytherapy: In vitro and in vivo analysis*. Journal of Controlled Release, 2006. **111**(3): p. 281-289.
73. Tibbitt, M.W. and K.S. Anseth, *Hydrogels as Extracellular Matrix Mimics for 3D Cell Culture*. Biotechnology and Bioengineering, 2009. **103**(4): p. 655-663.
74. Cushing, M.C. and K.S. Anseth, *Hydrogel cell cultures*. Science, 2007. **316**(5828): p. 1133-1134.
75. Bryant, S.J. and K.S. Anseth, *Hydrogel properties influence ECM production by chondrocytes photoencapsulated in poly(ethylene glycol) hydrogels*. Journal of Biomedical Materials Research, 2002. **59**(1): p. 63-72.
76. Sawhney, A.S., C.P. Pathak, and J.A. Hubbell, *BIOERODIBLE HYDROGELS BASED ON PHOTOPOLYMERIZED POLY(ETHYLENE GLYCOL)-CO-POLY(ALPHA-HYDROXY ACID) DIACRYLATE MACROMERS*. Macromolecules, 1993. **26**(4): p. 581-587.
77. Martens, P. and K.S. Anseth, *Characterization of hydrogels formed from acrylate modified poly(vinyl alcohol) macromers*. Polymer, 2000. **41**(21): p. 7715-7722.
78. Harris, J.M., et al., *New Polyethylene Glycols for Biomedical Applications*. Acs Symposium Series, 1991. **467**: p. 418-429.
79. Peyton, S.R., et al., *The use of poly(ethylene glycol) hydrogels to investigate the impact of ECM chemistry and mechanics on smooth muscle cells*. Biomaterials, 2006. **27**(28): p. 4881-4893.

80. Nemir, S., H.N. Hayenga, and J.L. West, *PEGDA Hydrogels With Patterned Elasticity: Novel Tools for the Study of Cell Response to Substrate Rigidity*. Biotechnology and Bioengineering, 2010. **105**(3): p. 636-644.
81. Hahn, M.S., J.S. Miller, and J.L. West, *Three-dimensional biochemical and biomechanical patterning of hydrogels for guiding cell behavior*. Advanced Materials, 2006. **18**(20): p. 2679-+.
82. Hahn, M.S., et al., *Photolithographic patterning of polyethylene glycol hydrogels*. Biomaterials, 2006. **27**(12): p. 2519-2524.
83. Liao, H.M., et al., *Influence of hydrogel mechanical properties and mesh size on vocal fold fibroblast extracellular matrix production and phenotype*. Acta Biomaterialia, 2008. **4**(5): p. 1161-1171.
84. Munoz-Pinto, D.J., A.S. Bulick, and M.S. Hahn, *Uncoupled investigation of scaffold modulus and mesh size on smooth muscle cell behavior*. Journal of Biomedical Materials Research Part A, 2009. **90A**(1): p. 303-316.
85. Moon, J.J., S.H. Lee, and J.L. West, *Synthetic biomimetic hydrogels incorporated with Ephrin-A1 for therapeutic angiogenesis*. Biomacromolecules, 2007. **8**(1): p. 42-49.
86. Gobin, A.S. and J.L. West, *Val-ala-pro-gly, an elastin-derived non-integrin ligand: Smooth muscle cell adhesion and specificity*. Journal of Biomedical Materials Research Part A, 2003. **67A**(1): p. 255-259.
87. Patel, D., R. Menon, and L.J. Taite, *Self-Assembly of Elastin-Based Peptides into the ECM: the Importance of Integrins and the Elastin Binding Protein in Elastic Fiber Assembly*. Biomacromolecules, 2011. **12**(2): p. 432-440.
88. Patel, D., et al., *Synergistic Activity of alpha(v)beta(3) Integrins and the Elastin Binding Protein Enhance Cell-Matrix Interactions on Bioactive Hydrogel Surfaces*. Biomacromolecules, 2012. **13**(5): p. 1420-1428.
89. Lau, Y.-K.I., A.M. Gobin, and J.L. West, *Overexpression of lysyl oxidase to increase matrix crosslinking and improve tissue strength in dermal wound healing*. Annals of Biomedical Engineering, 2006. **34**(8): p. 1239-1246.
90. Lee, S.-H., J.J. Moon, and J.L. West, *Three-dimensional micropatterning of bioactive hydrogels via two-photon laser scanning photolithography for guided 3D cell migration*. Biomaterials, 2008. **29**(20): p. 2962-2968.
91. Stapleton, T.W., et al., *Development and characterization of an acellular porcine medial meniscus for use in tissue engineering*. Tissue Engineering Part A, 2008. **14**(4): p. 505-518.

92. Yang, D., et al., *Tissue-Engineered Blood Vessel Graft Produced by Self-Derived Cells and Allogenic Acellular Matrix A Functional Performance and Histologic Study*. *Annals of Plastic Surgery*, 2009. **62**(3): p. 297-303.
93. Schmidt, C.E. and J.M. Baier, *Acellular vascular tissues: natural biomaterials for tissue repair and tissue engineering*. *Biomaterials*, 2000. **21**(22): p. 2215-2231.
94. Dahl, S.L.M., et al., *Decellularized native and engineered arterial scaffolds for transplantation*. *Cell Transplantation*, 2003. **12**(6): p. 659-666.
95. Tamura, N., et al., *A new acellular vascular prosthesis as a scaffold for host tissue regeneration*. *International Journal of Artificial Organs*, 2003. **26**(9): p. 783-792.
96. Lantz, G.C., et al., *Small intestinal submucosa as a small-diameter arterial graft in the dog*. *Journal of investigative surgery : the official journal of the Academy of Surgical Research*, 1990. **3**(3): p. 217-27.
97. Sandusky, G.E., et al., *HISTOLOGIC-FINDINGS AFTER INVIVO PLACEMENT OF SMALL-INTESTINE SUBMUCOSAL VASCULAR GRAFTS AND SAPHENOUS-VEIN GRAFTS IN THE CAROTID-ARTERY IN DOGS*. *American Journal of Pathology*, 1992. **140**(2): p. 317-324.
98. Badylak, S., et al., *Endothelial cell adherence to small intestinal submucosa: an acellular bioscaffold*. *Biomaterials*, 1999. **20**(23-24): p. 2257-2263.
99. Derham, C., et al., *Tissue Engineering Small-Diameter Vascular Grafts: Preparation of a Biocompatible Porcine Ureteric Scaffold*. *Tissue Engineering Part A*, 2008. **14**(11): p. 1871-1882.
100. Gui, L., et al., *Development of Decellularized Human Umbilical Arteries as Small-Diameter Vascular Grafts*. *Tissue Engineering Part A*, 2009. **15**(9): p. 2665-2676.
101. Cho, S.-W., et al., *Evidence for In Vivo Growth Potential and Vascular Remodeling of Tissue-Engineered Artery*. *Tissue Engineering Part A*, 2009. **15**(4): p. 901-912.
102. Grauss, R.W., et al., *Histological evaluation of decellularised porcine aortic valves: matrix changes due to different decellularisation methods*. *European Journal of Cardio-Thoracic Surgery*, 2005. **27**(4): p. 566-571.
103. Petersen, T.H., et al., *Matrix Composition and Mechanics of Decellularized Lung Scaffolds*. *Cells Tissues Organs*, 2012. **195**(3): p. 222-231.
104. Chrzanowski, P., et al., *ELASTIN CONTENT OF NORMAL AND EMPHYSEMATOUS LUNG PARENCHYMA*. *American Journal of Medicine*, 1980. **69**(3): p. 351-359.

105. Rosenbloom, J., W.R. Abrams, and R. Mecham, *EXTRACELLULAR-MATRIX .4. THE ELASTIC FIBER*. FASEB, 1993. **7**(13): p. 1208-1218.
106. Zorlutuna, P., N. Hasirci, and V. Hasirci, *Nanopatterned collagen tubes for vascular tissue engineering*. Journal of Tissue Engineering and Regenerative Medicine, 2008. **2**(6): p. 373-377.
107. Torikai, K., et al., *A self-renewing, tissue-engineered vascular graft for arterial reconstruction*. Journal of Thoracic and Cardiovascular Surgery, 2008. **136**(1): p. 37-U56.
108. Weinberg, C.B. and E. Bell, *A BLOOD-VESSEL MODEL CONSTRUCTED FROM COLLAGEN AND CULTURED VASCULAR CELLS*. Science, 1986. **231**(4736): p. 397-400.
109. Ishibashi, K. and T. Matsuda, *Reconstruction of a hybrid vascular graft hierarchically layered with three cell types*. ASAIO journal (American Society for Artificial Internal Organs : 1992), 1994. **40**(3): p. M284-90.
110. Girton, T.S., et al., *Mechanisms of stiffening and strengthening in media-equivalents fabricated using glycation*. Journal of Biomechanical Engineering-Transactions of the Asme, 2000. **122**(3): p. 216-223.
111. Berglund, J.D., et al., *A biological hybrid model for collagen-based tissue engineered vascular constructs*. Biomaterials, 2003. **24**(7): p. 1241-1254.
112. Berglund, J.D., R.M. Nerem, and A. Sambanis, *Incorporation of intact elastin scaffolds in tissue-engineered collagen-based vascular grafts*. Tissue Engineering, 2004. **10**(9-10): p. 1526-1535.
113. Seliktar, D., et al., *Dynamic mechanical conditioning of collagen-gel blood vessel constructs induces remodeling in vitro*. Annals of Biomedical Engineering, 2000. **28**(4): p. 351-362.
114. Barocas, V.H., T.S. Girton, and R.T. Tranquillo, *Engineered alignment in media equivalents: Magnetic prealignment and Mandrel compaction*. Journal of Biomechanical Engineering-Transactions of the Asme, 1998. **120**(5): p. 660-666.
115. Hirai, J. and T. Matsuda, *SELF-ORGANIZED, TUBULAR HYBRID VASCULAR TISSUE COMPOSED OF VASCULAR CELLS AND COLLAGEN FOR LOW-PRESSURE-LOADED VENOUS SYSTEM*. Cell Transplantation, 1995. **4**(6): p. 597-608.
116. Isenberg, B.C. and R.T. Tranquillo, *Long-term cyclic distention enhances the mechanical properties of collagen-based media-equivalents*. Annals of Biomedical Engineering, 2003. **31**(8): p. 937-949.

117. Mithieux, S.M. and A.S. Weiss, *Elastin*, in *Fibrous Proteins: Coiled-Coils, Collagen and Elastomers*, D.A.D.S.J.M. Parry, Editor 2005. p. 437-+.
118. Akagawa, M. and K. Suyama, *Mechanism of Formation of Elastin Crosslinks*. *Connective Tissue Research*, 2000. **41**(2): p. 131-141.
119. Karnik, S.K., et al., *A critical role for elastin signaling in vascular morphogenesis and disease*. *Development*, 2003. **130**(2): p. 411-423.
120. Long, J.L. and R.T. Tranquillo, *Elastic fiber production in cardiovascular tissue-equivalents*. *Matrix Biology*, 2003. **22**(4): p. 339-350.
121. Fung, Y.C. and S.Q. Liu, *ELEMENTARY MECHANICS OF THE ENDOTHELIUM OF BLOOD-VESSELS*. *Journal of Biomechanical Engineering-Transactions of the Asme*, 1993. **115**(1): p. 1-12.
122. Rodgers, U.R. and A.S. Weiss, *Cellular interactions with elastin*. *Pathologie Biologie*, 2005. **53**(7): p. 390-398.
123. Li, D.Y., et al., *Elastin is an essential determinant of arterial morphogenesis*. *Nature*, 1998. **393**(6682): p. 276-280.
124. Ayad S, B.-H.R., Humphries MJ, Kadler KE, Shuttleworth CA, *The extracellular matrix facts book*. London, Great Britain: Academic Press, 1994.
125. Wise, S.G. and A.S. Weiss, *Tropoelastin*. *Int. J. Biochem. Cell Biol.* , 2009. **41**(3): p. 494-497.
126. Daamen, W.F., et al., *Elastin as a biomaterial for tissue engineering*. *Biomaterials*, 2007. **28**(30): p. 4378-4398.
127. Floquet, N., et al., *Structural characterization of VGVAPG, an elastin-derived peptide*. *Biopolymers*, 2004. **76**(3): p. 266-280.
128. Fulop, T., et al., *Biological effects of elastin peptides*. *Pathologie Biologie*, 1998. **46**(7): p. 497-506.
129. Simionescu, A., K. Philips, and N. Vyavahare, *Elastin-derived peptides and TGF-beta 1 induce osteogenic responses in smooth muscle cells*. *Biochemical and Biophysical Research Communications*, 2005. **334**(2): p. 524-532.
130. Mecham, R.P., et al., *Elastin Binds to a Multifunctional 67-Kilodalton Peripheral Membrane-Protein*. *Biochemistry*, 1989. **28**(9): p. 3716-3722.
131. Grosso, L.E. and M. Scott, *PGAIPG, A REPEATED HEXAPEPTIDE OF BOVINE TROPOELASTIN, IS A LIGAND FOR THE 67-KDA BOVINE ELASTIN RECEPTOR*. *Matrix*, 1993. **13**(2): p. 157-164.

132. Faury, G., et al., *Action of tropoelastin and synthetic elastin sequences on vascular tone and on free Ca<sup>2+</sup> level in human vascular endothelial cells*. Circulation Research, 1998. **82**(3): p. 328-336.
133. Powell, J.T., N. Vine, and M. Crossman, *On the accumulation of d-aspartate in elastin and other proteins of the ageing aorta*. Atherosclerosis, 1992. **97**(2-3): p. 201-208.
134. Hinds, M.T., et al., *Development of a reinforced porcine elastin composite vascular scaffold*. Journal of Biomedical Materials Research Part A, 2006. **77A**(3): p. 458-469.
135. Kurane, A. and N. Vyavahare, *In vivo vascular tissue engineering: influence of cytokine and implant location on tissue specific cellular recruitment*. Journal of Tissue Engineering and Regenerative Medicine, 2009. **3**(4): p. 280-289.
136. Daamen, W.F., et al., *A biomaterial composed of collagen and solubilized elastin enhances angiogenesis and elastic fiber formation without calcification*. Tissue Engineering Part A, 2008. **14**(3): p. 349-360.
137. Lee, S.J., et al., *In vitro evaluation of electrospun nanofiber scaffolds for vascular graft application*. Journal of Biomedical Materials Research Part A, 2007. **83A**(4): p. 999-1008.
138. Paule, W.J., et al., *Calcification of Implanted Vascular Tissues Associated with Elastin in an Experimental Animal-Model*. J. Biomed. Mater. Res., 1992. **26**(9): p. 1169-1177.
139. Nimni, M.E., et al., *Factors which affect the calcification of tissue-derived bioprostheses*. Journal of Biomedical Materials Research, 1997. **35**(4): p. 531-537.
140. Schoen, F.J. and R.J. Levy, *Tissue heart valves: Current challenges and future research perspectives*. Journal of Biomedical Materials Research, 1999. **47**(4): p. 439-465.
141. Schinke, T. and G. Karsenty, *Vascular calcification - a passive process in need of inhibitors*. Nephrology Dialysis Transplantation, 2000. **15**(9): p. 1272-1274.
142. Liu, J.C. and D.A. Tirrell, *Cell Response to RGD Density in Cross-Linked Artificial Extracellular Matrix Protein Films*. Biomacromolecules, 2008. **9**(11): p. 2984-2988.
143. Welsh, E.R. and D.A. Tirrell, *Engineering the extracellular matrix: A novel approach to polymeric biomaterials. I. Control of the physical properties of artificial protein matrices designed to support adhesion of vascular endothelial cells*. Biomacromolecules, 2000. **1**(1): p. 23-30.

144. Di Zio, K. and D.A. Tirrell, *Mechanical properties of artificial protein matrices engineered for control of cell and tissue behavior*. *Macromolecules*, 2003. **36**(5): p. 1553-1558.
145. Nettles, D.L., A. Chilkoti, and L.A. Setton, *Applications of elastin-like polypeptides in tissue engineering*. *Advanced Drug Delivery Reviews*, 2010. **62**(15): p. 1479-1485.
146. Martin, L., et al., *Synthesis and Characterization of Macroporous Thermosensitive Hydrogels from Recombinant Elastin-Like Polymers*. *Biomacromolecules*, 2009. **10**(11): p. 3015-3022.
147. Kim, W. and E.L. Chaikof, *Recombinant elastin-mimetic biomaterials: Emerging applications in medicine*. *Advanced Drug Delivery Reviews*, 2010. **62**(15): p. 1468-1478.
148. Nagapudi, K., et al., *Viscoelastic and mechanical behavior of recombinant protein elastomers*. *Biomaterials*, 2005. **26**(23): p. 4695-4706.
149. Vrhovski, B., S. Jensen, and A.S. Weiss, *Coacervation characteristics of recombinant human tropoelastin*. *European Journal of Biochemistry*, 1997. **250**(1): p. 92-98.
150. Saunders, N.A. and M.E. Grant, *THE SECRETION OF TROPOELASTIN BY CHICK-EMBRYO ARTERY CELLS*. *Biochemical Journal*, 1985. **230**(1): p. 217-225.
151. Maki, J.M., et al., *Lysyl oxidase is essential for normal development and function of the respiratory system and for the integrity of elastic and collagen fibers in various tissues*. *American Journal of Pathology*, 2005. **167**(4): p. 927-936.
152. Sibon, I., et al., *Lysyl oxidase deficiency: a new cause of human arterial dissection*. *Heart*, 2005. **91**(5).
153. Lucero, H.A. and H.M. Kagan, *Lysyl oxidase: an oxidative enzyme and effector of cell function*. *Cellular and Molecular Life Sciences*, 2006. **63**(19-20): p. 2304-2316.
154. Kagan, H.M. and W.D. Li, *Lysyl oxidase: Properties, specificity, and biological roles inside and outside of the cell*. *Journal of Cellular Biochemistry*, 2003. **88**(4): p. 660-672.
155. Bax, D.V., et al., *Cell Adhesion to Tropoelastin Is Mediated via the C-terminal GRKRR Motif and Integrin alpha(V)beta(3)*. *Journal of Biological Chemistry*, 2009. **284**(42): p. 28616-28623.
156. Nakamura, T., et al., *Fibulin-5/DANCE is essential for elastogenesis in vivo*. *Nature*, 2002. **415**(6868): p. 171-175.

157. Yanagisawa, H., et al., *Fibulin-5 is an elastin-binding protein essential for elastic fibre development in vivo*. Nature, 2002. **415**(6868): p. 168-171.
158. Rodgers, U.R. and A.S. Weiss, *Integrin alpha(v)beta(3) binds a unique non-RGD site near the C-terminus of human tropoelastin*. Biochimie, 2004. **86**(3): p. 173-178.
159. Kothapalli, C.R., et al., *Transforming Growth Factor Beta 1 and Hyaluronan Oligomers Synergistically Enhance Elastin Matrix Regeneration by Vascular Smooth Muscle Cells*. Tissue Engineering Part A, 2009. **15**(3): p. 501-511.
160. Palamakumbura, A.H. and P.C. Trackman, *A fluorometric assay for detection of lysyl oxidase enzyme activity in biological samples*. Analytical Biochemistry, 2002. **300**(2): p. 245-251.
161. Urry, D.W., et al., *Elastin: a representative ideal protein elastomer*. Philosophical Transactions of the Royal Society of London Series B-Biological Sciences, 2002. **357**(1418): p. 169-184.
162. Bunda, S., N. Kaviani, and A. Hinek, *Fluctuations of intracellular iron modulate elastin production*. Journal of Biological Chemistry, 2005. **280**(3): p. 2341-2351.
163. Pratt, A.B., et al., *Synthetic extracellular matrices for in situ tissue engineering*. Biotechnology and Bioengineering, 2004. **86**(1): p. 27-36.
164. Davis, E.C., *ENDOTHELIAL-CELL CONNECTING FILAMENTS ANCHOR ENDOTHELIAL-CELLS TO THE SUBJACENT ELASTIC LAMINA IN THE DEVELOPING AORTIC INTIMA OF THE MOUSE*. Cell and Tissue Research, 1993. **272**(2): p. 211-219.
165. Gerrity, R.G. and W.J. Cliff, *AORTIC TUNICA INTIMA IN YOUNG AND AGING RATS*. Experimental and Molecular Pathology, 1972. **16**(3): p. 382-&.
166. Schwartz, S.M. and E.P. Benditt, *STUDIES ON AORTIC INTIMA .I. STRUCTURE AND PERMEABILITY OF RAT THORACIC AORTIC INTIMA*. American Journal of Pathology, 1972. **66**(2): p. 241-&.
167. Berry, C.L., Looker, T., Germain, J., *The growth and development of the rat aorta. I. Morphological aspects*. Journal of Anatomy, 1972. **113**(Part 1): p. 1-16.
168. Dingemans, K.P., et al., *Extracellular matrix of the human aortic media: An ultrastructural histochemical and immunohistochemical study of the adult aortic media*. Anatomical Record, 2000. **258**(1): p. 1-14.
169. Gerrity, R.G. and W.J. Cliff, *AORTIC TUNICA MEDIA OF DEVELOPING RAT .I. QUANTITATIVE STEREOLOGIC AND BIOCHEMICAL ANALYSIS*. Laboratory Investigation, 1975. **32**(5): p. 585-600.

170. Wolinsky, H. and S. Glagov, *A LAMELLAR UNIT OF AORTIC MEDIAL STRUCTURE AND FUNCTION IN MAMMALS*. *Circulation Research*, 1967. **20**(1): p. 99-&.
171. Mochizuki, S., B. Brassart, and A. Hinek, *Signaling pathways transduced through the elastin receptor facilitate proliferation of arterial smooth muscle cells*. *Journal of Biological Chemistry*, 2002. **277**(47): p. 44854-44863.
172. Faury, G., *Function-structure relationship of elastic arteries in evolution: from microfibrils to elastin and elastic fibres*. *Pathologie Biologie*, 2001. **49**(4): p. 310-325.
173. Cox, B.A., B.C. Starcher, and D.W. Urry, *COACERVATION OF TROPOELASTIN RESULTS IN FIBER FORMATION*. *Journal of Biological Chemistry*, 1974. **249**(3): p. 997-998.
174. Wu, W.J., B. Vrhovski, and A.S. Weiss, *Glycosaminoglycans mediate the coacervation of human tropoelastin through dominant charge interactions involving lysine side chains*. *Journal of Biological Chemistry*, 1999. **274**(31): p. 21719-21724.
175. Hinek, A., et al., *The Elastin Receptor - A Galactoside-Binding Protein*. *Science*, 1988. **239**(4847): p. 1539-1541.
176. Robinet, A., et al., *Elastin-derived peptides enhance angiogenesis by promoting endothelial cell migration and tubulogenesis through upregulation of MT1-MMP*. *Journal of Cell Science*, 2005. **118**(2): p. 343-356.
177. Grosso, L.E. and R.P. Mecham, *INVITRO PROCESSING OF TROPOELASTIN - INVESTIGATION OF A POSSIBLE TRANSPORT FUNCTION ASSOCIATED WITH THE CARBOXY-TERMINAL DOMAIN*. *Biochemical and Biophysical Research Communications*, 1988. **153**(2): p. 545-551.
178. Hinek, A. and M. Rabinovitch, *67-KD ELASTIN-BINDING PROTEIN IS A PROTECTIVE COMPANION OF EXTRACELLULAR INSOLUBLE ELASTIN AND INTRACELLULAR TROPOELASTIN*. *Journal of Cell Biology*, 1994. **126**(2): p. 563-574.
179. Kielty, C.M., M.J. Sherratt, and C.A. Shuttleworth, *Elastic fibres*. *Journal of Cell Science*, 2002. **115**(14): p. 2817-2828.
180. Wagenseil, J.E., Mecham, RP, *New Insights into Elastin Fiber Assembly*. *Birth Defects Research (Part C)*, 2007. **81**: p. 229-240.
181. Hinek, A., et al., *Lysosomal sialidase (neuraminidase-1) is targeted to the cell surface in a multiprotein complex that facilitates elastic fiber assembly*. *Journal of Biological Chemistry*, 2006. **281**(6): p. 3698-3710.

182. Yamamoto, Y., et al., *Possible involvement of increased glycooxidation and lipid peroxidation of elastin in atherogenesis in haemodialysis patients*. Nephrology Dialysis Transplantation, 2002. **17**(4): p. 630-636.
183. Hinek, A., F.W. Keeley, and J. Callahan, *RECYCLING OF THE 67-KDA ELASTIN BINDING-PROTEIN IN ARTERIAL MYOCYTES IS IMPERATIVE FOR SECRETION OF TROPOELASTIN*. Experimental Cell Research, 1995. **220**(2): p. 312-324.
184. Buttafoco, L., et al., *Electrospinning of collagen and elastin for tissue engineering applications*. Biomaterials, 2006. **27**(5): p. 724-734.
185. McHale, M.K., L.A. Setton, and A. Chilkoti, *Synthesis and in vitro evaluation of enzymatically cross-linked elastin-like polypeptide gels for cartilaginous tissue repair*. Tissue Engineering, 2005. **11**(11-12): p. 1768-1779.
186. Lee, J., *Elastin-mimetic synthetic polypentapeptide hydrogels*. Recent Research Developments in Polymer Science 2002. **6**: p. 27-43.
187. Mithieux, S.M., J.E.J. Rasko, and A.S. Weiss, *Synthetic elastin hydrogels derived from massive elastic assemblies of self-organized human protein monomers*. Biomaterials, 2004. **25**(20): p. 4921-4927.
188. Kaufmann, D., et al., *Chemical conjugation of linear and cyclic RGD moieties to a recombinant elastin-mimetic polypeptide - A versatile approach towards bioactive protein hydrogels*. Macromolecular Bioscience, 2008. **8**(6): p. 577-588.
189. Lee, J., C.W. Macosko, and D.W. Urry, *Elastomeric polypentapeptides cross-linked into matrixes and fibers*. Biomacromolecules, 2001. **2**(1): p. 170-179.
190. Ruoslahti, E. and M.D. Pierschbacher, *NEW PERSPECTIVES IN CELL-ADHESION - RGD AND INTEGRINS*. Science, 1987. **238**(4826): p. 491-497.
191. Hern, D.L. and J.A. Hubbell, *Incorporation of adhesion peptides into nonadhesive hydrogels useful for tissue resurfacing*. Journal of Biomedical Materials Research, 1998. **39**(2): p. 266-276.
192. Liaw, L., et al., *OSTEOPONTIN PROMOTES VASCULAR CELL-ADHESION AND SPREADING AND IS CHEMOTACTIC FOR SMOOTH-MUSCLE CELLS IN-VITRO*. Circulation Research, 1994. **74**(2): p. 214-224.
193. Liaw, L., et al., *ADHESIVE AND MIGRATORY EFFECTS OF OSTEOPONTIN ARE MEDIATED VIA DISTINCT CELL-SURFACE INTEGRINS - ROLE OF ALPHA(V)BETA(3) IN SMOOTH-MUSCLE CELL-MIGRATION TO OSTEOPONTIN IN-VITRO*. Journal of Clinical Investigation, 1995. **95**(2): p. 713-724.

194. Wachi Hiroshi, S.H., Murata Hayato, Nakazawa Junji, Mecham Robert P, and Seyakama, Yoshiyuki, *Tropoelastin inhibits vascular calcification via 67-kDa elastin binding protein in cultured bovine aortic smooth muscle cells*. Journal of Atherosclerosis and Thrombosis, 2004. **11**(3): p. 159-166.
195. Vrhovski, B. and A.S. Weiss, *Biochemistry of tropoelastin*. European Journal of Biochemistry, 1998. **258**(1): p. 1-18.
196. Debelle, L., et al., *The secondary structure and architecture of human elastin*. European Journal Of Biochemistry / FEBS, 1998. **258**(2): p. 533-539.
197. Mammi, M., L. Gotte, and G. Pezzin, *EVIDENCE FOR ORDER IN STRUCTURE OF ALPHA-ELASTIN*. Nature, 1968. **220**(5165): p. 371-&.
198. Urry, D.W., B. Starcher, and Partridge, S.M., *COACERVATION OF SOLUBILIZED ELASTIN EFFECTS A NOTABLE CONFORMATIONAL CHANGE*. Nature, 1969. **222**(5195): p. 795-&.
199. Tamburro, A.M., et al., *CONFORMATIONAL TRANSITIONS OF ALPHA-ELASTIN*. Biochimica Et Biophysica Acta, 1977. **492**(2): p. 370-376.
200. Tamburro, A.M., V. Guantieri, and D.D. Gordini, *HUMAN ALPHA-ELASTINS - LIPID-INDUCED CONFORMATIONAL-CHANGES*. International Journal of Biological Macromolecules, 1982. **4**(2): p. 111-115.
201. Urry, D.W., *WHAT IS ELASTIN - WHAT IS NOT*. Ultrastructural Pathology, 1983. **4**(2-3): p. 227-251.
202. Urry, D.W., *ENTROPIC ELASTIC PROCESSES IN PROTEIN MECHANISMS .1. ELASTIC STRUCTURE DUE TO AN INVERSE TEMPERATURE TRANSITION AND ELASTICITY DUE TO INTERNAL CHAIN DYNAMICS*. Journal of Protein Chemistry, 1988. **7**(1): p. 1-34.
203. Barczyk, M., S. Carracedo, and D. Gullberg, *Integrins*. Cell and Tissue Research, 2010. **339**(1): p. 269-280.
204. Charo, I.F., et al., *The Vitronectin Receptor Alpha-V-Beta-3 Binds Fibronectin and Acts in Concert with Alpha-5-Beta-1 in Promoting Cellular Attachment and Spreading on Fibronectin*. Journal of Cell Biology, 1990. **111**(6): p. 2795-2800.
205. Mann, B.K., R.H. Schmedlen, and J.L. West, *Tethered-TGF-beta increases extracellular matrix production of vascular smooth muscle cells*. Biomaterials, 2001. **22**(5): p. 439-444.
206. Mann, B.K., et al., *Smooth muscle cell growth in photopolymerized hydrogels with cell adhesive and proteolytically degradable domains: synthetic ECM analogs for tissue engineering*. Biomaterials, 2001. **22**(22): p. 3045-3051.

207. Moon, J.J., et al., *Micropatterning of Poly(Ethylene Glycol) Diacrylate Hydrogels with Biomolecules to Regulate and Guide Endothelial Morphogenesis*. Tissue Engineering Part A, 2009. **15**(3): p. 579-585.
208. Liu, V.A. and S.N. Bhatia, *Three-dimensional photopatterning of hydrogels containing living cells*. Biomedical Microdevices, 2002. **4**(4): p. 257-266.
209. DeLong, S.A., J.J. Moon, and J.L. West, *Covalently immobilized gradients of bFGF on hydrogel scaffolds for directed cell migration*. Biomaterials, 2005. **26**(16): p. 3227-3234.
210. Moore, S., *Amino Acid Analysis - Aqueous Dimethyl Sulfoxide as Solvent for Ninhydrin Reaction*. Journal of Biological Chemistry, 1968. **243**(23): p. 6281-&.
211. Zhu, J.M., *Bioactive modification of poly(ethylene glycol) hydrogels for tissue engineering*. Biomaterials, 2010. **31**(17): p. 4639-4656.
212. Mann, B.K., et al., *Modification of surfaces with cell adhesion peptides alters extracellular matrix deposition*. Biomaterials, 1999. **20**(23-24): p. 2281-2286.
213. Miller, D.C., et al., *Endothelial and vascular smooth muscle cell function on poly(lactic-co-glycolic acid) with nano-structured surface features*. Biomaterials, 2004. **25**(1): p. 53-61.
214. Hahn, M.S., et al., *Physiologic pulsatile flow bioreactor conditioning of poly(ethylene glycol)-based tissue engineered vascular grafts*. Annals of Biomedical Engineering, 2007. **35**(2): p. 190-200.
215. Gobin, A.S. and J.L. West, *Cell migration through defined, synthetic extracellular matrix analogues*. FASEB Journal, 2002. **16**(3): p. 751-+.
216. Hahn, M.S., et al., *Collagen composite hydrogels for vocal fold lamina propria restoration*. Biomaterials, 2006. **27**(7): p. 1104-1109.
217. Robert, L., A.M. Robert, and B. Jacotot, *Elastin-elastase-atherosclerosis revisited*. Atherosclerosis, 1998. **140**(2): p. 281-295.
218. Rabinovitch, M., *Elastase and cell matrix interactions in the pathobiology of vascular disease*. Acta Paediatrica Japonica, 1995. **37**(6): p. 657-666.
219. Szilagyi, L., *Pancreatic Elastase*. Handbook of Proteolytic Enzymes, 2004.
220. Levitz, D., et al., *Non-destructive label-free monitoring of collagen gel remodeling using optical coherence tomography*. Biomaterials, 2010. **31**(32): p. 8210-8217.

221. Cummings, C.L., et al., *Properties of engineered vascular constructs made from collagen, fibrin, and collagen-fibrin mixtures*. *Biomaterials*, 2004. **25**(17): p. 3699-3706.
222. Johnson, C. and Z.S. Galis, *Matrix metalloproteinase-2 and-9 differentially regulate smooth muscle cell migration and cell-mediated collagen organization*. *Arteriosclerosis Thrombosis and Vascular Biology*, 2004. **24**(1): p. 54-60.
223. Kanda, S., et al., *Matrix metalloproteinase and alpha v beta 3 integrin-dependent vascular smooth muscle cell invasion through a type I collagen lattice*. *Arteriosclerosis Thrombosis and Vascular Biology*, 2000. **20**(4): p. 998-1005.
224. Ramamurthi, A. and I. Vesely, *Evaluation of the matrix-synthesis potential of crosslinked hyaluronan gels for tissue engineering of aortic heart valves*. *Biomaterials*, 2005. **26**(9): p. 999-1010.
225. Venkataraman, L. and A. Ramamurthi, *Induced Elastic Matrix Deposition Within Three-Dimensional Collagen Scaffolds*. *Tissue Engineering Part A*, 2011. **17**(21-22): p. 2879-2889.
226. Lee, K.W., D.B. Stolz, and Y.D. Wang, *Substantial expression of mature elastin in arterial constructs*. *Proceedings of the National Academy of Sciences of the United States of America*, 2011. **108**(7): p. 2705-2710.
227. Ottani, V., M. Raspanti, and A. Ruggeri, *Collagen structure and functional implications*. *Micron*, 2001. **32**(3): p. 251-260.
228. Browning, M.B., et al., *Compositional control of poly(ethylene glycol) hydrogel modulus independent of mesh size*. *Journal of Biomedical Materials Research Part A*, 2011. **98A**(2): p. 268-273.
229. Browning, M.B. and E. Cosgriff-Hernandez, *Development of a Biostable Replacement for PEGDA Hydrogels*. *Biomacromolecules*, 2012. **13**(3): p. 779-786.
230. Gauvin, R., et al., *Dynamic mechanical stimulations induce anisotropy and improve the tensile properties of engineered tissues produced without exogenous scaffolding*. *Acta Biomaterialia*, 2011. **7**(9): p. 3294-3301.
231. Song, Y., et al., *Dynamic Culturing of Smooth Muscle Cells in Tubular Poly(Trimethylene Carbonate) Scaffolds for Vascular Tissue Engineering*. *Tissue Engineering Part A*, 2011. **17**(3-4): p. 381-387.
232. Gao, J., et al., *Co-expression of elastin and collagen leads to highly compliant engineered blood vessels*. *Journal of Biomedical Materials Research Part A*, 2008. **85A**(4): p. 1120-1128.

233. Syedain, Z.H., et al., *Implantable arterial grafts from human fibroblasts and fibrin using a multi-graft pulsed flow-stretch bioreactor with noninvasive strength monitoring*. *Biomaterials*, 2011. **32**(3): p. 714-722.
234. Porter, B., et al., *3-D computational modeling of media flow through scaffolds in a perfusion bioreactor*. *Journal of Biomechanics*, 2005. **38**(3): p. 543-549.
235. Kanda, K., T. Matsuda, and T. Oka, *Mechanical stress induced cellular orientation and phenotypic modulation of 3-D cultured smooth muscle cells*. *ASAIO journal (American Society for Artificial Internal Organs : 1992)*, 1993. **39**(3): p. M686-90.
236. Tranquillo, R.T., et al., *Magnetically orientated tissue-equivalent tubes: Application to a circumferentially orientated media-equivalent*. *Biomaterials*, 1996. **17**(3): p. 349-357.
237. Punshon, G., et al., *Assessment of the potential of progenitor stem cells extracted from human peripheral blood for seeding a novel vascular graft material*. *Cell Proliferation*, 2008. **41**(2): p. 321-335.
238. Bondar, B., et al., *Functionality of endothelial cells on silk fibroin nets: Comparative study of micro- and nanometric fibre size*. *Biomaterials*, 2008. **29**(5): p. 561-572.
239. Orlova, Y., et al., *Electrospun nanofibers as a tool for architecture control in engineered cardiac tissue*. *Biomaterials*, 2011. **32**(24): p. 5615-5624.
240. Patel, S., et al., *Regulation of endothelial cell function by GRGDSP peptide grafted on interpenetrating polymers*. *Journal of Biomedical Materials Research Part A*, 2007. **83A**(2): p. 423-433.
241. Comisar, W.A., et al., *Engineering RGD nanopatterned hydrogels to control preosteoblast behavior: A combined computational and experimental approach*. *Biomaterials*, 2007. **28**(30): p. 4409-4417.
242. Murugan, R. and S. Ramakrishna, *Design strategies of tissue engineering scaffolds with controlled fiber orientation*. *Tissue Eng*, 2007. **13**(8): p. 1845-1866.